Technische Universität München

Lehrstuhl für Organische Chemie II

Aldehyde Dehydrogenase 1 – A Novel Target of Duocarmycins
and
Activity Based Protein Profiling during Bacterial Invasion

Tanja Wirth

Für meine Familie

Parts of this thesis have been published in international journals

TABLE OF CONTENTS

°C	degree Celsius
μL	microliter
μM	micromolar
μmol	micromole
Å	Angström
AA	amino acid
ABC	ATP-binding cassette
ABPP	activity based protein profiling
Act	actine
ADEPT	antibody-directed enzyme prodrug therapy
ADP	adenosine diphosphate
Ala	alanine
ALDH	aldehyde dehydrogenase
ATP	adenosine triphosphate
BHB	Brain-Heart-broth
BOC	t-butyloxycarbonyl
BSA	bovine serum albumin
$CaCl_2$	calcium cholride
CBI	1,2,9,9a-tetrahydro**c**yclopropa[c]**b**enz[e]**i**ndol-4(2H)-one
CC	click chemistry
CDC	cholesterol-dependent cytolysin
cDNA	complementary DNA
CHES	N-Cyclohexyl-2-aminoethanesulfonic acid
CI	2,3-dihydro-1H-**c**yclopropa[c]**i**ndol-5(1aH)-one
ClpP	caseinolytic protein protease
cm^2	square centimeter
CO_2	carbon dioxide
CPI	7-methyl-1,2,8,8a-tetrahydro**c**yclopropa[c]**p**yrrol[3,2-e]**i**ndol-4(5H)-one
$CuSO_4$	Copper(II) sulfate
Cys	cysteine
DA	(6R)-methyl 6-methyl-4-oxo-1,2,4,5,6,7,8,8a-octahydrocyclopropa[c]pyrrol[3,2-e]indole-6-carboxylate
DAPI	4',6-diamidino-2-phenylindole
DMEM	Duolbeco's Modified Eagle's Medium
DMF	dimethylformamid
DMSO	dimethylsulfoxid
DNA	deoxyribonucleic acid
dNTP	deoxyribonucleotide triphosphate
DSA	methyl 4-oxo-1,2,4,5,8,8a-hexahydrocyclopropa[c]pyrrol[3,2-e]indole-6-carboxylate
dsDNA	double stranded DNA
DTT	dithiothreitol

EDC	1-ethyl-3-(3-dimethylaminopropyl)-carbodiimide
EDTA	ethylene diamine tetraacetat
e.g.	exempli gratia = for example
eq.	equivalents
ESI-MS	electrospray ionization mass-spectrum
EtOAc	ethylacetat
FAS	fatty acid synthesis
FBS	fetal bovine serum
g	gram
h	hour
HCl	hydrochloric acid
HEPES	2-(4-(2-Hydroxyethyl)- 1-piperazinyl)-ethansulfonsäure
HGF	hepatocyte growth factor receptor
HILIC	ydrophilic interaction chromatography
Hpt	hexose-phosphate translocase
HTCFA	human tumor colony forming ability assay
IC_{50}	half maximal inhibitory concentration
Inl	internalin
kDA	kilo dalton
LB	Luria-broth
LC	liquid chromatography
LLO	listeriolysin O
Lpl	lipoate protein ligase
LTQ-FT	Linear trap quadrupole - Fourier Transform
M	molar
MALDI	Matrix-assisted laser-desorption ionization
MAPK	mitogen-activated protein kinase
MES	2-(N-morpholino)-ethanesulfonic acid
mg	milligram
min	minute
mL	milliliter
mM	millimolar
MOI	multiplicity of infection
MS	mass spectrometry
MTT	3-(4,5-Dimethylthiazol-2-yl)-2,5-diphenyltetrazolium bromide
MW	molecular weight
NaCl	sodium chloride
NAD	nicotinamide adenine dinucleotide
NECH	neutral cholesterol ester hydrolase
nL	nanoliter
nM	nanomolar
nm	nanometer

nmol	nanomole
OD	optical density
ORF	open reading frame
PAGE	polyacrylamide gel electrophoresis
PAMP	pathogen-associated molecular patterns
PBS	Phosphate Buffered Saline
PCR	polymerase chain reaction
PEG	polyethylene glycol
PEP	phosphenolypyruvate ADP
PKM	pyruvate kinase isozyme M
Plc	phospholipase
pM	picomolar
pmol	picomole
ppm	parts per million
PTM	post-translational modification
RNA	ribonucleic acid
rpm	rotations per minute
RT	room temperature
scr	scrambled
SDS	sodium dodecyl sulfate
sec	second
siRNA	small interfering RNA
TBTA	Tris-[(1-benzyl-1H-1,2,3-triazol-4-yl)methyl]amin)
TCEP	Tris-(2-carboxyethyl)-phosphine
TEV	Tobacco Etch Virus
TLR	Toll-like receptor
TMI	5,6,7-trimethoxy-1H-indole
TNF	tumor necrosis factor
Tris	Tris-(hydroxymethyl)-aminomethan

1 INTRODUCTION

1   THE HISTORY OF DRUG DISCOVERY

Throughout history humans have been threatened by diseases and explored natural resources for abatement and cure. The first attempts can be dated back to prehistoric times, as residuals of medicinal herbs were discovered in 60,000 year old Neanderthal remains.[1] Ancient civilizations such as the Egyptians gathered their knowledge of herbal treatments in written compendia. The Ebers Papyrus (1500 BC) is one important example and contains 800 prescriptions for over 700 cures.[2, 3] But this knowledge was more a result of trial and error or accidental discoveries, rather than systematic research. Furthermore the tinctures of alcoholic or aqueous plant extracts did not fit an exact chemical composition, since they contained various constituents in differing amounts.[2] The scientific foundation for today's therapeutic agents as well as for modern drug discovery was laid in the 19th century. Due to the development of organic and analytical chemistry (Figure I-1) the tools for isolation, purification and characterization of active herbal ingredients were provided.
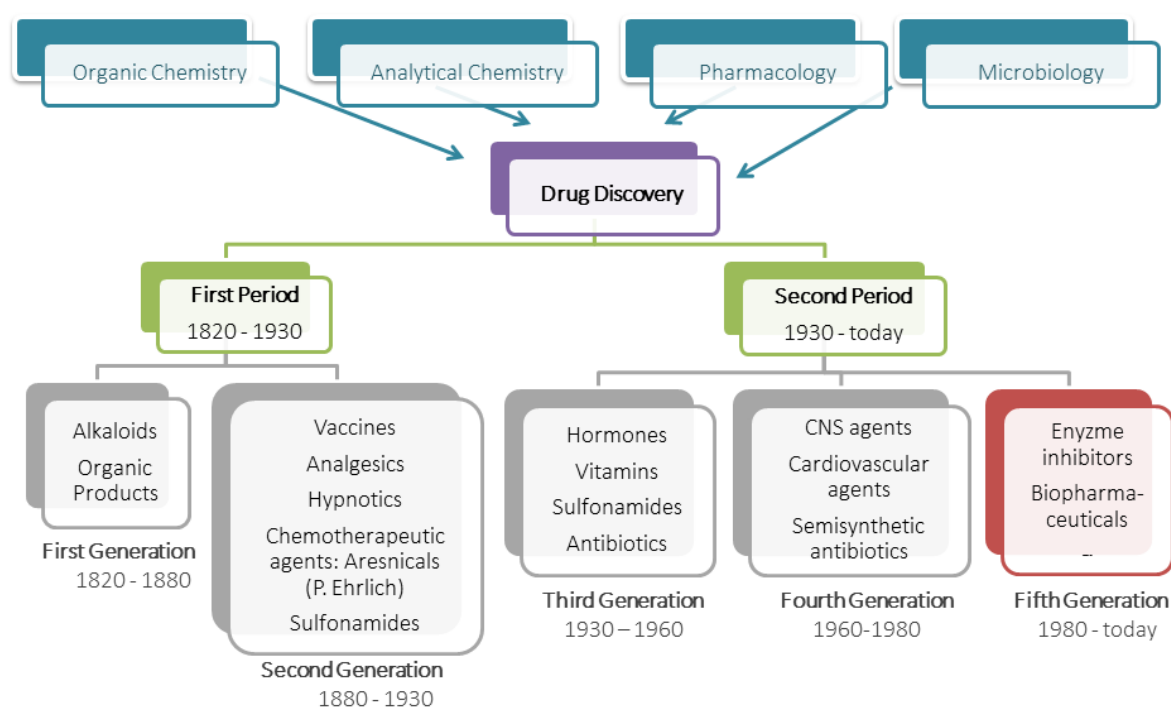
Figure I-1: Important periods of drug discovery (modified from original source, p 16).[2]

The first generation of "modern" drugs was launched with the isolation of morphine[4] from opium by Sertürner (1815).[2, 5] Through the access of pure alkaloids and synthetic

organic products, the door was opened to a new and independent scientific discipline: pharmacology. Further disciplines as medicinal chemistry, biochemistry and microbiology followed soon and gave birth to second-generation drugs (e.g. vaccines) and new types of drug therapies such as chemotherapy to treat cancer. An underlying concept of "chemoreceptors" was first introduced by Paul Ehrlich[6] (1872-1874), who postulated that cancer cells, parasites or microorganisms possess particular chemoreceptors, which are absent in host tissues or healthy cells. He further demonstrated these receptors could be exploited for a selective treatment and cure of infectious disease.[2, 5]

With the discovery of Penicillin[7] by Alexander Fleming (1929) and Prontosil[8] (the first sulfonamide antibiotic, 1932) a new age of drug discovery had begun. In the following years further sulfonamide derivatives, hormones, vitamins and antibiotics reached the market and revolutionized the pharmaceutical industry.[2] With the emerging knowledge in biological structures and functions in the 1960s, rational drug discovery and design through structural variations grew popular. The resulting fourth generation of drugs furthermore expanded the scope of treatments to central nerve system or cardiovascular diseases.[2, 5] Today we have reached the fifth generation of drugs consisting of small molecule enzyme inhibitors and biologics, such as monoclonal antibodies and recombinant proteins. But apart from these new types of drugs, a huge progress in technology and methodology was achieved, resulting in the new concept of structure-based drug discovery.[2, 5] This strategy is focused on the molecular mechanism of cellular processes and diseases to identify potential drug targets and to optimize drug candidates. Methods and techniques as high-throughput screening, combinatorial chemistry, X-ray crystallography, bioinformatics, genomics and proteomics (to name but a few) are utilized to solve this task.[2, 5] Hence, drug discovery has become a highly interdisciplinary field with increasing complexity. Nonetheless the evolution will go on and further techniques and strategies have to be developed for target identification and drug optimization.

2 FROM GENOME TO PROTEOME

With finishing the sequence of the human genome (Human Genome Project, 1990 – 2003) the foundation for functional analysis at the molecular level of cellular processes was laid. However, the genome – the total set of genes of an organism - is a static system, independent from environmental conditions or cell type. Compared to the genome of nematodes ($\sim$12,000 – 24,000 genes, depending on the species)[9] the human genome ($\sim$20,000 genes)[10] itself cannot explain the obviously increased biological complexity. Therefore, an explanation can only be found at the level of the dynamic and highly diverse transcriptome and proteome (Figure I-2).
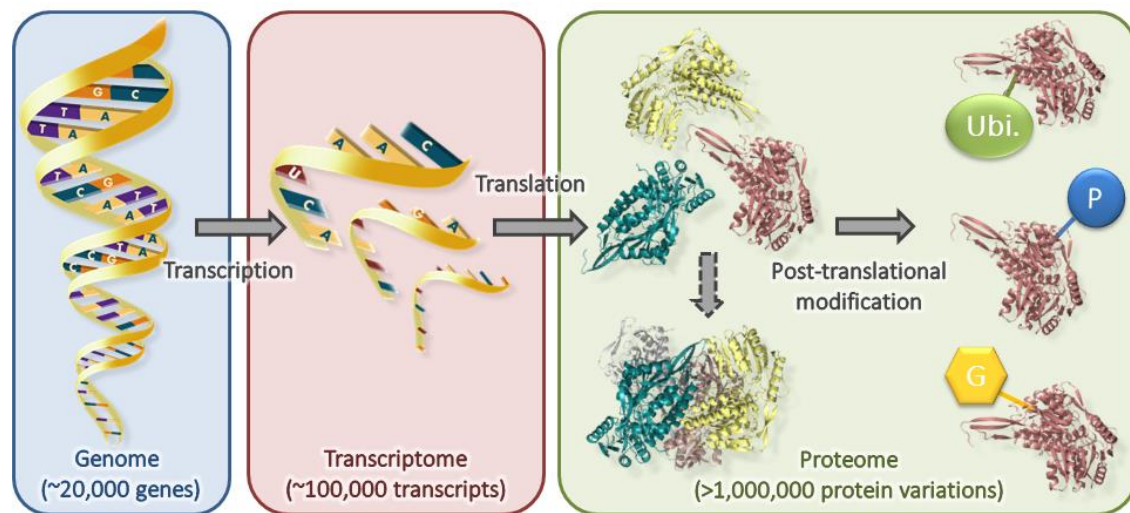
Figure I-2: From genome to proteome. The proteome complexity is increased through protein complexes and post-translational modifications. The examples shown here are only a few of the over 400 types of known protein modifications (Ubi = ubiquitination, P = Phosphorylation, G = Glycosylation).The figure was partially prepared by the Biological and Environmental Research Information System, Oak Ridge National Laboratory.

Due to changes in the environmental conditions, such as stress, drug exposure or disease, their composition can alter dramatically, as a result of transcriptional regulation, RNA processing, protein synthesis and modification.[11] The transcriptome – the total set of mRNA in a given cell or cellular state – is generated from the genome, whereby one gene may encode different transcripts by alternative splicing or alternative promoters. The transcriptome in turn is translated to produce the proteome, the total set of proteins in a given cell or cellular state.[11] The expressed proteins can act as single molecules or as

subunits of homo- (same subunits) and heteromeric (different subunits) protein complexes. Moreover, the proteome complexity is increased through post-translational modifications (PTMs), which can emerge at any stage of a proteins life cycle. Taking PTMs into account, there are over one million possible protein variations according to estimations.[12] These chemical modifications exert influence over protein activity, localization, degradation, expression and the interaction with other macromolecules.

Today's major goal for drug discovery and basic research is focused on the detailed understanding of biological systems, to create pathways and networks. One approach to resolve the functions of genes and their products is based on the transcriptome (transcriptomics). But DNA and mRNA are "solely" information carriers, which cannot predict the structure, interaction, abundance or activity of a protein. However, the activity and function of a protein depends greatly on the cellular localization and eventual post-translational modifications.[11] In contrast to DNA and mRNA, proteins provide a direct link to the various biological functions in the cell, as they control biochemical reactions, intracellular transport, cell shape, signal transduction and many more. Hence the analysis of the proteome (proteomics) presents a powerful tool to determine altered protein expression, interaction or activity.

3 ENZYME INHIBITORS

Enzyme catalysis and the control of biochemical reactions are essential for all life. Furthermore altered regulation of activity, substrate specificity and expression can either be caused by diseases or result in a pathologic state, making enzymes attractive drug targets. Beside the attractiveness and pathophysiologic relevance, enzymes are highly druggable for several reasons. First the active site and ligand binding pockets are well attuned to interact with small molecule drugs. That is because enzyme pockets are small, shielded from bulk solvent and show large surfaces relative to volume with a distinct topography, which contains specific groups for hydrogen bonding and electrostatic interactions with ligands.[13, 14] Second minor changes in the surface topography, induced through ligand or drug binding, are enough to alter the enzymatic activity drastically. Third enzymes are highly dynamic molecules, rearranging shape and structure to

facilitate the catalysis of chemical reactions. Thus one enzyme offers various conformational forms and transition states, whereas each form represents a unique point of application that can be addressed by small molecule drugs.[13, 14]

As mentioned before, proteins are responsible for diverse biological functions and can therefore be further divided into subclasses, such as cytoskeletal proteins, coagulation factors, ion channels, receptors, chaperones, enzymes and many more. But concerning the druggability and the actual application in modern medicine, enzymes and G-protein-coupled receptors represent the predominant drug targets (Figure I-3A/B).[15, 16]
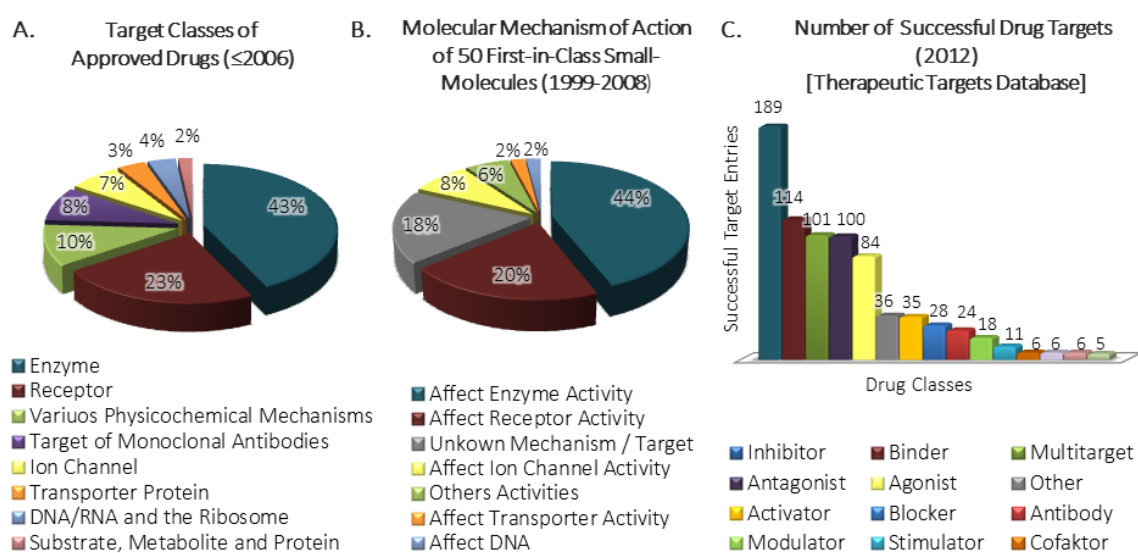
Figure I-3: A. Target classes of approved drugs. Similar target molecules of different drugs were counted once. B. Molecular mechanism of action (MMOA) of the 50 first-in-class small-molecule drugs (with new MMOA) approved by the FDA between 1999 and 2008. C. Number of successful drug targets sorted by drug classes. The Data was derived from the Therapeutic Target Database (TTD 2012) and considers also targets of multiple drug classes. Therefore the successful target entries are shown in absolute numbers.

A more detailed view on the molecular mode of action is shown in Figure I-3C. Successful and clinically used targets are divided by the classes of attacking drugs, revealing enzyme inhibitors as major class.[17] As a conclusion the pathophysiologic relevance and druggability of enzymes makes inhibitors attractive for drug discovery and applicable in any human disease, such as cancer, infectious, metabolic, inflammatory or cardiovascular diseases.

4   ACTIVITY BASED PROTEIN PROFILING (ABPP)

For analyzing *in vitro* functions, expression patterns and interactions of proteins, several proteomic methods have been developed, such as yeast two-hybrid methods[18, 19] or protein microarrays[20]. Though these are valuable techniques, they do not give any information on the activity of proteins, since the abundance of a protein is not necessarily related to its activity or its pathophysiological function.[21, 22] Thus a new chemical proteomic strategy termed activity based protein profiling (ABPP) was established by Cravatt[23, 24] and Bogyo[25, 26], based on previous work from Walker[27] and Powers[28, 29]. This method provides a powerful screening tool for the identification and functional characterization of enzymes and enzyme families in complex biological systems.[21, 22] The applied probes usually consist of three main elements. First a reactive group (green triangle, Figure I-4), which exhibits a moderate reactivity towards proteins to ensure a selective recognition of structural related active sites and thus covalent binding of a limited subset of the proteome. Reactive groups are in general derived from mechanism-based inhibitors[30], natural products[22, 31] and other electrophilic scaffolds[32]. Second, an alkyne handle, which serves for the attachment of an azide containing reporter tag (pink star, Figure I-4). This attachment is mediated via an bio-orthogonal Cu(I)-catalyzed-Huisgen-[3+2]-cycloaddition (click chemistry)[33-35] and results in the formation of a triazole. The reporter tag typically consists of a fluorescent dye or biotin which serves for visualization or enrichment and identification of labeled enzymes, respectively. The final structural element is a spacer, which separates the first two elements.
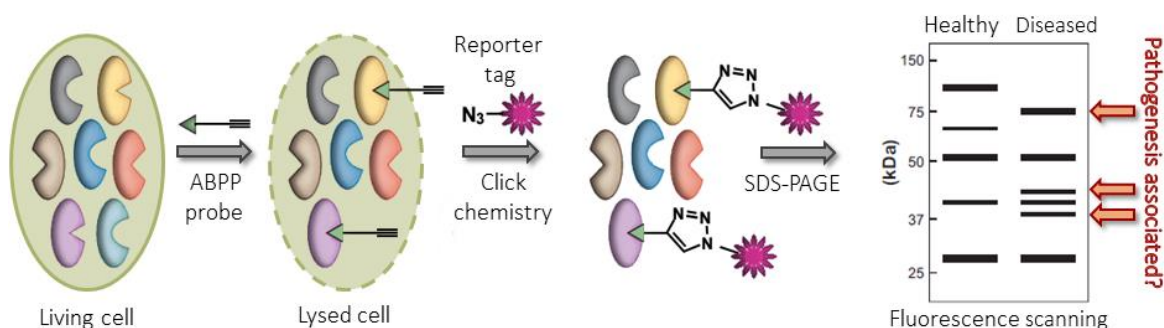
Figure I-4: Schematic representation of ABPP. 1. *In situ* labeling with alkyne probe. 2. Cell lysis. 3. Click chemistry to attach reporter tag. 4. SDS-gel electrophoresis for protein separation. The figure was partially taken from *Cravatt* et al.[24]

The schematic representation of a general ABPP experiment is shown in Figure I-4. A cell permeable probe is first incubated with living cells. A small subset of the enclosed proteome is covalently labeled *in situ*. After cell lysis, the reporter tag is attached via click chemistry and the enzymes are separated by gel electrophoresis. Finally the labeled enzymes are visualized through in-gel fluorescence scanning.

The most popular application of ABPP is comparative target discovery.[24] In this application, proteomes with different characteristics, such as healthy versus diseased (eukaryotic cells/tissues) or pathogenic versus non-pathogenic (bacterial strains), are compared. Varying levels of activity or differences in the resulting labeling patterns, as presented in Figure I-4, indicate potential targets with a possible pathogenesis association. For a detailed target investigation the enzymes are labeled with a biotinylated tag, enriched on avidin beads, digested and the resulting peptides are analyzed by LC-MS/MS. The identified proteins are then further characterized and evaluated by different biochemical methods such as kinetic assays, mutations, knock downs, crystallizations and affinity determinations.

Another application is the target discovery of potent natural products.[22] Though they are widely spread and applied as pharmacologically active substances, their actual targets and molecular mechanisms of action are often unknown or merely partially elucidated. Furthermore protein-reactive natural products are well-suited as ABPP probes due to their fine attuned reactivity and therefore excellent selectivity and high affinity for a small and specific subset of target molecules. Beside the elucidation of unknown molecular mechanism, ABPP can be deployed to determine possible proteinogenic off-targets of well characterized natural products.

II ALDEHYDE DEHYDROGENASE 1 – A NOVEL TARGET OF DUOCARMYCINS

1 Special Introduction

1.1 Duocarmycins

The duocarmycins, a small class of natural products, have been known since 1978, when the first member the (+)-CC-1065 (**1**) (Figure II-1) was isolated from a soil culture of *Streptomyces zelensis*.[36, 37] (+)-CC-1065 soon aroused the curiosity of the scientific community as it showed an exceptional high *in vitro* cytotoxicity of 20 pM[38] (L1210 cell line) as well as antimicrobial and antitumor activity.[36, 37, 39] To expand the library of potent antitumor antibiotics different *Streptomyces* strains were screened, which led to the identification of further duocarmycins such as duocarmycin SA[40, 41] (**2**) and B$_2$[42] (**3**) shown in Figure II-1.
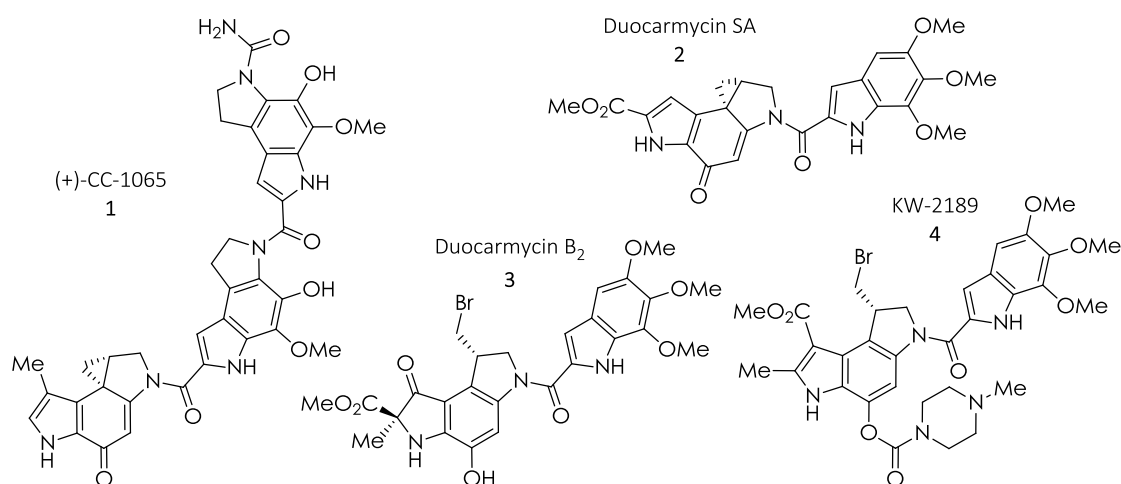
Figure II-1: Structures of (+)-CC-1065, duocarmycin SA, duocarmycin B$_2$ and KW-2189.

Due to the promising anticancer activity, different analogs progressed into clinical phase I and II. One example is the semisynthetic compound KW-2189 (**4**), a more soluble and stable derivative of duocarmycin B$_2$. However, treatment resulted in prolonged hematologic toxicity and severe side effects, which led to the termination of the different trials. [43, 44]

The cytotoxicity of duocarmycins originates from sequence specific DNA alkylation and interstrand crosslinking as shown in Figure II-2A/B.[45-48]
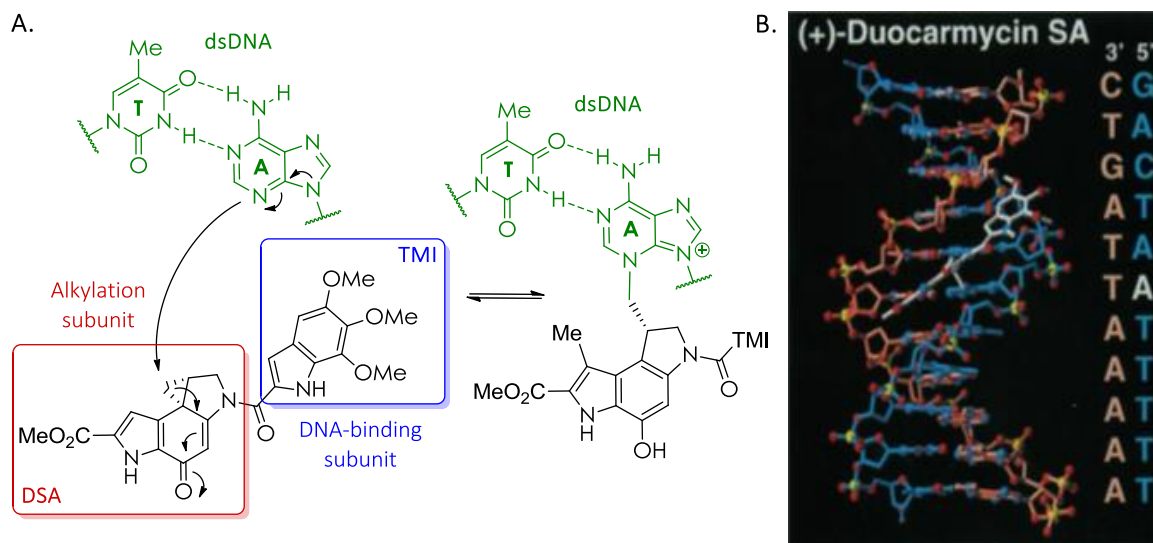
Figure II-2: Scheme of *N*3-alkylation at 3'adenine (green) by duocarmycin SA, which consists of two main elements: alkylation subunit (red) and DNA-binding subunit (blue). **B.** DNA alkylation model of (+)-Duocarmycin SA within w794 DNA: duplex 5'd(GACTA**A**TTTTT) with binding in the 3'→5' direction across the sequence 5'-CTAA, taken from *Boger* et al.[47]

The alkylation is achieved by a dual mode of action, as the structure consists of two main elements (Figure II-2A): the right-hand DNA-binding subunit and the left-hand alkylation subunit. According to the theoretical mechanism, postulated by *Boger* et al.[38, 47-52], the TMI DNA-binding subunit first incorporates non-covalently into AT-rich sequences of the minor groove by a shape-selective recognition, which leads to hydrogen bonding. Due to hydrogen bonding, the vinylogous amide conjugation is disrupted, which results in a conformational change and activation of the DSA alkylation subunit followed by nucleophilic attack of the 3'adenine *N*3-nitrogen on the cyclopropyl ring (Figure II-2A).To clarify the structural requirments of the sequence-selective DNA alkylation, different synthetic analogs of the right-hand TMI motive, as well as chemical variations of the left-hand DSA, were designed by *Boger* et al. (Figure II-3A, p. 12).

	k (pH3)	$t_1/_2$	IC_{50}
DSA-Boc	1.1×10^{-6} /s	177 h	6 nM
CBI-Boc	1.5×10^{-6} /s	133 h	80 nM
CPI-Boc	5.3×10^{-6} /s	37 h	330 nM
SA-Boc	1.7×10^{-5} /s	11 h	1000 nM
CI-Boc	2.0×10^{-2} /s	0.01 h	18000 nM
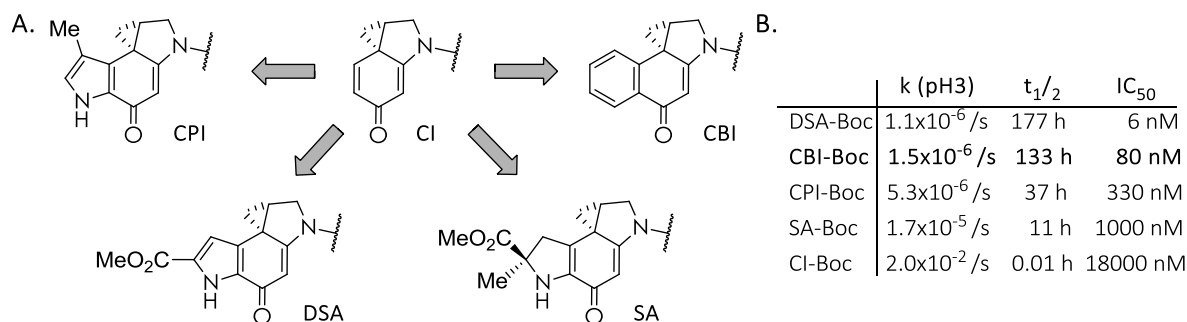
Figure II-3: **A.** Analogs of duocarmycin alkylation subunits derived from the parental core structure CI: CPI = alkylation subunit of (+)-CC-1065, DSA= alkylation subunit of (+)-Duocarmycin SA, SA= alkylation subunit of (+)-Duocarmycin A and CBI = synthetically simplified alkylation subunit. **B.** The table shows rate constants k and half-life periods $t_{1/2}$ for solvolysis at pH 3 and *in vitro* cytotoxicities IC_{50} (L1210 mouse melanoma cell line) of Boc protected derivatives.[53]

DSA, SA and CPI represent naturally occurring alkylation subunits with a cyclopropapyrrolindole core structure, originating from duocarmycins SA, duocarmycins S and CC-1065, respectively. Further dissection of this core structure resulted in the minimum potent pharmacophore, the cyclopropaindole CI. Despite limiting stability due to solvolysis, CI derivatives showed exceptionally high reactivities and decreased cytotoxic activities with comparable incorporations and sequence-selective covalent alkylations of DNA to (+)-CC-1065.[38, 54] Further variation of the alkylation subunit led to simplified cyclopropabenzindole CBI derivatives, which exhibited a higher cytotoxicity and lower reactivity compared to their CPI-based analogs.[55] In addition, DNA alkylation occurred more efficient and with higher selectivity.[38, 49, 56] Further studies of several simple and advanced analogues led to the observation of a nearly linear inverse relationship between cytotoxicity and solvolytic reactivity. Rate constants and half-life periods of solvolysis (pH 3), as well as *in vitro* cytotoxicities of Boc protected derivatives are exemplarily presented in Figure II-3B.[38, 53, 55, 57]

In addition to the extensive research on the mechanism of DNA alkylation, the affinity of duocarmycins towards conventional nucleophiles such as glutathione was evaluated, which exhibited poor reactivity.[58] Hence DNA was thought to be the only specific target of these natural products.

1.2   ANTIBODY-DIRECTED ENZYME PRODRUG THERAPY

Since conventional chemotherapeutics typically affect all fast proliferating cells and are unable to distinguish between healthy and cancerous cells and tissues, side effects as immunosuppression and gastrointestinal disorders are the consequences.[59] To overcome these side effects several approaches have been made in developing cancer-selective chemotherapeutics. One promising strategy is the antibody-directed enzyme prodrug therapy[59-66] (ADEPT), shown in Figure II-4, which combines the use of "nontoxic" prodrugs and antibody conjugated enzymes that control drug release.
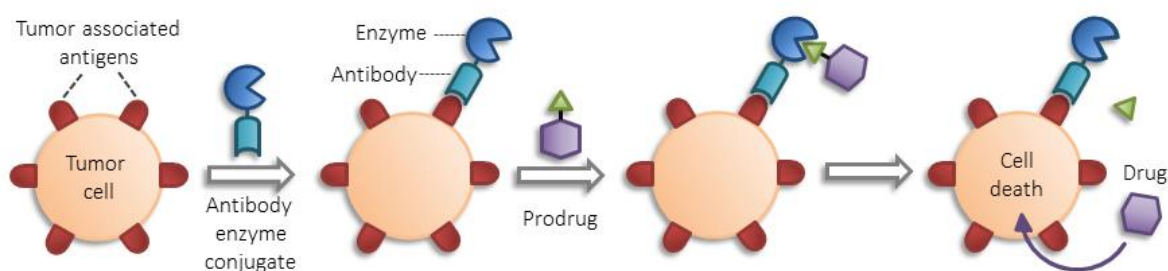
Figure II-4: Schematic representation of antibody-directed enzyme prodrug therapy.

For selective treatments antibody conjugated enzymes are utilized, which recognize and specifically bind tumor associated antigens. After binding, a "nontoxic" prodrug is administered, which is only activated at the antibody enzyme conjugate. The release of the highly cytotoxic drug is therefore limited to the tumor tissue. *Tietze* et al achieved excellent results for ADEPT with duocarmycin prodrug **5** (Figure II-5), as the cytotoxicity of **7** could be reduced from 0.75 nM to 3.6 µM through the incorporation of a galactosidic group at the enaminone oxygen.[67]
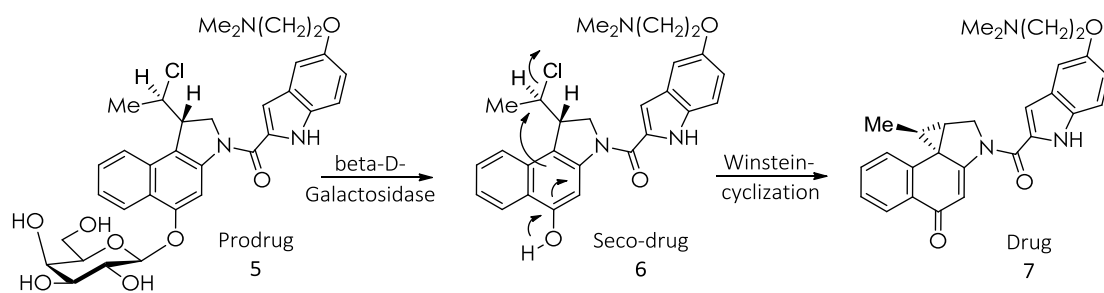
Figure II-5: Activation of the "nontoxic" galactosidic CBI prodrug **5** by β-D-galactosidase in two steps over a Winstein-cyclization of seco-drug **6** to provide the highly cytotoxic duocarmycin analog **7**.

For drug release, a deglycosylation is mediated by β-D-galactosidase, which leads to the corresponding seco-drug **6**. The intermediate **6** is further processed *in situ* by a base catalyzed Winstein-cyclization to afford the highly cytotoxic drug **7**. The driving force which leads to a break of aromaticity is not fully described in literature. Yet intramolecular displacement of the hydrated chloride by the phenolate anion leads to the formation of a highly stabile enaminone.[68-70]

1.3 BIFUNCTIONAL DUOCARMYCIN DERIVATIVES

In 2010, *Tietze* et al. presented a novel class of duocarmycin-related bifunctional derivatives **8a-c** as shown in Figure II-6, which exceeded the potency of duocarmycin SA (**2**) or (+)-CC-1065 (**1**) with IC_{50} values down to 0.11 pM (*in vitro* cytotoxicity, A549 cell line).[71]
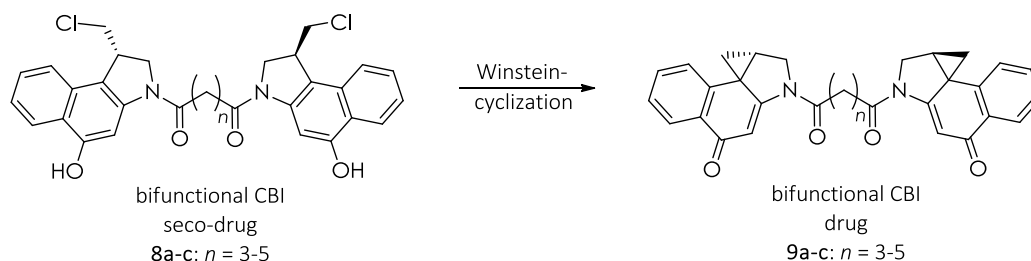
Figure II-6: Winstein-cyclization of bifunctional CBI seco-drugs **8a-c**, yielding bifunctional CBI drugs **9a-c**.

These compounds consist of two CBI alkylation subunits, coupled through a dicarboxylic acid of varying chain lengths, which has a remarkable influence on the biological activity and cytotoxicity. As determined by the human tumor colony forming ability assay (HTCFA) on A549 human bronchial carcinoma cell line, the *in vitro* cytotoxicity of **8a-c** decreases within the sequence *n*=3>5>4 with 9 pM, 1 pM and 0.11 pM.[71] However, the analysis of the reactivity towards double-stranded DNA exhibited 'no indication of a characteristic interaction of the active compounds with the oligodeoxynucleotides'. This caused the hypothesis of DNA as the only target of duocarmycins to be put into question and resulted in the conclusion that 'the cause of the high cytotoxicity is presumably another, as yet unknown mechanism'.[71]

2   RESEARCH APPROACH AND OBJECTIVES

As explained in the last chapter, the reason of the high cytotoxicity of bifunctional duocarmycin derivatives is unlikely attributed solely to DNA alkylation and interstrand cross-linking. One can therefore hypothesize that additional proteinogenic targets may contribute to the potent activity of the duocarmycins. In order to address this question, activity based protein profiling and LC-MS/MS methods have been applied. The isolation and identification of the only prominent protein target of the duocarmycins revealed aldehyde dehydrogenase 1A1 (ALDH1A1) as major hit. With the discovery of this enzyme target further questions evolved, including the biological value and possible drugability of ALDH1A1 and the characteristics of the duocarmycin-enzyme interaction. Further research objectives comprised the identification of the ALDH1A1 binding site via LC-MS/MS, active site point mutation and the elucidation of the precise inhibitory mechanism through crystallization. In addition, time-dependent enzymatic assays, cell imaging and knock-down studies should further clarify the role of ALDH1A1 in the cytotoxicity of duocarmycins and in lung cancer cell proliferation.

3   RESULTS AND DISCUSSION

3.1   IDENTIFICATION OF DUOCARMYCIN PROTEIN TARGETS VIA ABPP

3.1.1   DESIGN OF AN ALKYNYLATED DUOCARMYCIN ABPP-PROBE

One prerequisite for ABPP target discovery is the incorporation of an alkyne handle, which serves for the attachment of an azide-containing reporter tag via click chemistry (Chapter I-4, p. 7). However, the incorporated alkyne should not affect or significantly reduce the biological activity of the ABPP-probe. Amine derivatives of 5-aminoindole DNA-binding subunits as present in **10** (Figure II-7A) are perfectly suited for alkyne incorporation since varying *N*-alkylation showed low effects on biological activity.[65, 72]
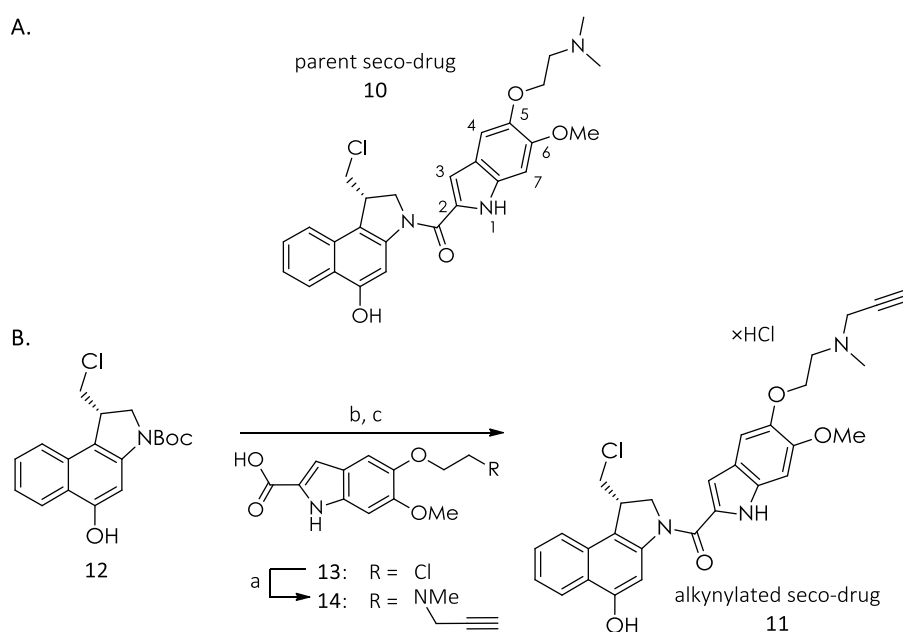
Figure II-7: A. Structure of parental seco-drug **10 B**. Synthetic scheme of the alkyne containing seco-drug **11**. a) N-methylpropargylamine, H_2O, 80 °C, 13.5 h, b) 4 M HCl/EtOAc, 3 h, RT; c) **14**, EDC·HCl, DMF, 13 h, RT.[73]

The synthetic strategy is detailed in Figure II-7B and was carried out by Dr. Kianga Schmuck of the Tietze group at the University of Göttingen. In brief, seco-drug probe **11** was prepared starting from enantiomeric pure Boc-protected seco-CBI **12**.[74, 75] Deprotection of **12** was subsequently followed by an EDC-activated coupling with the alkynylated DNA-binder **14**, obtained through nucleophilic substitution of chloride **13**.[73, 76, 77] A direct comparison of the individual *in vitro* cytotoxicities with the human tumor colony forming ability assay (HTCFA) by Dr. Ingrid Schuberth of the Tietze group at the

University of Göttingen resulted in IC_{50} values with 9 pM and 14 pM for **10** and **11**, respectively.[73] Thus the attached alkyne tag results in no loss of compound potency.

3.1.2 TARGET IDENTIFICATION OF *IN SITU* LABELED A549 LUNG CARCINOMA CELLS

The first *in situ* labelings were conducted with varying amounts of seco-drug **11** in A549 lung cancer cells. The probe was incubated with an adherent culture of A549 cells (70%-80% confluence) in culture medium at 37 °C and 5% CO_2. After labeling, the cells were washed with PBS, trypsinized, resuspended in medium and centrifuged. The pellet was lysed and the soluble and membrane cellular components were separated by ultracentrifugation at 45.000 rpm for 30 min. The membrane fraction was resuspended and the proteomes were treated with rhodamine azide under click chemistry conditions. Relevant control experiments were carried out to verify the labeling of ALDH1A1 by **11** and the results are shown in Figure II-8.
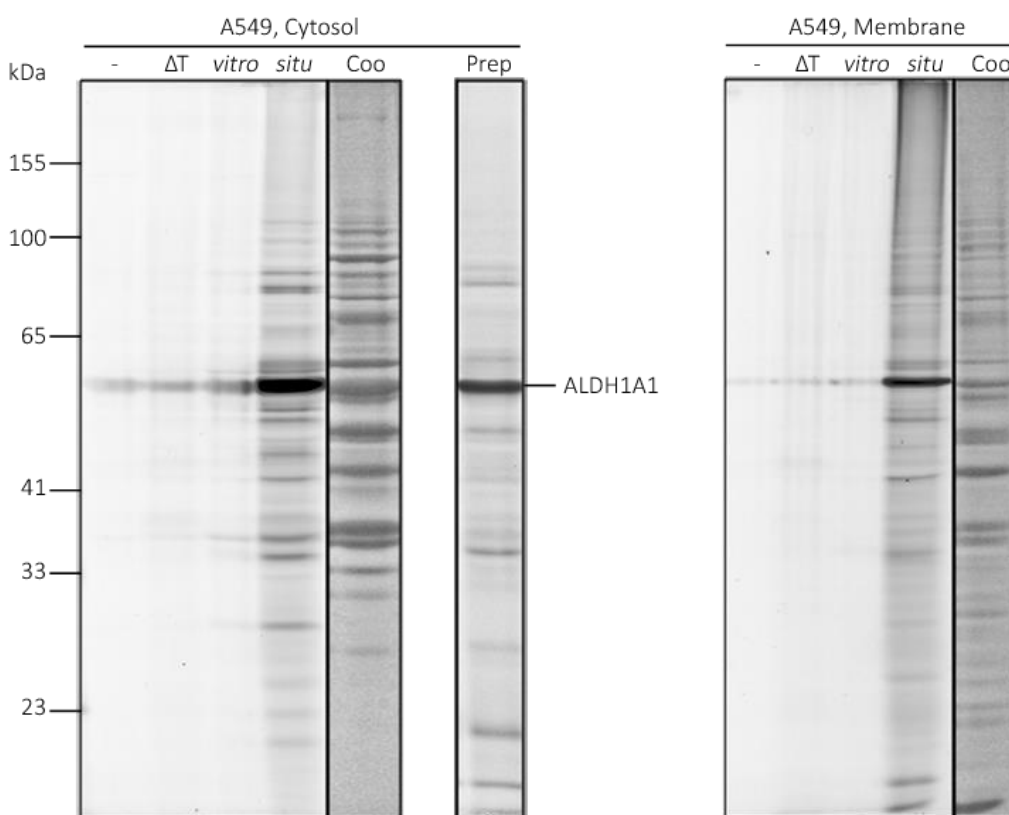
Figure II-8 (previous page): Fluorescent SDS-PAGE analysis of *in situ* labeled A549 cells (= *situ*) compared to *in vitro* labeling (= *vitro*), heat control (= ΔT) and DMSO control (= -). Beside the DMSO control, all labeling experiments were conducted with 20 µM seco-drug **11** for 4 h. A 60 kDa protein band is the only prominent target in living cells. LC-MS/MS analysis of the corresponding preparative labeled band revealed ALDH1A1. (Coo = corresponding coomassie staining, Prep = preparative labeling after enrichment via biotin).

The fluorescent readout of *in situ* labeled living A549 cells (*situ*) reveals one single prominent protein band at a molecular weight of ~60 kDa. Compared to the coomassie staining (Coo) a corresponding band is observed, which indicates the high abundance of the target. Interestingly, this band appears only as a weak signal in cellular lysates (*vitro*) compared to living, intact cells. As the labeling pattern of membrane and cytosol appeared similar, without additional targets in the membrane fraction, Figure II-8 was focused on the cytosol. In addition, further experiments were restricted to the cytosolic or the complete proteome of A549 cells.

In order to identify the targeted protein, the labeling was repeated with **11** (20 µM, 4 h, 37 °C) on a larger scale, using a trifunctional rhodamine-biotin-azide linker that allows the selective enrichment of probe labeled proteins with avidin beads. The following fluorescent SDS-PAGE (Prep) revealed the same strong ~60 kDa band, which was isolated and subject to mass spectrometry (LS-MS/MS). The obtained peptide fragments were analyzed applying the SEQUEST search algorithm and aldehyde dehydrogenase 1A1 (ALDH1A1) was identified as a strong hit (Table II-1).[73]

Table II-1: Target protein identification reveals ALDH1A1 via LC-MS/MS. The table shows Protein ID, molecular weight (MW), the number of replicates conducted (R), the minimal reached p value (Min p value), the maximal reached X-correlation (Max Xcorr) and the number of peptides found (NP) in a single LC-MS/MS run.

Protein	Protein ID	MW	R	Min p value	Max Xcorr	NP
ALDH1A1, Aldehyde dehydrogenase 1A1 or	NP_000680.2	54827.0	1	$2.00 \cdot 10^{-14}$	228.31	23
RALDH1, retinal dehydrogenase 1	"	"	2	$1.00 \cdot 10^{-30}$	356.32	36

To independently confirm the results of the mass spectrometry analysis, commercially available ALDH1A1 (Abcam) was labeled with **11** (1 µM, 4 h, RT). *In vitro* labeled A549 proteome (P) and heat denaturated recombinant ALDH1A1 (=ΔT) served as controls. The results of the fluorescent SDS-PAGE compared with the corresponding coomassie staining is presented in Figure II-9.
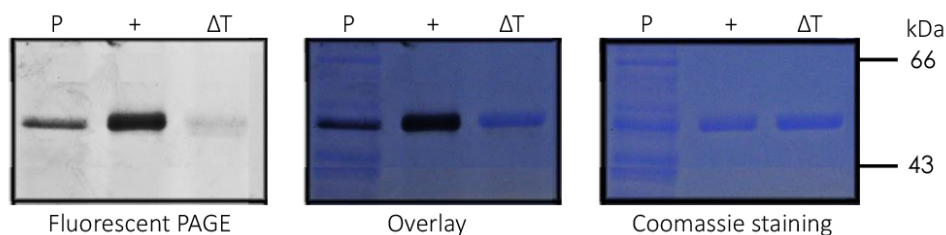
Figure II-9: Recombinant ALDH1A1 (2 µg) is selectively labeled by seco-drug **11** in its native form (P = native proteome, + = recombinant ALDHA1, ΔT = heat denaturated ALDHA1).

The native proteome as well as the recombinant ALDH1A1 both exhibit an intense band at the same height of ~60 kDa, which disappears after heat denaturation. This indicates a specific binding of **11** and provides further evidence for ALDH1A1 as the protein target of **11**.

3.1.3 ALDEHYDE DEHYDROGENASE 1A1

The aldehyde dehydrogenase 1 is a ubiquitous enzyme occurring in diverse tissues, built up by four identical monomers, forming the active state homotetramer. The co-factor NAD$^+$ plays an essential role for enzyme activity, whereas monovalent ions such as K$^+$ represent non-essential activators.[78] ALDH1A1 takes part in the oxidative formation of retinoic acid and thus influences gene expression and differentiation.[79] High expression of ALDH1A1 in malignancies such as pancreatic[80], breast[81] and lung cancers[82] correlates with increased proliferation and results in an aggressive phenotype with poor prognosis. Furthermore, exposure of tobacco smoke leads to an ALDH1A1 upregulation in pneumocytes that may correlate with oncogenesis of lung cells.[83] Besides those crucial effects this enzyme is responsible for the detoxification of cyclophosphamide and other antitumor agents and hence overexpression serves as a protective mechanism in lung cancer cells. [84, 85]

ALDH1A1 exhibits a broad substrate tolerance (retinal, cyclophosphamides, acetaldehyde, cancerogenous aldehydes), which correlates with a diversity of functions, which have probably not all been discovered yet. Moreover, several knockdown studies with ALDH1A1 specific siRNA have shown that this enzyme is important for cell proliferation and survival.[86-88] Therefore, selective inhibition of ALDH1A1 by duocarmycin analogs such as **10** and **11** may represent an additional route by which these molecules exhibit their activity. Moreover, this might be the preferred mode of action for the dimeric seco-drugs **8a-c** lacking the DNA-binding subunit.

3.1.4   EVALUATING THE SELECTIVITY OF SECO-DRUG 11 TOWARDS ALDH1A1

To assess the selectivity of **11** towards ALDH1A1, serial dilutions were conducted and incubated with intact A549 cells for 4 h. The result of the fluorescent SDS-PAGE is presented in Figure II-10, which exhibits visible labeling down to a concentration of 100 nM.

	ΔT	vitro		situ		
c [µM]	20	20	1	0.5	0.2	0.1
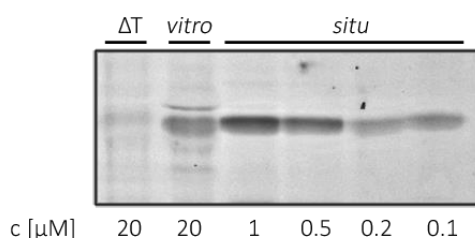
Figure II-10: *In situ* dose down of seco-drug **11** in A549 cells (*situ*) and comparison to *in vitro* labeled (*vitro*) and heat denatured proteome (ΔT).

Furthermore ALDH1A1 is the only detectable target at a concentration below 1 µM, emphasizing a specific protein recognition and high affinity binding. Compared to the *in situ* labeling, a 40- to 100-fold excess of **11** is necessary in *in vitro* experiments for achieving an equal band intensity, which indicates a significant inactivation of ALDH1A1 after cell rupture. This emphasizes the value of *in situ* over *in vitro* in biological studies.

3.1.5   VERIFICATION OF ALDH1A1 AS TARGET OF BIFUNCTIONAL SECO-DRUG 8B

As **8a-c** lack a DNA binding motif, ALDH1A1 inhibition might be the preferred mode of action concerning these bifunctional compounds. Out of these three compounds, **8b** is the most potent (Chapter II-1.3, p 14) and was therefore chosen to verify ALDH1A1 binding. A competitive labeling of recombinant ALDH1A1 was conducted with bifunctional **8b** versus alkynylated seco-drug **11**. Prior to labeling with **11**, ALDH1A1 was pre-incubated with either DMSO or a 10- to 40-fold excess of **8b**. The fluorescent SDS-PAGE of the competitive labeling is shown in Figure II-11.
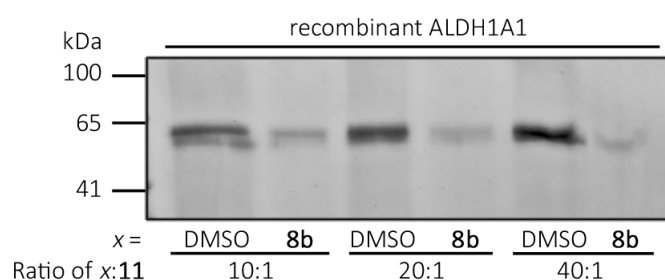
Figure II-11: Competitive labeling of recombinant ALDH1A1 by seco-drug probe **11** and a 10- to 40-fold excess of dimeric seco-drug **8b**.

A 10-fold excess of **8b** is sufficient to significantly decrease the signal intensity compared to the DMSO control. This indicates that bifunctional seco-drug **8b** covalently binds ALDH1A1 in a strong and irreversible manner and competes for the same binding site as probe **11**.

3.2   IDENTIFICATION AND VERIFICATION OF THE DUOCARMYCIN BINDING SITE

3.2.1   BINDING SITE IDENTIFICATION

To investigate the ALDH1A1 binding site of **11**, recombinant ALDH1A1 (Abcam) was covalently labeled with **11** (10 µM, 4 h, RT), digested with chymotrypsin, desalted and analyzed by LC-MS/MS. A search for cysteines bearing an modification with the molecular mass of **11**, resulted in the identification of two different peptide fragments. The fragmentation and the peptide sequence are shown in Figure II-12 and Table II-2 (p. 22), with ^ indicating a modification by **11**.
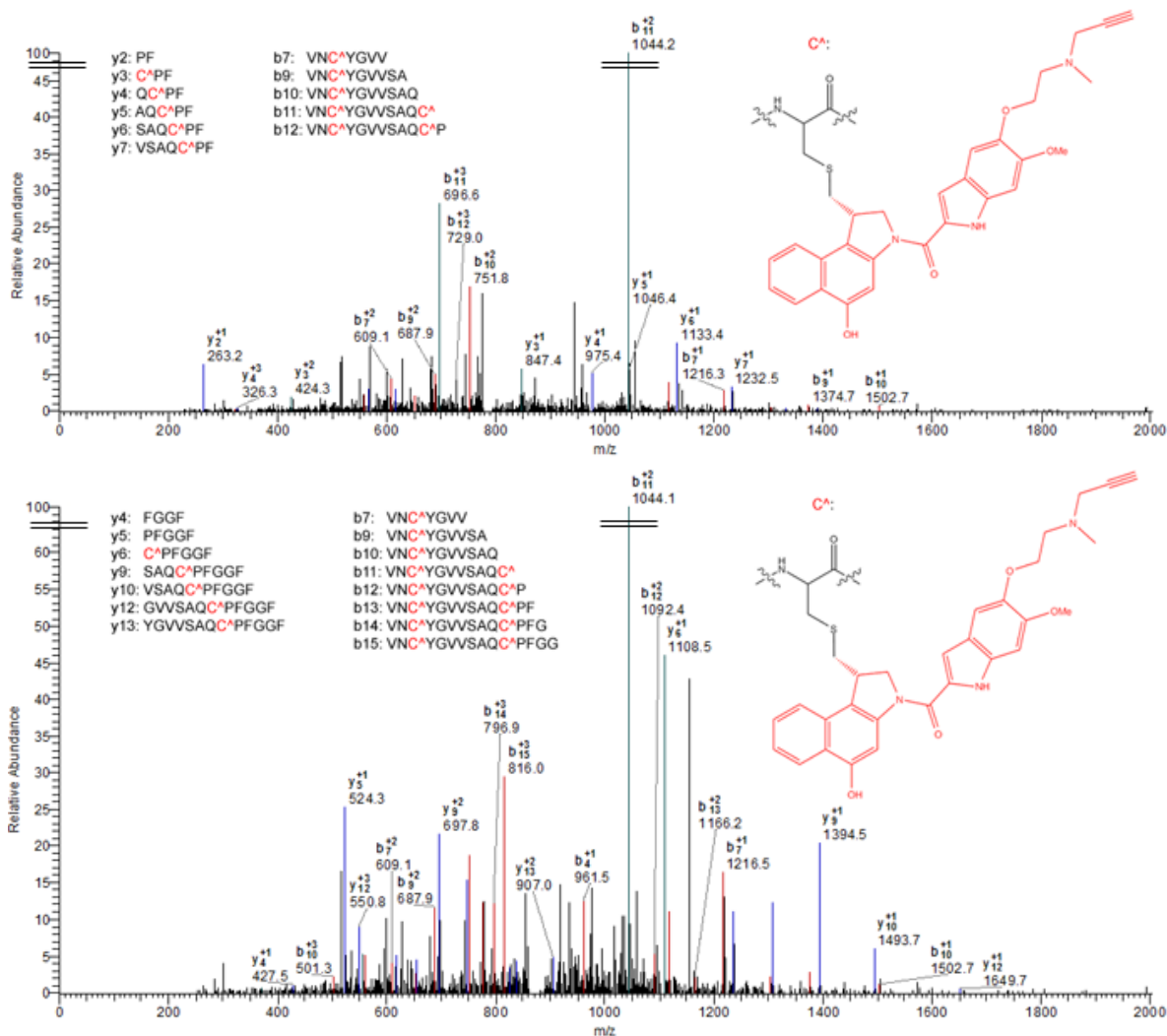
Figure II-12: MS/MS sequencing data reveals the binding of seco-drug **11** to Cys456 and Cys464 for two different peptide fragments.[73]

Table II-2: Peptides identified by mass spectrometry containing modified cysteine residues C^ (highlighted in red). The table shows the fragment ion mass (MH⁺), the fragment ion charge (z), the minimal reached p value (Min p value) and the maximal reached X-correlation (Max Xcorr).

Peptide	MH⁺	z	Min p value	Max Xcorr
VNC^YGVVSAQC^PF	2349.0	3	$2.40 \cdot 10^{-4}$	2.99
VNC^YGVVSAQC^PFGGF	2610.1	3	$4.38 \cdot 10^{-6}$	3.92

Each fragment exhibits two probe bound cysteine residues: 456 and 464, indicating that two molecules **11** bind per enzyme subunit. Previous crystallographic data[89, 90] shows that Cys456 and Cys464 are located close to the C-terminus of ALDH1A1 and in a

proximal range to the enzyme active site, Cys303, which was not observed to be alkylated.[73]

3.2.2 BINDING SITE VERIFICATION VIA POINT MUTATION

For verifying the determined duocarmycin binding sites, point mutations were introduced via site-directed mutagenesis. For this purpose, cysteines 456 and 464 were specifically exchanged for alanine residues, as alanine represents the closest structural analogue without thiol group. Special mismatching sense and antisense primers were designed for every binding site cysteine, containing a codon change to alanine. These mismatching primers were then applied in a polymerase chain reaction (PCR), for inserting the corresponding mutation into the wild type ALDH1A1 cDNA (Gene Copoeia). The mutant cDNA was further cloned into a pDEST 007 expression vector using the Gateway recombination cloning technology (Invitrogen). Subsequent heat shock transformation into *E. coli* BL21 and overexpression resulted in two single (C456A and C464A) and one double point mutated (C456A+C464A) versions of ALDH1A1. To evaluate the accessibility towards duocarmycin binding, *E. coli* BL21 lysates containing the different overexpressed mutants were labeled with seco-drug **11** (1 μM, 3 h, RT) and compared to recombinant wild type ALDH1A1 (Figure II-13A).
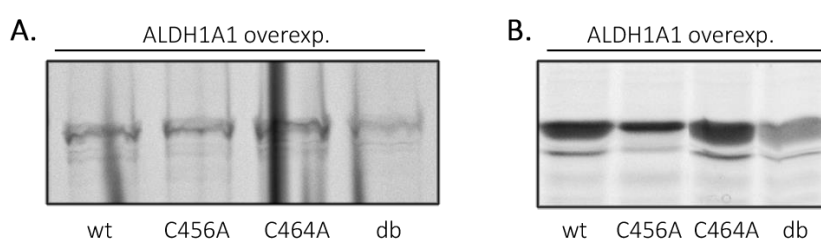
Figure II-13: Labeling of overexpressed ALDH1A1 wild type (wt), single mutants C456A and C464A and the double mutant C456A+C464A (db) with **A.** 1 μM **11** for 3 h and **B.** 40 μM seco-drug **11**, 15 h. The wild type and single mutant ALDH1A1 exhibit similar signal intensities, while the double mutant is significantly reduced.

Since the resulting fluorescent PAGE exhibits only weak labeling intensity, the experiment was repeated with an extended incubation time of 15 h and an increased concentration of 40 μM, as presented in Figure II-13B. Within both labeling experiments,

the wild type and both single mutants exhibit comparable band intensities, which indicates an equal binding to both identified cysteine residues by seco-drug **11**. In contrast, the intensity of the double mutant is significantly decreased, whereas minor labeling was always observed. This suggests either unspecific labeling due to a high excess of unreacted probe, or the existence of a so-far overlooked third binding site of seco-drug **11**. However, the latter explanation seems unlikely, due to the significant signal drop.

3.2.3 BINDING SITE OF BIFUNCTIONAL DUOCARMYCIN DERIVATIVES - THE HYPOTHESIS OF CYSTEINE 456 AND 464 CROSSLINKING

As previously shown in Chapter II-3.1.5 (p. 21) and Figure II-11, pre-incubation of ALDH1A1 with bifunctional seco-drug **8b** and subsequent addition of probe **11** abolished labeling, suggesting that both compounds compete for the same binding site. A look at the crystal structure of the sheep ALDH1A1 homotetramer[90], as presented in Figure II-14, reveals a distance of 10.4 Å (red) between the cysteines 456 and 464 (yellow).
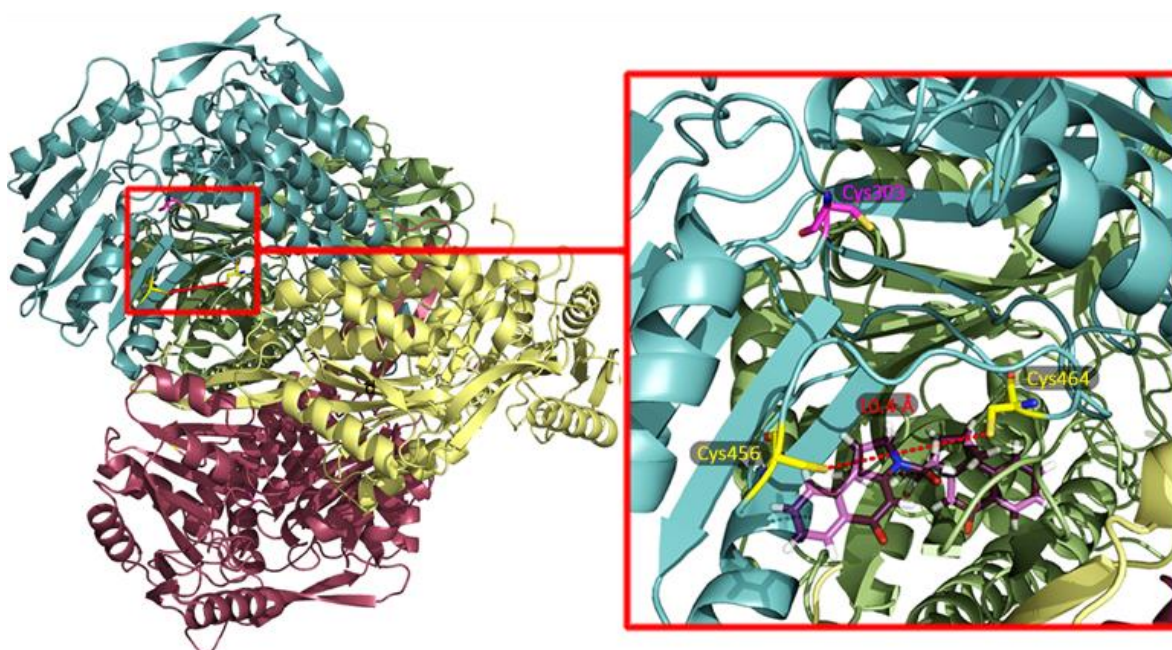
Figure II-14: Crystal structure of the sheep liver cytosolic ALDH1A1 homotetramer.[90] The catalytic active cysteine 303 (pink) of one monomer is enlarged. The nearby cysteines 456 and 464 (yellow) show a suitable distance (red) of 10.4 Å for a modification by the bifunctional drug **9b** (purple).[73]

Both are further in a proximal range to the enzyme active site cysteine 303 (pink). As the sequence identity of sheep and human ALDH1A1 is approximatly 91%, it is assumed that both enzymes virtually share an identical structure.[91] Thus, the distances of the active site environment of sheep ALDH1A1 should also apply for the human homologue. To assess the possibility of a bridging event whereby one molecule of seco-drug **8b** reacts with both binding cysteines, the structure of the corresponding drug **9b** (purple) was theoretically calculated and refined with Coot[92] by Dr. Sabine Schneider at the Technische Universität München. The theoretical structure was further superimposed onto the sheep crystal structure, using PyMOL.[93] This revealed a distance between cysteines 456 and 464 suitable to allow reaction with both cyclopropyl moieties of **9b**. In addition, the *in vitro* cytotoxicities of **8a**-**c** decrease with an increasing spacer length of *n*=3>5>4 = **8a**>**c**>**b** (Chapter II-1.3, p. 14), which indicates a less effective binding.[71] This fact supports the hypothesis of a crosslinking event by **8b**. Yet, the hypothesis could not be proved by mass spectrometry, since the modified peptide was not detected. Despite varying digestion methods, such as enzymatic digest with trypsin or chymotrypsin and chemical digest with cyanogen bromide, a modified peptide with improved ionization properties could not be obtained. Further mass experiments, analyzing the modified full-length enzyme with MALDI and LTQ-FT lead to no results either. Apparently, co-crystallization of bifunctional CBI-drug **9b** with human ALDH1A1 is the most promising method to prove the hypothesis and to clarify the mechanism of inhibition.

3.3   CRYSTALLIZATION OF HUMAN ALDH1A1

For determining a crystal structure, the electron density map has to be obtained from X-ray diffraction experiments. These experiments enable the direct observation of X-ray amplitudes but not their phase. However, to reconstruct the electron-density distribution from the diffraction pattern, the phase angle of the scattered waves has to be known. For macromolecular crystals this is known as the Phase Problem and can be solved by isomorphous replacement (introduction of heavy atoms), anomalous scattering (e.g. substitution of methionine with selenomethionine) or molecular replacement (using related solved structures as model).[94]

Concerning the human ALDH1A1, the closely related sheep crystal structure provides an excellent model for calculating the electron density map via molecular replacement, without the need of further protein modification.
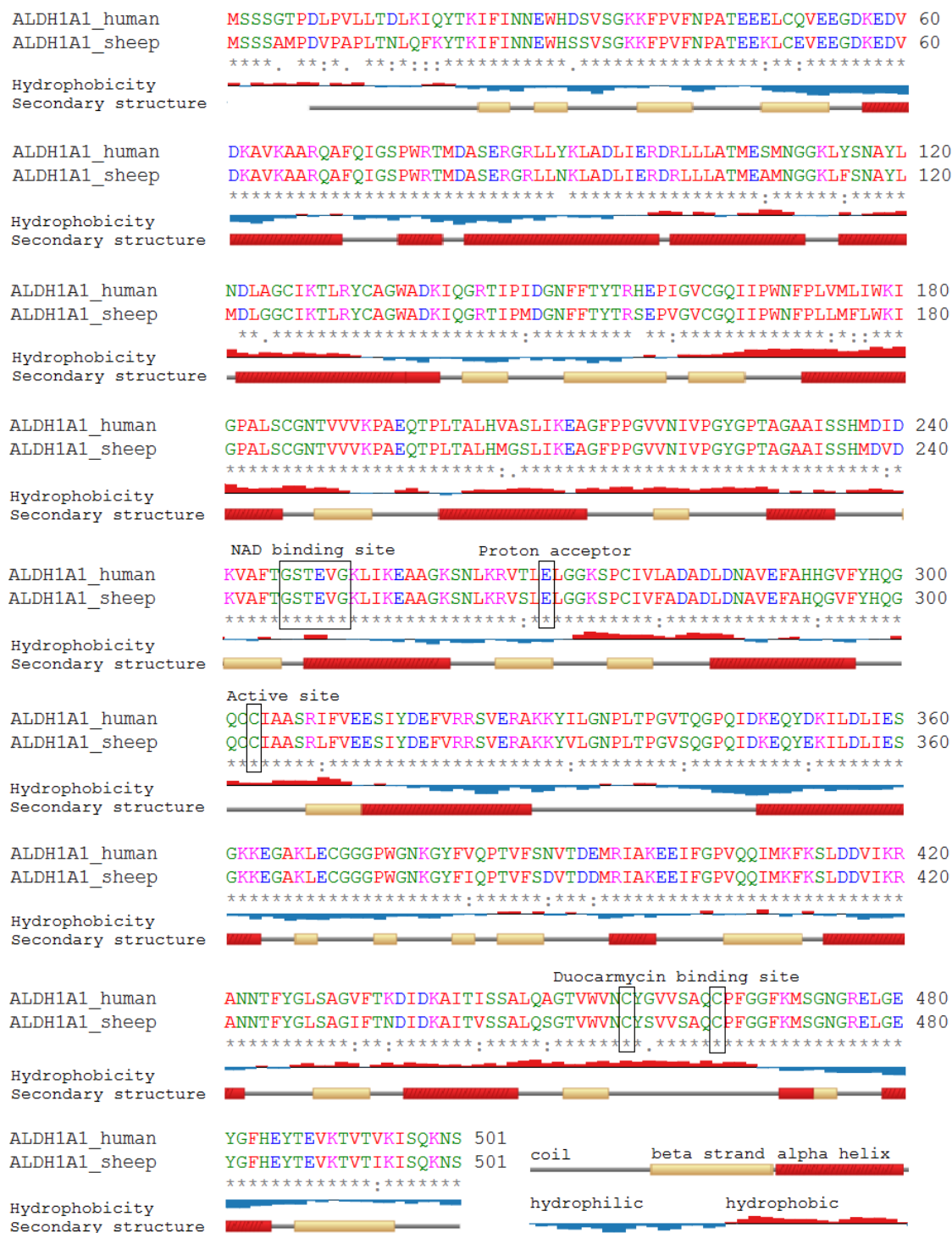
Figure II-15: ClustalW2.1[95, 96] multiple sequence alignment of human and sheep ALDH1A1, Score= 91.0% (* fully conserved, : strongly similar properties, . weakly similar properties, red: small AAs, blue= acidic AAs, pink= basic AAs, green= hydroxyl + sulfhydryl + amine + G). The hydrophobicity and the secondary structure data of sheep ALDH1A1 were taken from the RSCB Protein Date Bank (PDB).[97]

26

A comparison of human and sheep ALDH1A1 is presented in Figure II-15 (p. 26) by a ClustalW2.1 multiple sequence alignment, which exhibits a high conservation with a score of 91.0%. In addition important sites including the duocarmycin binding site remain unchanged.

Initial high-throughput crystallization screening was carried out for ALDH1A1-Strep with the sitting-drop vapor diffusion method in 96-well microlike plates, as described in Chapter V-2.4.1 (p. 97). Conditions from 10 commercially available crystallization screening suits were tested at varying protein concentrations, drop ratios (protein:reservoir) as well as incubation temperatures. Crystals were obtained at 4 °C with 0.2 M sodium formate, 0.1 M bis-tris propane (pH 8.5) and 20% PEG 3350 and could be reproduced in a manual grid screen around the initial hit conditions (Figure II-16A).
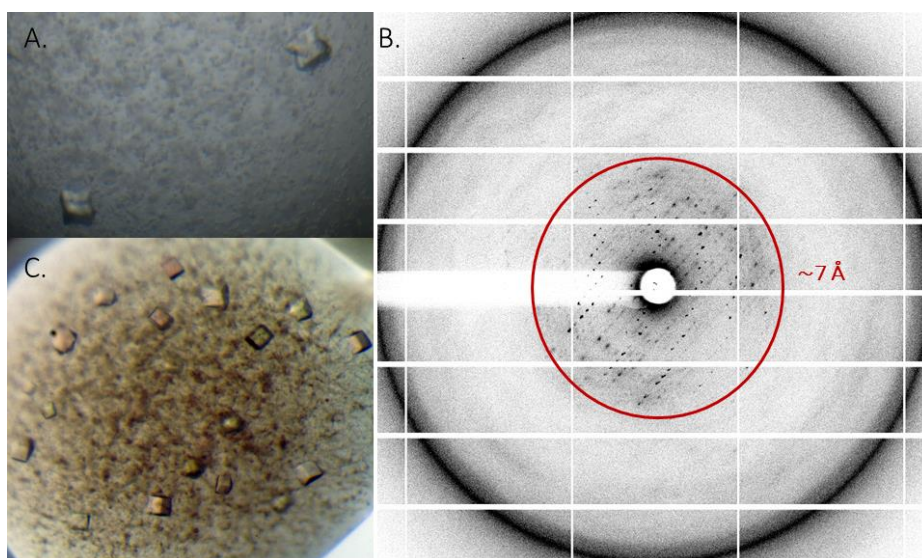
Figure II-16: A. Crystals of recombinant human ALDH1A1 containing Strep-Tag / *att*B site grown at 4°C with 5-10 μg/μL ALDH1A1-Strep, 0.1-0.2 M sodium formate, 0.1 M bis-tris propane (pH 8.5) and 18-21% PEG 3350. **B.** Diffraction pattern of one crystal of A with a limited resolution to ～7 Å. **C.** Crystals of human wild type ALDH1A1 grown at 4 °C with 5-10 μg/μL ALDH1A1, 0.3 M NaCl, 0.1 M CHES (pH 9.5) and 16% PEG 8000.

Despite the sufficient size and the clean shape, the crystals only diffracted X-ray to about 7 Å, which could not be improved (Figure II-16B). This indicates loose crystal packing, which might be caused by the long unnatural N-terminal chain bearing the Strep-tag connected to an *att*B site, a remnant of the cloning methodology. Thus, to obtain the wild type ALDH1A1, a TEV restriction site (Tobacco Etch Virus) was introduced between

the Strep-tag / *att*B site and the open reading frame (ORF). After a strep purification, the enzyme was completely digested with the TEV protease over night at 4 °C and separated via gel filtration the next day. Initial high-throughput crystallization screening was carried out for wild type ALDH1A1 as described above. Crystals were obtained in a number of conditions in the presence of PEG at 4 °C and 20 °C and could be reproduced in a manual grid screen around the initial hit conditions (Figure II-16B). However, the diffraction resolution was not increased with wild type ALDH1A1. In order to improve the diffraction resolution, crystal dehydration[98-101], different cryobuffers as well as additives were trailed but were unsuccessful (Chapter V-2.4.3, p. 100).

Despite the low resolution of about 7 Å, the crystal lattice packing of human ALDH1A1 was analyzed using the coordinates of sheep ALDH1A1[90] as a model. Data processing yielded the tetragonal space group *P*222. The structure is presented in Figure II-17 in comparison to the sheep homologue.
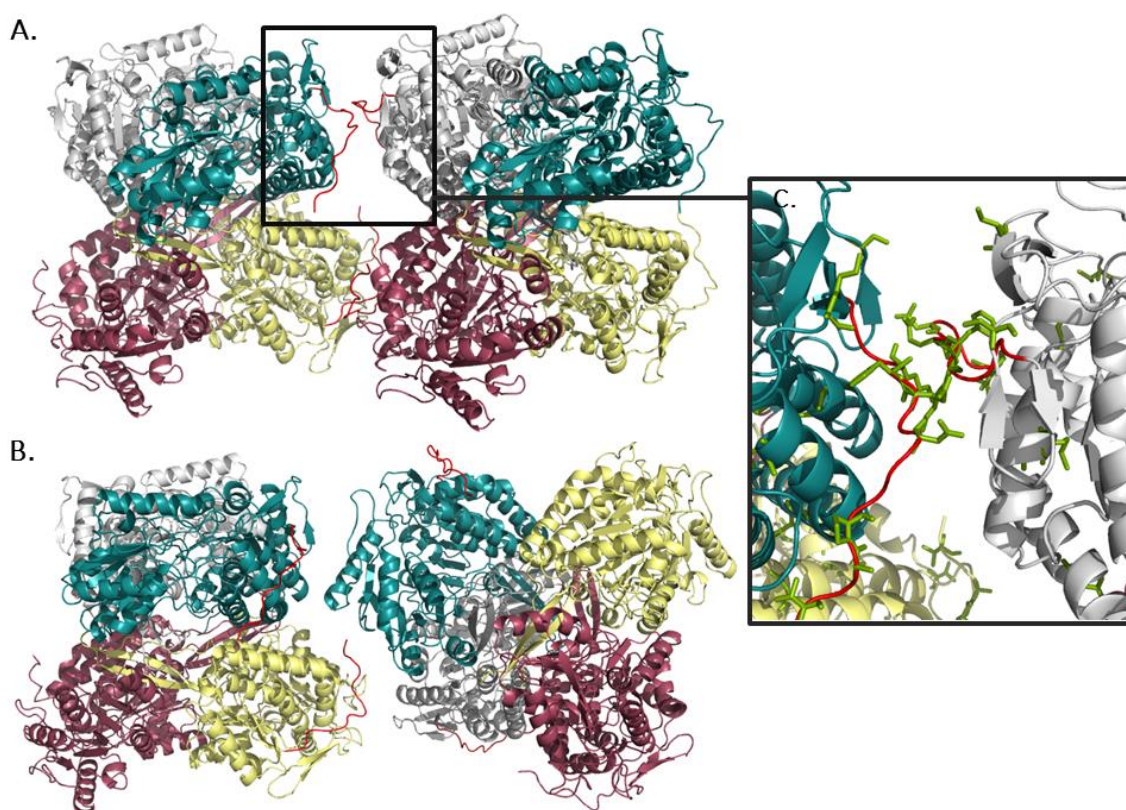
Figure II-17: A. Triclinic crystal structure of sheep ALDH1A1.[90] **B.** Tetragonal crystal structure of human (wild type) ALDH1A1 (resolution ～7 Å). **C.** Crystal lattice contacts of sheep ALDH1A1 (red= N-terminal coil, green= sequence differences of human homologue).

Data collection and processing was conducted by Dr. Sabine Schneider at the Technische Universität München. In the published triclinic sheep crystal structure the asymmetric unit contains the entire tetrameric ALDH1A1 (Figure II-17A), with crystal contacts involving parts of the N-terminal coil (residues 15-22). In contrast the asymmetric unit of the tetragonal human homologue contains one monomer, while the tetramer is completed by the crystal symmetry. Despite the high sequence identity of human and sheep ALDH1A1 (91.0%), different crystal lattice contacts can be seen in Figure II-17B. A look at the sequence differences reveals, that most differences occur in the N-terminal coil (Figure II-15, Figure II-17C), which might explain the loose crystal packing and the altered crystal symmetry in comparison to the sheep homologue.

Despite the low resolution of human ALDH1A1 crystals, a co-crystallization of the closely related sheep homologue with **9b** is a promising strategy to clarify the interaction of bifunctional duocarmycins with ALDH1A1. Thus, a sheep *ALDH1A1* construct, containing a TEV-restriction site, was already designed and cloned into expression-ready *E. coli* (Chapter V-3.2.4, p. 108). However, initial crystallization screens have to be conducted.

3.4   CLARIFYING THE ROLE OF ALDH1A1 IN DUOCARMYCIN CYTOTOXICITY

3.4.1   INHIBITION STUDIES OF ALDH1A1

To evaluate the inhibitory effect of duocarmycins on ALDH1A1 activity, an aldehyde dehydrogenase activity assay was conducted according to published procedures.[85, 86, 88, 102] Enzyme inactivation can be described according to the following scheme:

$$[E] + [I] \; \underset{}{\overset{K_I}{\rightleftharpoons}} \; [E \cdot I] \; \overset{k_{inact}}{\longrightarrow} \; [E-I]$$
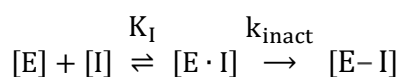
In case of reversible inhibition, the inhibitor $[I]$ forms a non-covalent inhibitor-enzyme complex $[E \cdot I]$ with free enzyme $[E]$ until equilibrium is achieved. In contrast, irreversible inhibitors, such as the duocarmycins, further transform the non-covalent complex $[E \cdot I]$ into an irreversibly inactivated form $[E-I]$ until completion.[103, 104] There are therefore two parameters which govern an irreversible inhibitor: the equilibrium disassociation constant K_I and the rate constant for irreversible inactivation k_{inact}. Despite the

mechanistic interpretation, K_I can be defined as inhibitor concentration that produces the half-maximal rate of inactivation, whereas the maximal rate of inactivation is defined by the product of the active enzyme concentration and k_{inact}.[103, 104] Both parameters can be determined in a time depended activity assay according to the method of Kitz and Wilson, which is based on equations (I-V).[105-107] The overall concentration of enzyme $[E]_0$ is composed of the sum of free enzyme $[E]$, inhibitor-enzyme complex $[E·I]$ and irreversibly inactivated enzyme $[E-I]$ (equations (I)):

$$[E]_0 = [E] + [E \cdot I] + [E- I] = [E]_A + [E- I] \tag{I}$$

As an excess of substrate results in a release of reversible bound inhibitor from the inhibitor-enzyme complex $[E·I]$, the active enzyme $[E]_A$ is defined as sum of free enzyme $[E]$ and $[E·I]$. The increase of irreversibly inactivated enzyme $[E-I]$ is described by equation (II), which corresponds to the decrease of $[E]_A$ with the assumption of $[E]_0 = $ constant and $[I] >> [E]$ (reaction of pseudo first order):

$$\frac{d[E- I]}{dt} = k_{inact} \times [E \cdot I] = - \frac{d[E]_A}{dt} \tag{II}$$

$$- \frac{d[E]_A}{dt} = k_{inact} \times \frac{[E]_A}{1 + \frac{K_I}{[I]}} \qquad \text{with (I) and } K_I = \frac{[E] \times [I]}{[E \cdot I]} \tag{III}$$

Integration of equation (III) results in equation (IV):

$$ln \frac{[E]_A}{[E]_0} = - \frac{k_{inact} \times t}{1 + \frac{K_I}{[I]}} = -k_{obs} \times t = ln\, A_R \tag{IV}$$

$[E]_A/[E]_0$ is determined by measuring the relative enzyme activity A_R for several inhibitor concentrations $[I]$ and time points t. The rate of enzyme inactivation at a given inhibitor concentration is referred to the apparent inactivation rate k_{obs}.[103, 105, 107] It can be derived from the slope by plotting the rate of enzyme inactivation against the time. As k_{obs} is depending on $[I]$, K_I and k_{inact}, equation (IV) can be linearized to obtain K_I and k_{inact} as presented in equation (V):

$$\frac{1}{k_{obs}} = \frac{K_I}{k_{inact} \times [I]} + \frac{1}{k_{inact}} \qquad\qquad\qquad (V)$$

$$\triangleq \quad y = ax + t \qquad\qquad \text{with } y = \frac{1}{k_{obs}}; x = \frac{1}{[I]}; a = \frac{K_I}{k_{inact}} \text{ and } t = \frac{1}{k_{inact}}$$

Thus plotting $1/k_{obs}$ against $1/[I]$ results in a linear curve with a slope of K_I/k_{inact} and an intercept of $1/k_{inact}$.[103, 105-107]

To determine the rate of ALDH1A1 inactivation for duocarmycins, a time depended activity assay was conducted. In an initial study, the enzyme activity in presence of inhibitor A_{EI*} was measured for purchased recombinant ALDH1A1 (ProSpec) using retinal as a substrate. In the assay, a complete conversion of seco-drugs **8b** and **11** into the corresponding active drugs was ensured by pre-incubating **8b** and **11** for 2 h at RT in reaction buffer (50 mM Tris-HCl, pH 8.5). Analysis via LC/MS revealed an approximate transformation of 100% and 85% for **8b** and **11**, respectively. After pre-incubation the activated drugs were added to the enzyme at various concentrations and incubated for different periods of time at RT. In Figure II-18 a sigmoidal plot of A_R against [I] is presented for several time points.
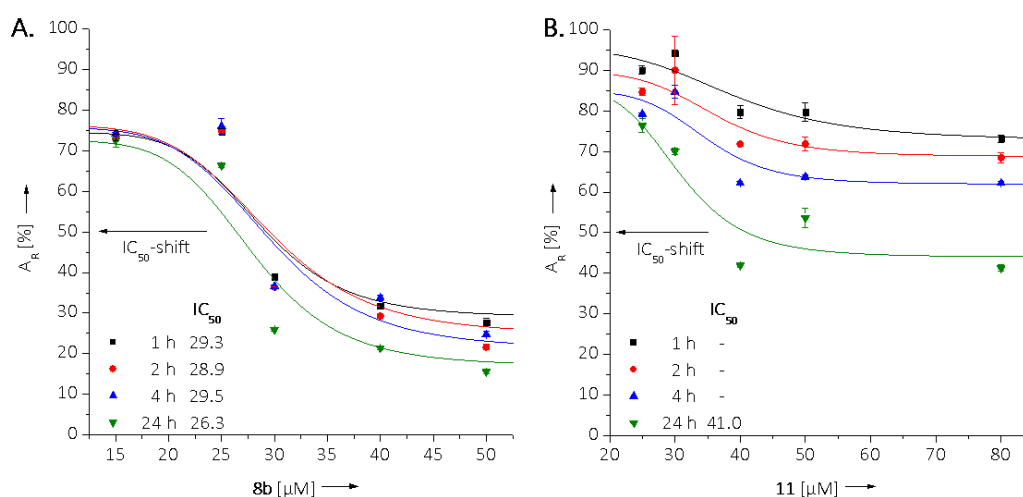
Figure II-18: Inactivation plots of **8b** and **11** with purchased recombinant ALDH1A1 (ProSpec), measured with retinal as substrate. **A.** Time-dependent IC_{50} shift of **8b**. **B.** Time-dependent IC_{50} shift of **11**.[73]

The sigmoidal plot of A_R against **8b** and **11** reveals a time-dependent inhibition for both compounds. In contrast to reversible inhibitors this plot exhibits an IC_{50} shift to lower

concentrations for increasing incubation time. This emphasizes the inadequacy of the description of irreversible inhibitors with single IC_{50} values at one time point. Regarding the velocity of inactivation, **8b** reveals a faster inhibition than **11** (Figure II-18). After 24 h of pre-incubation, seco-drug **11** barely achieves the half maximal enzyme inhibition with an apparent IC_{50} of 41.0 µM (Figure II-18B). In contrast, the recombinant ALDH1A1 exhibits already a strong inhibition after 1 h of incubation with seco-drug **8b**, which is further increased after 24 h with an apparent IC_{50} of 26.3 µM (Figure II-18A).

However, purchased recombinant ALDH1A1 may not exhibit its full catalytic power and binding affinity outside its natural environment (Chapter II-3.1.4, p. 20) in addition to partial degradation and inactivation by freezing and thawing. Thus A549 lung cancer cell lysates were directly incubated with **8b** and **11** at various concentrations and A_R was monitored by the measurement of propanal turnover (Figure II-19A and Figure II-20A, p. 33).
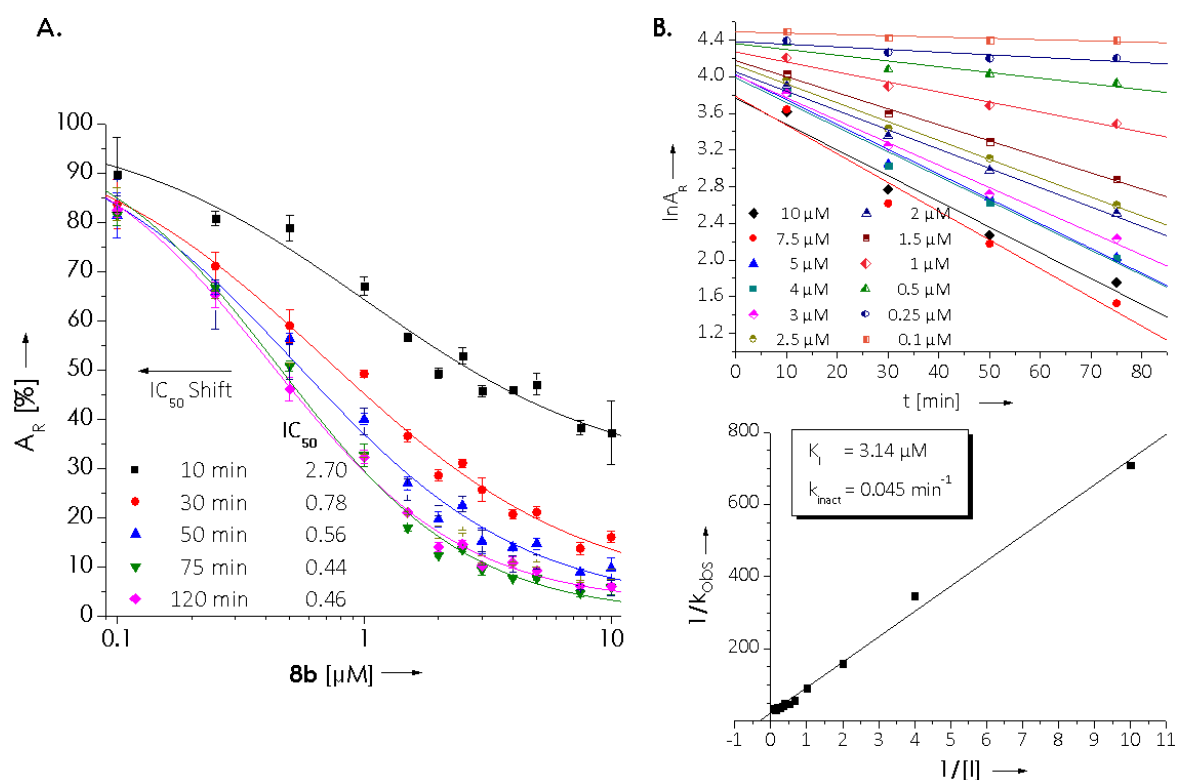
Figure II-19: Inactivation plots of **8b** measured with propanal in A549 lysates. **A.** Time-dependent IC_{50} shift. **B.** Plots of **equation** (II) to determine k_{obs} and **equation** (III) to determine k_{inact} and K_I.[73]
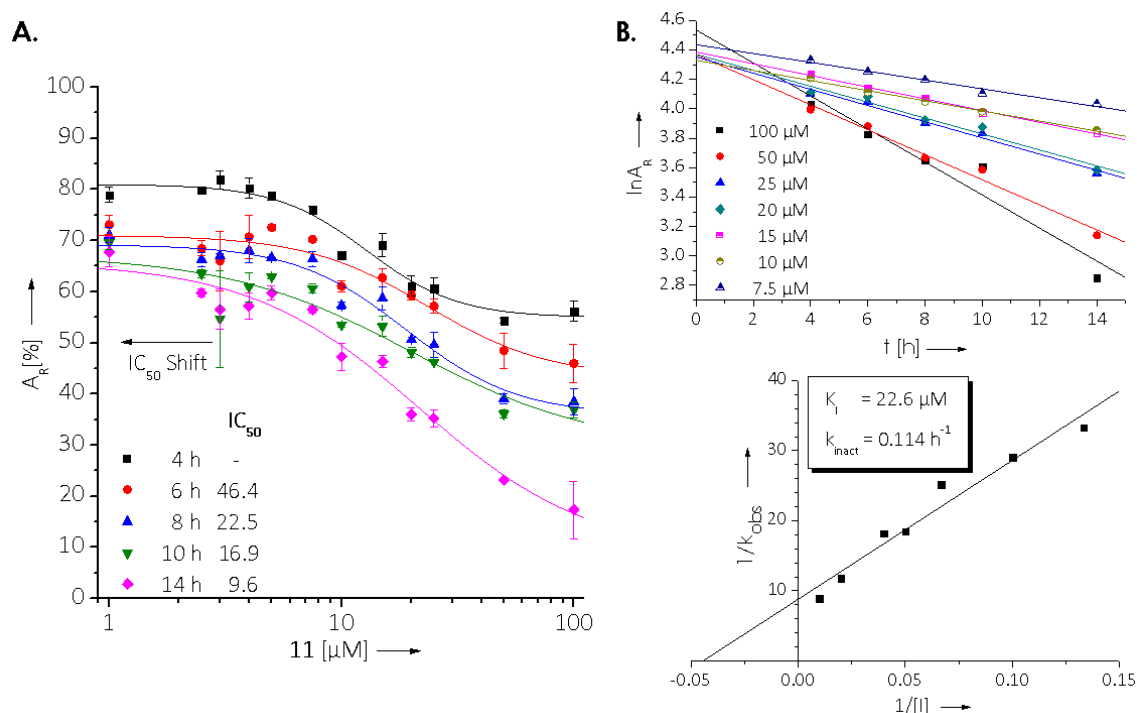
Figure II-20: Inactivation plots of **11** measured with propanal in A549 lysates. **A.** Time-dependent IC_{50} shift. **B.** Plots of **equation** (II) to determine k_{obs} and **equation** (III) to determine k_{inact} and K_I.[73]

Compared to the recombinant enzyme, inactivation of ALDH1A1 in its native environment with **8b** and **11** occurs at an obviously higher velocity, since first apparent IC_{50} values can be obtained after 10 min and 6 h, respectively. Over time the apparent IC_{50} values further decrease to 0.44 µM (75 min =1.25 h) and 9.6 µM (14 h) for **8b** and **11**, respectively. Thus in comparison to the monofunctional seco-drug **11**, the bifunctional seco-drug **8b** reveals an approximately 11 times faster inhibition of ALDH1A1 with an inhibitor concentration of 1/22 in relation to **11**. This pronounced difference is in line with the suggested binding mode (Chapter II-3.2.3, p. 24) and further supports that crosslinking of the cysteines 456 and 464 by the bifunctional compound leads to a faster and more efficient inhibition of substrate turnover. This binding mode is not only preferred for entropic reasons but also represents an optimal probe-enzyme alignment.

In Figure II-19B and Figure II-20B, (pp. 32/33) the kinetic parameters of inactivation K_I and k_{inact} were determined according to equations (IV) and (V). To determine k_{obs} (equation (IV)) a plot of the natural logarithm of the relative enzyme activity A_R was plotted against the incubation time t for several inhibitor concentrations. The apparent rate of inactivation k_{obs} was then derived from the negative slopes of the linear fits in

Figure **II-19**B and Figure II-20B. A further double reciprocal plot of k_{obs} against the inhibitor concentration $[I]$ (equation (V)) gave K_I and k_{inact}. The resulting kinetic parameters are K_I = 3.14 µM and k_{inact} = 0.045 min^{-1} = 2.7 h^{-1} for the bifunctional seco-drug **8b** and K_I = 22.6 µM and k_{inact} = 0.114 h^{-1} for the monomeric seco-drug **11**. As a result, the maximal rate of enzyme inactivation of **8b** is higher and achieved at lower probe concentration compared to **11**.

As all calculated parameters and the apparent IC$_{50}$ values are depending on the enzyme concentration applied in the activity assay, the ALDH1A1 concentration was estimated to determine independent molecular ratios as described in Chapter V-2.3.2 (p. 96). The volume of lysate applied in the activity assay corresponds to 5.3 pmol or 106 nM of ALDH1A1 (in 50 µL). Compared to the obtained IC$_{50}$ values for **8b** of 0.44 µM (1.25 h) and **11** of 9.6 µM (14 h), only 4.2 molecules of **8b** per molecule of ALDH1A1 are already sufficient to inhibit 50% of the enzyme activity. In contrast, a high excess of 90.6 molecules of **11** over enzyme is needed to achieve the same effect.

A direct ALDH1A1 inhibition with both compounds in living A549 cells failed since immediate apoptosis and loss of activity within the duration of the assay was observed. Therefore, it is difficult to compare *in vitro* enzyme inhibition data with cell toxicity (HTCFA). However, a time-dependent Aldefluor assay[108, 109], which allows determining the intracellular aldehyde dehydrogenase activity by FACS analysis, could provide a direct link.

3.4.2 CHARACTERISTICS OF THE DUOCARMYCIN DNA-BINDING SUBUNIT

As already described the duocarmycins consist of two main elements (Figure II-2A, p. 11), a DNA-binding and an alkylation subunit. Several studies revealed the importance of the DNA-binding subunit for DNA alkylation, by replacement for different heteroaromatic cycles and short residues. *Boger* et al.[110] analyzed the effect on DNA alkylation and cytotoxicity for various dimeric mono-, bi- and tricyclic heteroaromatic substitutions of the DNA-binding subunit of CBI analogues, e.g. compounds **15a-d** as illustrated in Figure II-21A (p. 35).

A.

15a: monocyclic IC$_{50}$ >10000 pM

15b: monocyclic IC$_{50}$ 400 pM

15c: bicyclic IC$_{50}$ 19 pM

15d: tricyclic IC$_{50}$ 5 pM

B.

16a-f

	R	IC$_{50}$
a:	H	nd
b:	SO$_2$Et	24 nM
c:	OtBu	80 nM
d:	COEt	110 nM
e:	CO$_2$Me	140 nM
f:	CONHMe	200 nM

C.

17a: CPI-Ac   **17b:** CPI-Boc
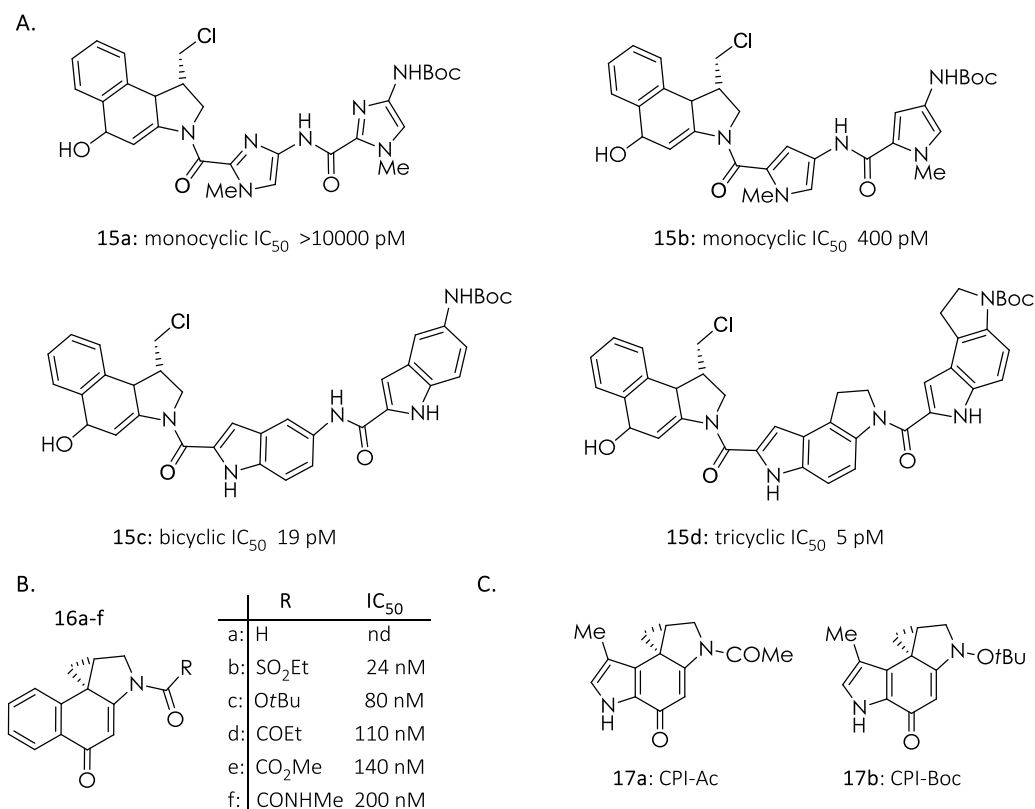
Figure II-21: Replacing the DNA-binding subunit of CBI by **A.** heteroaromatic mono-, di- and tricycles **15a-d**[110] and **B.** diverse short heteroatomic residues **16a-f**[53, 111] results in a wide variety of IC$_{50}$ values. The *in vitro* cytotoxicity of all compounds was determined in L1210 mouse melanoma cell line. **C.** Structures of CPI-Ac (**17a**) and CPI-Boc (**17b**).

With a few exceptions, an exchange for two monocyclic subunits resulted in a cytotoxic potency of 1-10 nM. In contrast, and exchange for dimeric bi- or tricyclic substituents mostly revealed cytotoxicities of 3-80 pM. Concerning the selectivity of DNA alkylation, no changes were observed. Yet, the efficiency was increased from mono-, over bi- to tricycles, with a range spanning over a magnitude of ≥10,000.[110] Smaller heteroatomaric substituents as presented in Figure II-21B by compounds **16a-f** were further analyzed for several alkylation subunits.[53, 54, 111-113] In contrast to **15a-d**, the sequence selectivity of DNA alkylation is drastically altered. In addition the cytotoxicity and the efficiency of DNA alkylation are further decreased. Using the example of CPI-Ac (**17a**) and CPI-Boc (**17b**) (Figure II-21C), the loss of sequence selectivity and efficiency is illustrated in Figure II-22 (p. 36).[112]
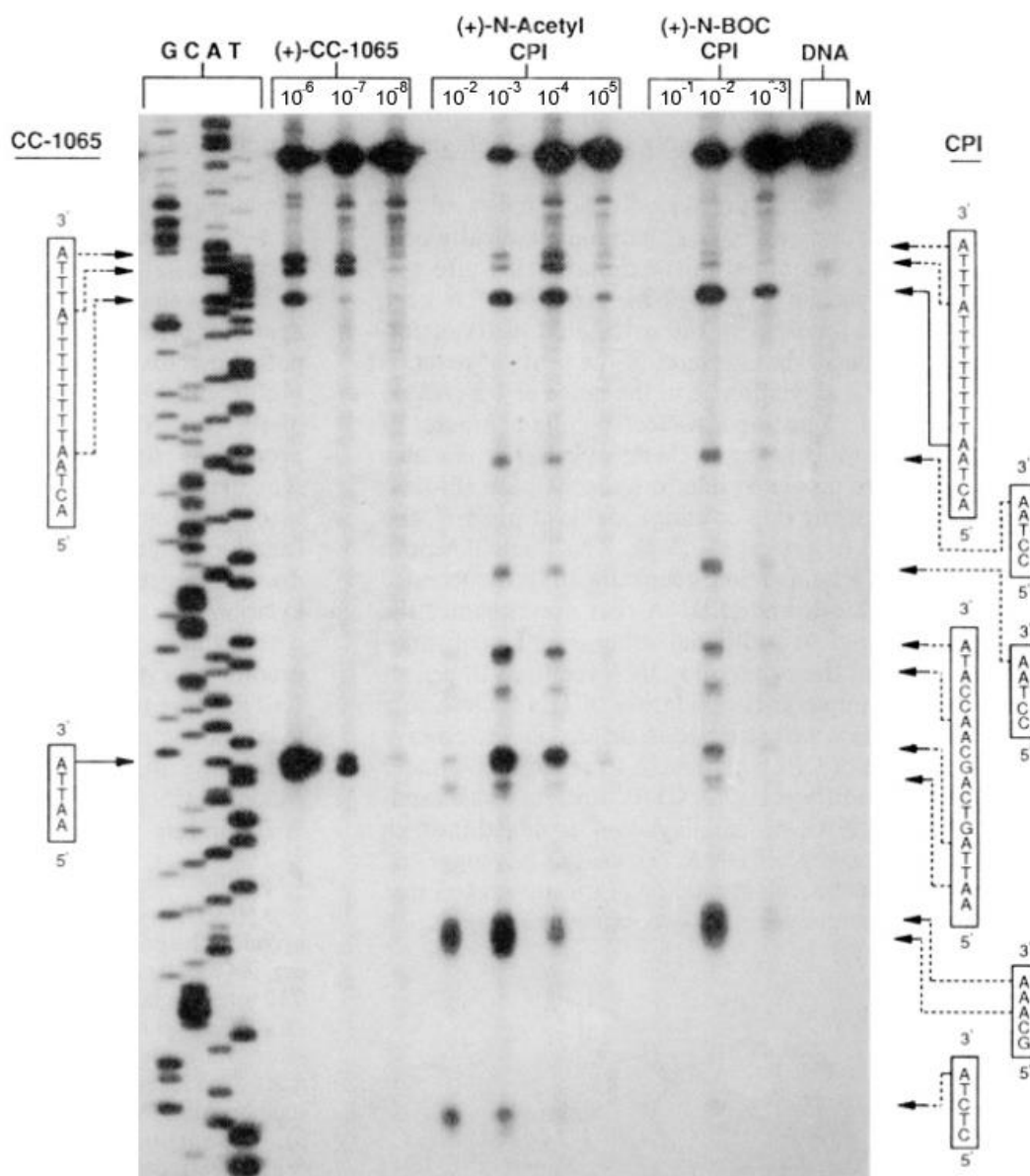
Figure II-22: DNA alkylation pattern of CPI-Ac (**17a**) and CPI-Boc (**17b**) in comparison to CC-1065 for an incubation time of 24 h at 37 °C. Taken from *Boger* et al.[112]

As both compounds require the 10^4-10^7-fold concentration of CC-1065 for DNA alkylation, the efficiency decreased. The major alkylation site of **17a-b**, a minor site of CC-1065, is 5'-d(ACTA**A**)-3' (bold arrow) in addition to numerous minor sites, not alkylated by CC-1065. Thus the alkylation pattern of **17a-b** substantially differs from CC-1065 and alkylation occurs less.[112] Even small changes in the substitution pattern of an indole moiety of compounds **18a-e**, as presented in Figure II-23 (p. 37), result in a wide range of cytotoxic potency.[72]

Figure II-23: Small changes in the substitution pattern of an indole DNA-binding unit at position 4 or 5 as presented in **18a-e** result in a wide variety of IC_{50} values.[72]

'Combined with related studies, these results highlight that the role of the DNA-binding domain goes beyond simply providing DNA-binding selectivity and affinity, consistent with the proposal that it contributes significantly to catalysis of the DNA alkylation reaction.'[110]

3.4.3   DISSECTION OF THE DUOCARMYCINS

The individual contribution of ALDH1A1 to the cytotoxic potency of duocarmycins could not be specified so far. In addition the individual structural elements of duocarmycin analogues that contribute solely to ALDH1A1 inhibition are unknown to date. Referring to Chapter II-3.4.2, removal of the DNA recognition sequence in **11** should result in a loss of DNA binding and subsequent alkylation. This would then enable the evaluation of ALDH1A1 inhibition towards biological activity. In order to identify the targets of the pure CBI motive and visualize the binding preferences to proteins and/or DNA, an alkyne handle was incorporated for visualization.

Figure II-24: Synthetic scheme of click-able seco-drug **19**, control compound **20** and dimeric seco-drug **21** without DNA-binding subunit. a) 4 N HCl/ethyl acetate, r.t., 3 h; b) **22-24**, EDC•HCl, DMF, r.t., 15-18 h, **19**: 67%, **20**: 29%, **21**: 31%.

The synthetic scheme is presented in Figure II-24 (p. 40). Seco-drugs **19-21** were synthesized by Dr. Galina Pestel of the Tietze group at the University of Göttingen starting from enantiopure Boc-protected seco-CBI **12**.[74, 75] An HCl-mediated deprotection of **12** was subsequently followed by an EDC-activated coupling with the alkynoic and alkanoic acids **22** and **23** and the diacid **24**.[113] To preclude any adverse effects of the alkyne handle, **20** was designed as a control compound.

For determining the effects on cell proliferation of the novel seco-drugs **19**-**21** together with the established DNA-binding seco-drug **11**, an HTCFA assay was conducted in A549 cells by Dr. Ingrid Schuberth. As already described, the assay is based on the capability of cells to form new clones after small molecule treatment and reflects the long term cytotoxicity after 10 days of initial exposure. While **11** exhibited the best cytotoxicity with an IC_{50} value of 14 pM, **19**, **20** and **21** revealed higher IC_{50} values of 5.3 nM, 17.6 nM, and 0.11 nM, respectively.[113] Still all novel compounds exhibited potent cytotoxicity in the low nM and high pM range.

In order to validate ALDH1A1 as target of **19-21** they were applied to ABPP studies as well as **11** and incubated *in situ* with A549 cells for 4 h at 37 °C and 5% CO_2. After cell lysis, the labeled proteins were tagged with rhodamine azide via click chemistry and separated by gel electrophoresis (Figure II-25A).
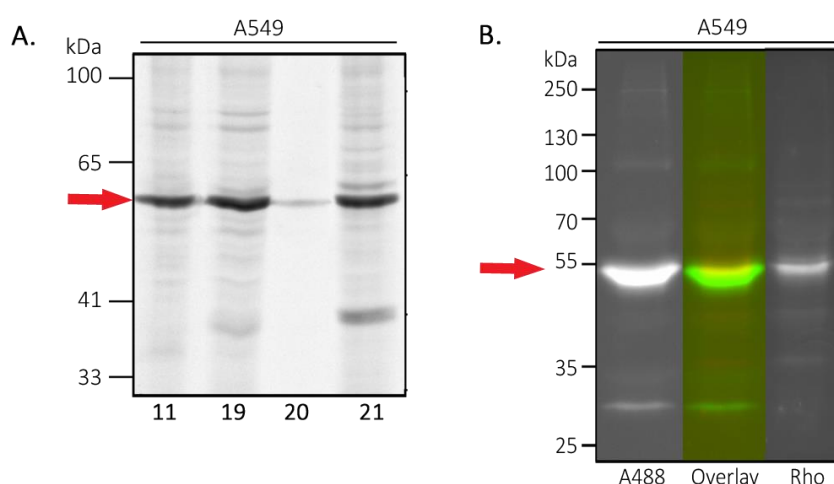
Figure II-25: A. Comparison of *in situ* labeling pattern with seco-drugs **11** and **19**-**21** (10 µM, 4 h) of A549 cells on fluorescent SDS-PAGE. The aldehyde dehydrogenase is marked with a red arrow. **B.** Fluorescent Western blot of **19** (10 µM, 4 h) labeled A549 cells (A488 = Alexa 488, Rho = rhodamine).[113]

The fluorescent SDS-Page reveals a similar labeling pattern for all probes, containing only one prominent fluorescent band at the height of ALDH1A1 (red arrow), with the exception of **20**, which lacks the alkyne tag. In addition, the identity of this band was independently confirmed by Western blot analysis of **19**. Therefore the labeled lysate of Figure II-25A was blotted to a nitrocellulose membrane after separation by SDS-Page and incubated first with an anti-ALDH1A1 primary antibody and subsequently with an Alexa Fluor 488 secondary antibody. The fluorescent readout is presented in Figure II-25B. It reveals an overlay of rhodamine and Alexa 488 labeling, which confirms ALDH1A1 as target of **19** and thus of **20** and **21**.

3.4.4 DETERMINATION OF ALDH1A1 AFFINITY AND SELECTIVITY

To evaluate the affinity and selectivity of the new CBI-seco-drugs **19** and **21** in comparison to DNA-binding CBI-seco-drug **11** for the aldehyde dehydrogenase 1, labeling with serial dilutions and the ALDH1A1 inhibition assay were conducted. In the former case A549 cells were incubated with serial dilutions of DNA-binding CBI-seco-drug **11** and CBI-seco-drug **19** without DNA-binding unit for 4 h at 37 °C and 5% CO_2. The fluorescent SDS-Page is presented in Figure II-26.

39
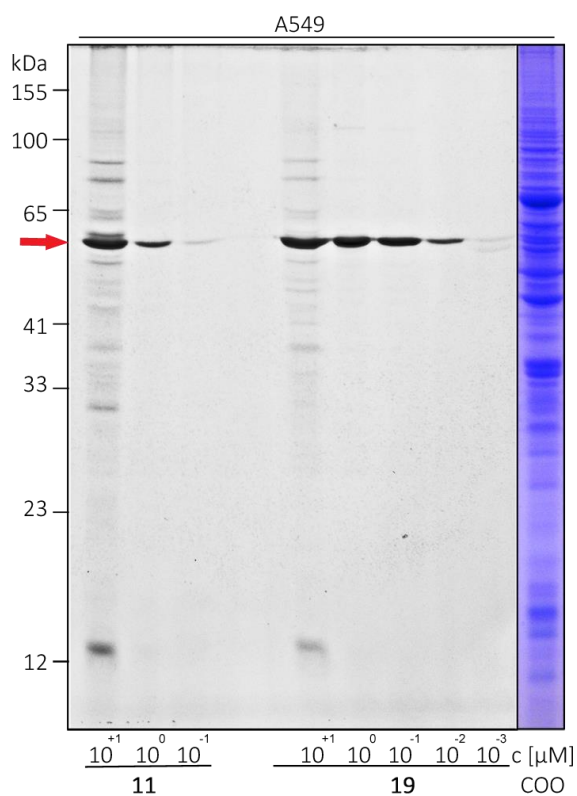
Figure II-26 (previous page): Fluorescent SDS-PAGE and coomassie staining (COO) of *in situ* labeled A549 cells (4 h) showing a comparative dose down of compounds **11** (with DNA-binding subunit) and **19** (without DNA-binding subunit).[113]

While **11** shows a visible band down to a concentration of 100 nM, labeling with **19** is achieved down to a concentration of even 1 nM. These results suggest that removal of the DNA binding motif indeed results in compounds with a significantly increased affinity for ALDH1A1. Moreover, no labeling of other proteinogenic targets could be observed of **19** at concentrations below 1 µM (Figure II-26). This is astonishing in respect of the coomassie staining, which reveals a high abundance of different proteins and underlines the high selectivity of **19**.

Next, the *in vitro* inhibitory efficacy of DNA-binding seco-drug **11** was compared with CBI-seco-drugs **19** and **21** against recombinantly expressed and purified ALDH1A1 by using the ALDH1A1 activity assay with propanal as a substrate. As above, the enzyme activity was measured after incubation of 3 h, 8 h and 24 h with different compound concentrations to observe the corresponding time-dependent IC_{50} shifts. Of note, the minimal observable IC_{50S} are limited by the concentration of recombinant enzyme used in the *in vitro* assay of 0.08 µM. As expected, the IC_{50} values decrease with increasing incubation time down to 0.40 µM and 0.34 µM for **19** and **21** after 24 h (Figure II-27B/C, p. 41), while DNA-binding seco-drug **11** (Figure II-27A, p. 41) shows a weaker inhibition of 12.4 µM.
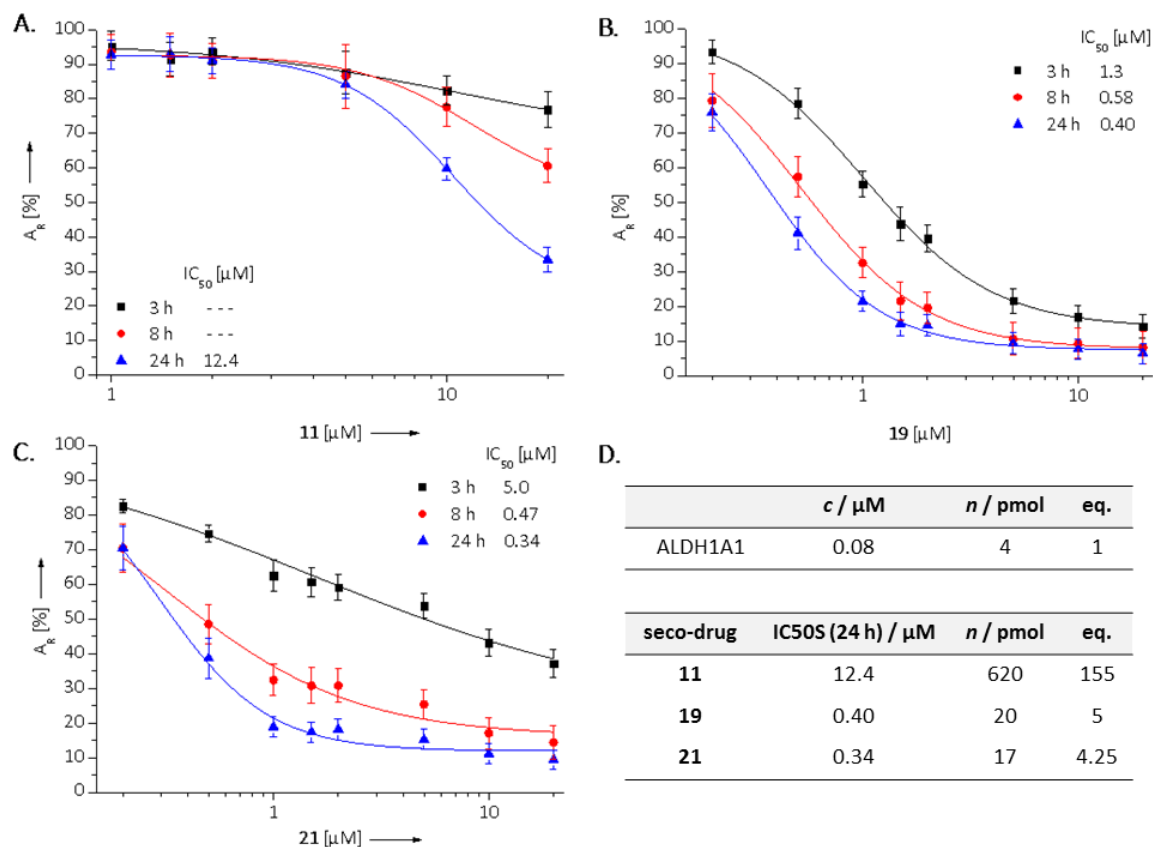
Figure II-27: A-C. *In vitro* inhibitory efficiency of CBI derivatives **11**, **19** and **21** at 2 h, 8 h and 24 h. **D.** Calculation of the equivalents of seco-drugs **11**, **19** and **21** needed to inhibit 50% of ALDH1A1 activity after 24 h of incubation.[113]

In addition, **11** exhibits the slowest and **19** the fastest inhibition. The reduced velocity of **21** may be caused by the introduction of the alkyne moiety at the spacer, as small variations in the chain length of bifunctional duocarmycin **8b** resulted in a loss of cytotoxicity (Chapter II-1.3, p.14).[71] In relation to the used enzyme concentration, the IC_{50} values correspond to only 5 and 4.25 molecules of **19** and **21** per molecule of enzyme, which is already sufficient to inhibit 50% of the ALDH1A1 activity after 24 h (Figure II-27D). These results are in line with the serial dilution experiment and further demonstrate an improved affinity of ALDH1A1 for those compounds that lack the DNA binding motif.

3.4.5   FLUORESCENT IMAGING OF A549 CELLS

In order to investigate if the increased affinity for ALDH1A1 correlates with a decrease of DNA-binding, whole cell imaging in combination with fluorescent immunostaining was

conducted. Therefore, A549 cells were grown on gelatin coated coverslips and incubated *in situ* with 1 µM seco-drugs **11** and **19** for 2 h or **21** for 4 h at 37°C and 5% CO_2. The incubation time of compound **21** was increased to 4 h due to the slower inhibition. For determining the background fluorescence of the rhodamine-N_3 dye, control seco-drugs **8b** and **20** were also applied. The cells were subsequently fixed with 4% paraform-aldehyde, permeabilized with 0.05% saponine and blocked with 3% BSA. The coverslips were incubated with the primary ALDH1A1 antibody over night at 4°C and tagged with a secondary antibody containing Atto 488 as a fluorophore for 3 h. Thereafter the cells were treated with rhodamine azide under click chemistry conditions and finally the DNA was stained with DAPI. The images shown in Figure II-28 were recorded with a confocal microscope by Dr. Vanessa Ganal of the Rein group at MPI of Psychiatry in Munich and visualize the distribution of compounds in red (rhodamine), ALDH1A1 in green (Atto 488) and DNA in blue (DAPI).
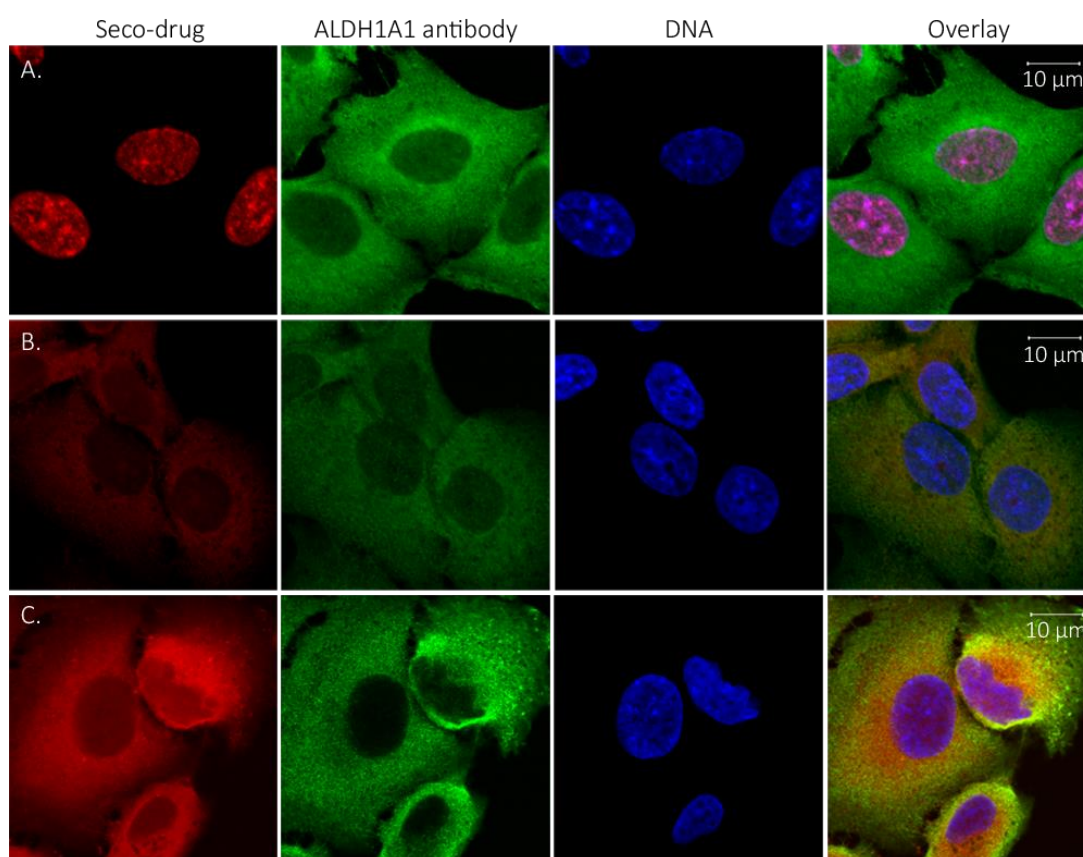
Figure II-28: Cell imaging of A549 cells with different duocarmycin derivatives and immunostaining with ALDH1A1 antibody. Red = compound (rhodamine azide), green = ALDH1A1 (Atto 488), blue = DNA (DAPI). The corresponding negative controls are presented in **Figure II-29** (p. 45). **A.** With DNA-binder (1 µM **11**, 2 h). **B.** With non DNA-binder (1 µM **19**, 2 h). **C.** Bifunctional CBI (1 µM **21**, 4 h).

As expected, **11** shows a high affinity for DNA (Figure II-28A) as intense fluorescent staining is observed in the nucleus. Compared to the labeling intensity of **19** and **21**, the intensity of **11** is increased. This is due to an enrichment of **11** in the smaller nucleus in contrast to a dilution of **19** and **21** throughout the cytosol. This effect is more pronounced for recording the images at the same laser adjustments (Figure II-32, p. 45). However, despite the high DNA-alkylation, **11** exhibits weaker fluorescent labeling in the cytosol, illustrated by the overexposed images of 1 µM and 20 µM (Figure II-30).
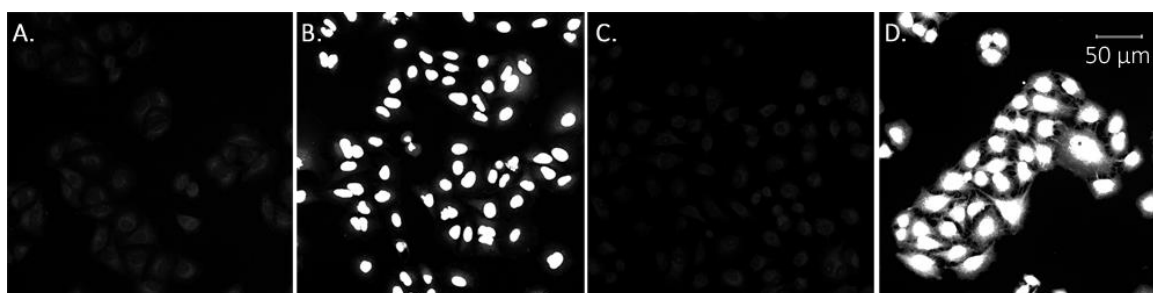
Figure II-30: Overexposure of **11** reveals labeling in cytosol. **A**. 1 µM **20** (2 h, neg. control). **B**. 1 µM **11** (2 h). **C**. 20 µM **20** (2 h, neg. control). **D**. 20 µM **11** (2 h).[113]

Contrary to **11**, **19** and **21** exhibit negligible DNA labeling as shown by the very weak fluorescence of the nucleus, indicating that in a native environment these seco-drugs likely do not exert their biological activity through DNA alkylation (Figure II-28B/C). Importantly, strong fluorescent signals can be observed in the cytosol, suggesting binding to a protein target. Immunostaining of the cells with an ALDH1A1 specific antibody (green) reveals a co-labeling in the cytosol between the signals of **19** and **21** and ALDH1A1 immunofluorescence. When the incubation time of **19** is increased to 24 h, this signal is even observed at concentrations down to 10 nM (Figure II-31, p. 44), emphasizing a high binding affinity.
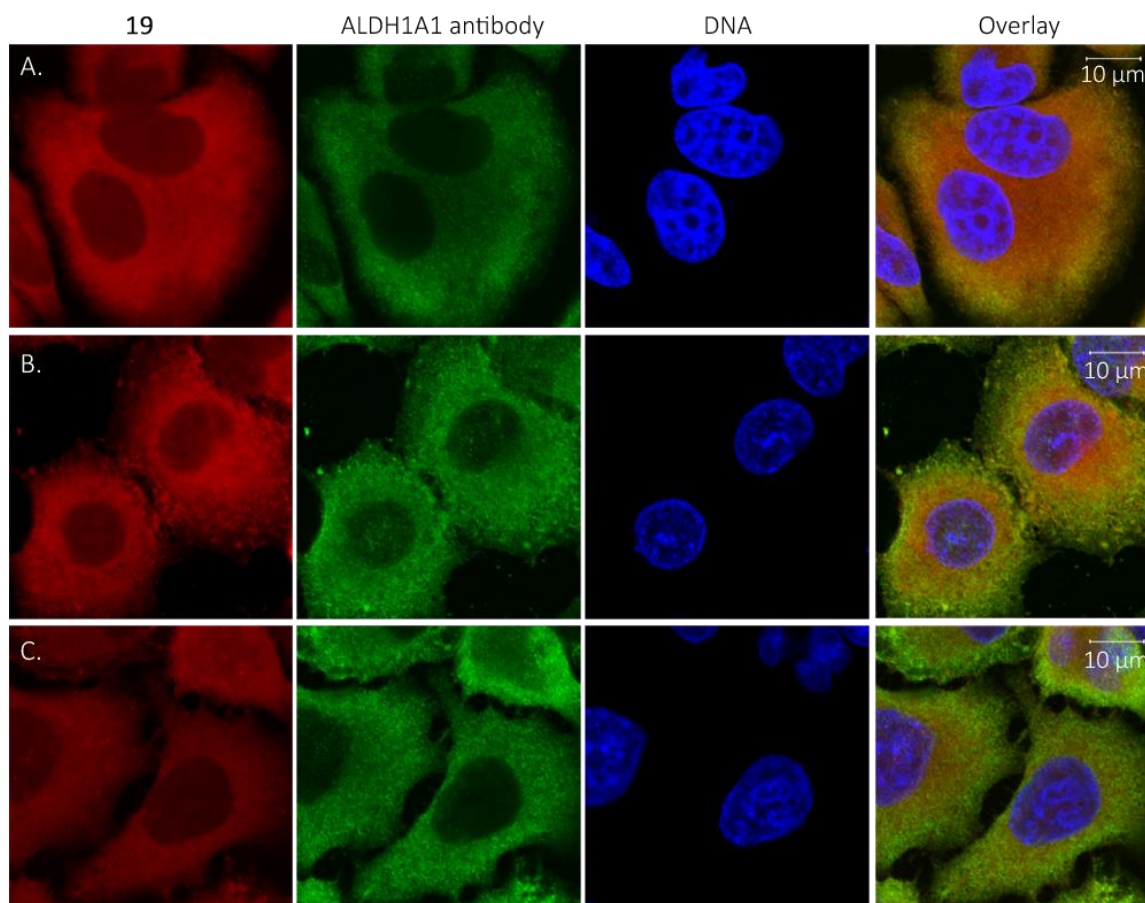
Figure II-31: A-C. Cell imaging of A549 cells with different concentrations of seco-drug **19**. **A.** 1 µM **19** (2 h). **B.** 100 nM **19** (24 h). **C.** 10 nM **19** (24 h).[113]

However, due to the high delocalization of compound and antibody, it is difficult to determine a distinct correlation, thus interaction with other proteinogenic targets cannot be excluded. In contrast to **11**, **19** and **21**, the control compounds **8b** and **20** lacking the alkyne for click chemistry modifications exhibit no fluorescent signal. These Images, taken at lower magnification and with the same laser adjustments in relation to the corresponding probes**,** are shown in Figure II-32 (p. 45).

Seco-drug	ALDH1A1 antibody	DNA	Overlay
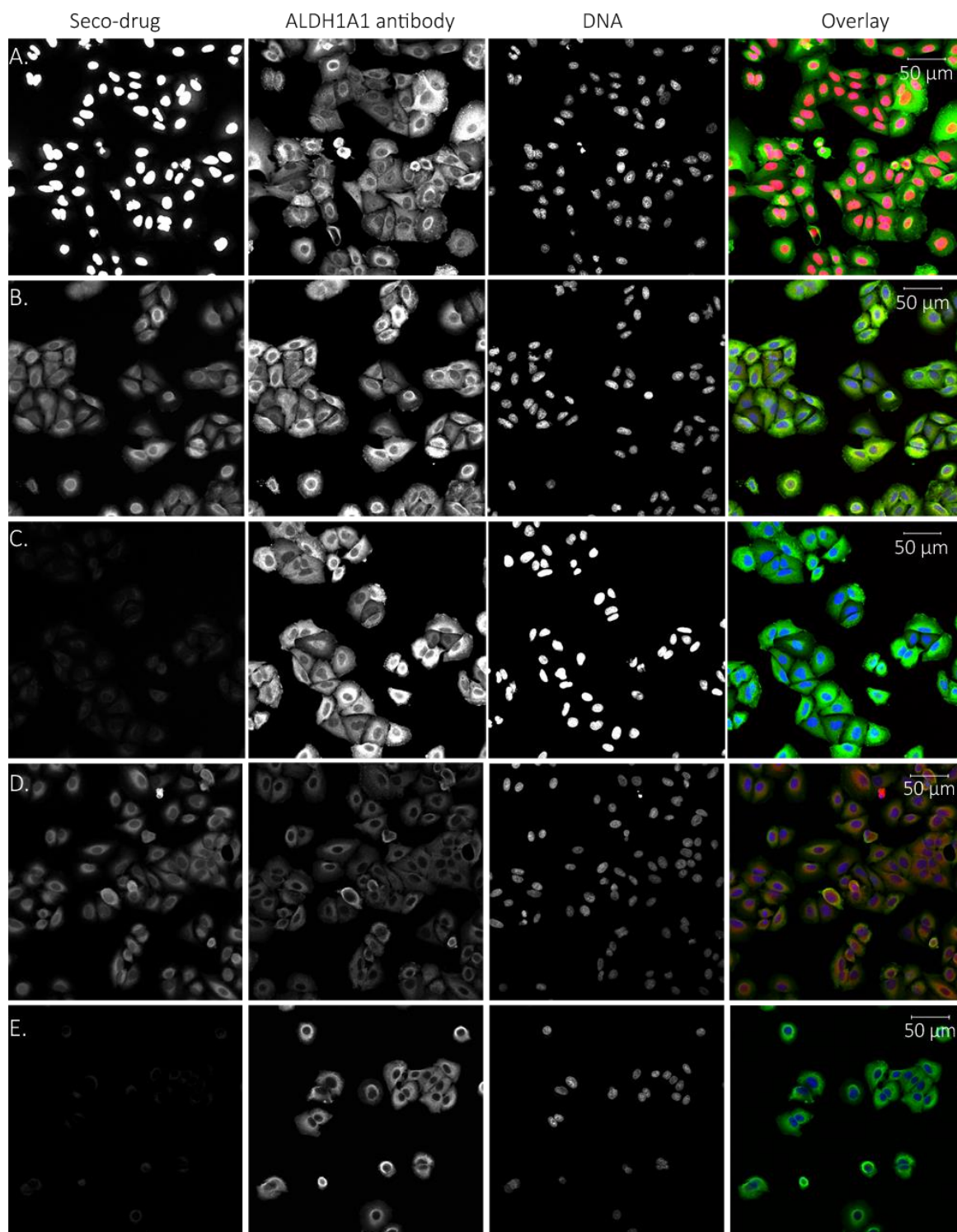
Figure II-32: Comparison of **11**, **19** and **21** with negative control compounds **8b** and **20**. The images **A-C** and **D-E** are taken with the same laser adjustments. **A.** With DNA-binder (1 µM **11**, 2 h). **B.** Without DNA-binder (1 µM **19**, 2 h). **C.** Without alkyne (1 µM **20**, 2 h) **D.** Bifunctional CBI (1 µM **21**, 4 h). **E.** Bifunctional CBI without alkyne (1 µM **8b**, 4 h).[113]

3.4.6 KNOCK DOWN STUDIES OF ALDH1A1 IN A549 CELLS

In order to establish a connection between the cytotoxicity of seco-drugs lacking the DNA-binding subunit and ALDH1A1, siRNA was utilized to knock down the expression and to investigate the corresponding effects on cell proliferation. Therefore A549 cells were transfected with one approved siRNA #1 and three *Silencer*® Select siRNAs #2-4. The RNA sequence of all siRNAs is presented in Chapter V-1.1.7 (p. 81). Beside the four different ALDH1A1-specific siRNAs a scrambled siRNA scr was used as a control. The transfection was carried out with Lipofectamine RNAiMAX (Invitrogen) and the resulting expression levels of ALDH1A1 were monitored via Western blot (by Anna-Maria Werner of the Rein group at MPI of Psychiatry in Munich) for six days. (Figure II-33). In addition to ALDH1A1, actin was immunostained to eliminate concentration dependent fluctuations of the different A549 lysates.
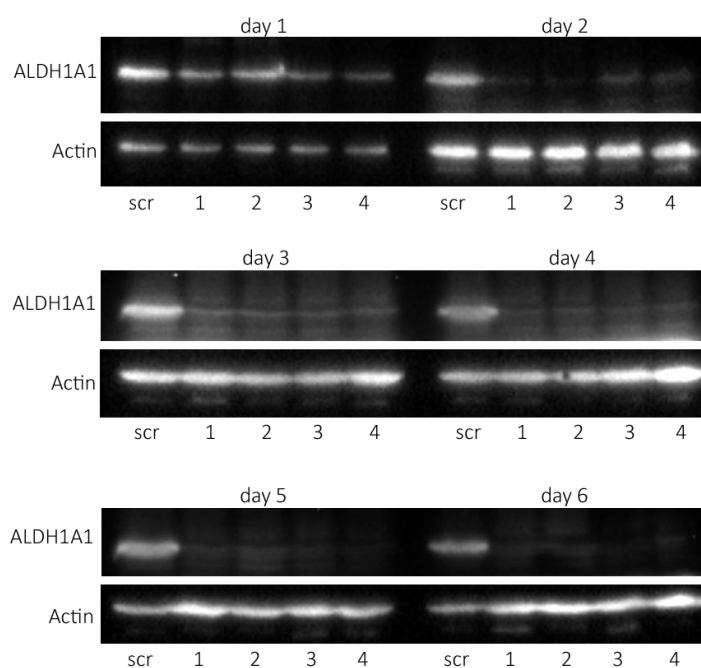
Figure II-33: Western blot of four different siRNA knock downs 1-4 compared to the scrambled control siRNA scr. The transfection was monitored for six days. After Three days of transfection all siRNAs provided a high knock down efficiency of ALDH1A1 with an expressional reduction of over 80%.[113]

The Western blot reveals a decrease in the expression of ALDH1A1 over the first three days for all siRNAs. After three days a knock down efficiency with over 80% is achieved in comparison to the scrambled control siRNA (scr). To ensure a maximal effect on cell proliferation, further experiments were conducted at least three days after transfection.

Therefore, the increase of cell density from the third to the sixth day after transfection with siRNAs 1, 3 and scr was colorimetrically monitored by the metabolic formation of formazan. The optical densities of the third and the sixth day were read out at λ = 570 nm and λ = 630 nm with a microplate reader. To determine the number of replication, the absorption of the sixth day was divided by the third day, which was defined as "1".
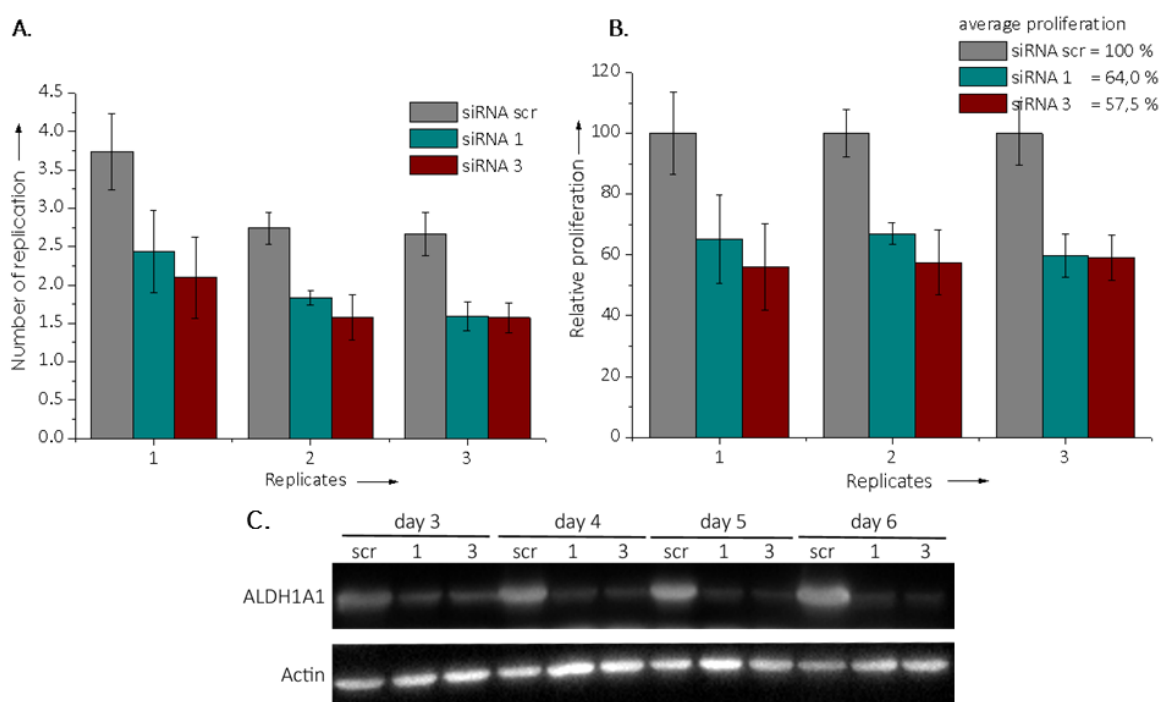
Figure II-34: Proliferation assay of transfected A549 cells with ALDH1A1 specific siRNAs 1 and 3 and a scrambled control siRNA scr for 3 days. **A.** Number of replication of three independent measurements **B.** Relative proliferation of A with siRNA scr set as 100%. **C.** Western blot of transfected A549 cells used in A. (knock down efficiency > 80%).[113]

After three days of growth, cells treated with the scrambled control divided themselves approximately 2.75 to 3.75 times, whereas the treatment with ALDH1A1 specific siRNA 3 led to a reduced cell division of approximately 1.5 to 2.0 times (Figure II-34A).

$$\nu = \frac{\lg(\frac{N}{N_0})}{\lg(2)\, dt} \quad ; \quad t_g = \frac{1}{\nu} \qquad \text{with } \nu = \text{Growth rate}; \ t_g = \text{Doubling time} \qquad \text{(VI)}$$

Applying the equation (VI) with the assumption of exponential growth, the numbers of replication correspond to a maximal doubling time of 2.0 days and 5.3 days for siRNAs scr

and 3, respectively. Hence, the knock down of ALDH1A1 results in a strikingly decreased growth rate, which has a pronounced impact on long-term growth in relation to regular ALDH1A1 expression.

To determine the relative proliferation after three days, the scrambled controls of each replicate was set as 100%. The results are presented in Figure II-34B, which demonstrates a significantly reduced proliferation to approximately 64% and 57.5 % of siRNA 1 and 3, respectively. To monitor and verify a constant knock down efficiency, samples were taken and analyzed via Western blot by Anna-Maria Werner of the Rein group at MPI of Psychiatry in Munich, which reveals an efficiency > 80% over the whole period of time for both ALDH1A1 specific siRNAs (Figure II-34C).

In order to establish a connection between siRNA knock down and seco-drug treatment, the proliferation assay was slightly modified and repeated with the scrambled control siRNA. Beside the siRNA, the A549 cells were incubated with different concentrations of **19** and **21** in between the third and sixth day after transfection. After the readout, the absorptions of the different concentrations were calculated in relation to DMSO treated cells, which were set as 100%. The results are shown in Figure II-35.
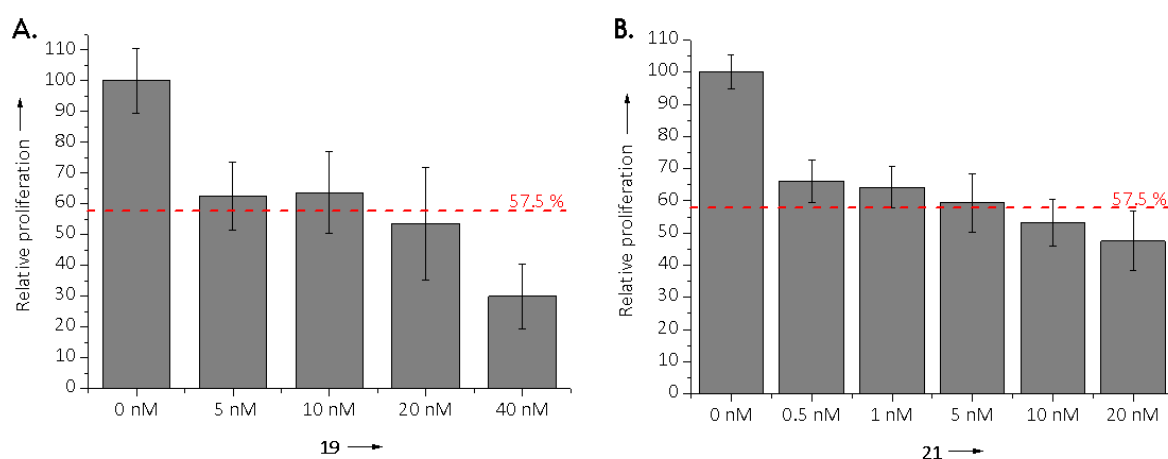
Figure II-35: A. Reduction of proliferation after incubation of siRNA scr transfected A549 cells with seco-drug **19** for three days. **B.** Reduction of proliferation after incubation of siRNA scr transfected A549 cells with seco-drug **21** for three days.[113]

An incubation of 10-20 nM **19** and of approximately 5 nM **21** for three days results in a comparable reduction of proliferation (42.5%) as a treatment with siRNA 3. Furthermore

lower concentrations down to 5 nM and 0.5 nM for **19** and **21**, respectively, exhibit only a slight recovery with an approximate proliferation of 65%, which is comparable to a treatment with siRNA 1. These concentrations are in line with the corresponding *in vitro* cytotoxicities of 5.3 nM (**19**) and 0.11 nM (**21**) and confirm that ALDH1A1 is an essential enzyme for proliferation in A549 cells. Thus treatment of cells with low nM concentrations of **19** and **21** reveal phenotypes comparable to ALDH1A1 siRNA knock downs.

4   SUMMARY AND CONCLUSION

It was shown, that derivatives of the duocarmycin family do not only target DNA but also the aldehyde dehydrogenase 1A1, which is an essential enzyme that plays an important role in viability and detoxification of cancer cells. The target was identified by ABPP in combination with LC/MS-MS analysis and further confirmed by labeling of recombinantly expressed ALDH1A1. The binding sites of duocarmycin derivatives Cys456 and Cys464 located in a proximal range to the enzyme active site, were identified via LC/MS-MS and confirmed by the insertion of point mutations. These cysteines provided a suitable distance to react with both alkylation subunits of bifunctional seco-drugs **8b** or **21** at once. To prove the hypothesis of Cys456 / Cys464 crosslinking by **8b** a co-crystallization of human ALDH1A1 with **8b** was attempted. However, the resolution of the obtained crystals was too low to verify the interaction of bifunctional duocarmycins with ALDH1A1.

Novel seco-drugs **19-21**, containing the pure CBI motif, were synthesized in order to identify the targets of CBI and evaluate the binding preferences to ALDH1A1 versus DNA. These compounds exhibited a reduced *in vitro* cytotoxicity compared to seco-drug **11** or (+)-CC-1065 (**1**), but were still highly potent with IC_{50} values in the low nM range. The inhibitory activity was determined by the application of an aldehyde dehydrogenase activity assay, which revealed that all tested duocarmycin derivatives inhibited ALDH1A1. However, compounds lacking the DNA-binding motif exhibited a more pronounced inhibitory efficiency. This was in line with *in situ* ABPP experiments of serial dilutions, which showed labeling at 100-fold lower concentrations of seco-drug **19** versus seco-drug **11**. In combination with the increased inhibitor efficiency, these results confirmed that removal of the DNA binding motif results in compounds with a significantly increased selectivity and affinity for ALDH1A1. Furthermore the affinity for DNA is drastically decreased as proven by *in situ* labeling of A549 cells in combination with fluorescent imaging. In order to establish a connection between the cytotoxic potency of seco-drugs lacking the DNA-binding subunit and ALDH1A1, an siRNA knock down in combination with a proliferation assay were conducted. As a result the siRNA knock down of ALDH1A1 exhibited a comparable reduction of proliferation as incubation with seco-drugs **19** and **21** at concentrations in the range of their corresponding *in vitro* cytotoxicities of 5.3 nM and 0.11 nM, respectively. In addition, the siRNA knock down

confirmed ALDH1A1 as an essential enzyme for proliferation in A549 cells, as an ALDH1A1 reduction of over 80% led to a decreased growth rate.

In conclusion, bifunctional seco-drugs, as well as monofunctional seco-drugs without DNA-binder exert a large fraction of their bioactivity via inhibition of ALDH1A1, as they loose DNA affinity and gain specificity for ALDH1A1. Despite the reduced potency, CBI compounds **19**-**21** still exhibit remarkable cytotoxicities that are matched by the essential role of ALDH1A1 in lung cancer cell proliferation. However, the conducted experiments do only allow the identification of covalent targets. Thus interaction with non-covalent targets could contribute to the cytotoxicity of duocarmycins. Though duocarmycin derivatives with intact indole moiety bind ALDH1A1 as well, DNA alkylation is the major mechanism of action.

5   OUTLOOK

As all improved strategies for obtaining high resolution crystals of human ALDH1A1 remained unsuccessful, co-crystallization of duocarmycin derivative **9b** with the closely related sheep ALDH1A1 seems to be the most promising alternative. Due to the sequence identity of approximately 95%, all results should be applicable to the human enzyme. Therefore important questions could be solved such as the actual mechanism of ALDH1A1 inhibition and the binding mode of bifunctional duocarmycin derivatives. Moreover co-crystallization of monofunctional versus bifunctional seco-drug could indicate whether the hypothetical crosslinking of bifunctional compounds contributes to their improved potency.

Since a direct ALDH1A1 inhibition in living A549 cells failed, due to immediate apoptosis and loss of activity, it is difficult to compare *in vitro* enzyme inhibition data with cell toxicity (HTCFA). In order to establish a direct connection, a time-dependent Aldefluor assay, which allows determining the intracellular aldehyde dehydrogenase activity by FACS analysis, could be conducted. However, this method is not specific for ALDH1A1 and detects the activity of several aldehyde dehydrogenases according to the manufacturer

protocol and a previous publication.[108] Yet, as ALDH1A1 is highly abundant in A459, this assay may give a good indication on intracellular ALDH1A1 inhibition.

Furthermore as reversible binding to other potential protein or non-proteinogenic targets could not be excluded, further studies with focus on non-covalent targets should be conducted. One strategy for identifying reversible targets is the incorporation of a photocrosslinking moiety instead of the DNA-binding site of duocarmycins. After irradiation, the photoactivatable probe is transformed into a reactive intermediate, which generates covalent crosslinks to nearby residues or biomolecules.

In addition, investigations could be expanded to CPI derivatives, found in duocarmycin (**1**) and CC-1065 (**2**).

III ACTIVITY BASED PROTEIN PROFILING DURING BACTERIAL INVASION

1   SPECIAL INTRODUCTION

1.1   BACTERIAL INVASION

Over millions of years microbial pathogens have developed a myriad of strategies to successfully infect host cells, elude or resist the immune system, divide intracellularly and to spread through diverse tissues. Invasive bacteria possess the ability to actively induce a phagocytic uptake in nonphagocytic cells for example, epithelial cells.[114] For studying host-pathogen interactions, bacterial invasion and host immune response, *Listeria monocytogenes* is one of the best characterized bacterial invasive pathogens. By various immunological and microbiological studies, important questions concerning intra- and intercellular movement of bacteria, mechanisms of invasion or intracellular survival have been solved, giving 'one of the most comprehensive pictures of the "battle" between host and microorganism'[115].[116]

1.2   LISTERIA MONOCYTOGENES: A PARADIGM FOR HOST-PATHOGEN INTERACTIONS

L. monocytogenes is a Gram-positive, nonspore-forming, motile pathogen that causes listeriosis. This infection manifests itself as gastroenteritis, meningitis, encephalitis and mother-to-fetus infections.[116-118] Though listeriosis appears rarely, *L. monocytogenes* is categorized as one of the most deadly human foodborne pathogens due to a high mortality rate of 25-30%.[116, 117] As an opportunistic pathogen, it manly affects immunocompromised individuals, newborn, elderly and pregnant women. It can be found in various different environments such as, water, soil, food products, animals and the human. However, uptake occurs primarily through consumption of contaminated food.[115-117] After oral ingestion, *L. monocytogenes* invades into intestinal epithelial cells at the gastrointestinal tract, enabled by the cell surface protein internalin A (InlA). InlA interacts with epithelial cadherin (E-cadherin), which induces a cytoskeletal rearrangement to form a vacuole that engulfs the bacterium.[114-117, 119] After transition through the epithelial-cell layer, the bacteria spread to other organs via the bloodstream. In addition to the intestinal barrier, *L. monocytogenes* possesses the ability to cross the blood-brain barrier and the fetoplacental barrier.[116, 118] Reaching the liver, the bacteria are internalized by hepatic macrophages or actively enter hepatocytes with the aid of the surface protein internalin B (InlB). InlB binds to the hepatocyte growth factor receptor

(HGF), which activates different pathways and the protein-tyrosine-kinase Met, which results in a bacterial uptake via vacuole formation.[114-116, 120] After internalization, the bacteria escape the phagosome by secretion of the pore-forming toxin listeriolysin O (LLO) and the phospholipases PI-Plc and PC-Plc (Figure III-1).[114-116, 118, 121]
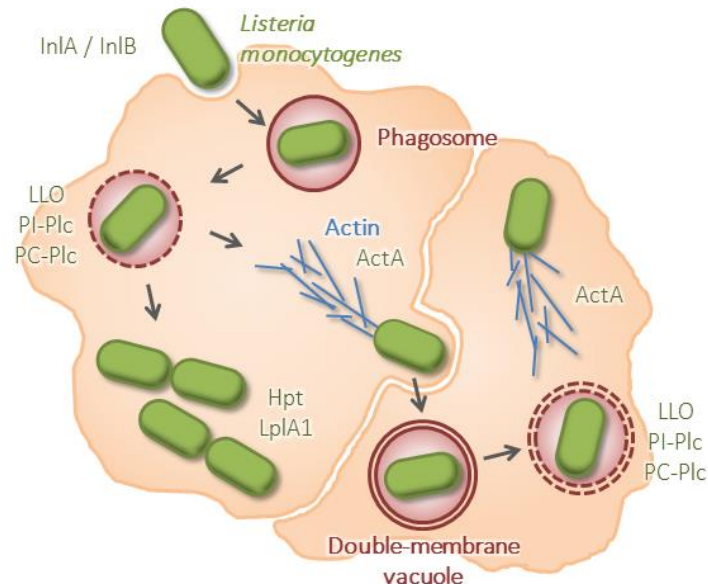
Figure III-1: Schematic mechanism of the intracellular life-cycle of *Listeria monocytogenes.*

L. monocytogenes is able to replicate and survive in the cytosol of various cell types such as macrophages and epithelial cells. However, intracellular growth requires an adaption to novel nutritional sources. Facing this challenge, *L. monocytogenes* expresses hexose-phosphate translocase (Hpt), allowing it to exploit glucose-1-phosphate as carbon source and lipoate protein ligase A1 (LplA1), which is proposed to derive lipoyl from host molecules.[115, 116, 122, 123] For intracellular movement, host actin is polymerized by the actin-assembly-inducing protein (ActA), which produces an actin tail that propels the bacteria through the cytoplasm and into neighboring cells.[114-116, 118, 124] Cell to cell spread occurs via endocytosis of neighboring cells resulting in a double-membrane vacuole, which is again destroyed by LLO, PI-Plc and PC-Plc. Thus *L. monocytogenes* disseminates from cell to cell, protected from the adaptive immune system as it circumvents the extracellular milieu.[114, 116, 117]

For clearance of *L. monocytogenes*, an early innate immune response upon infection is essential, whereas macrophages and neutrophils are predicted to be the major mediator

of killing.[115, 117, 125] However, the innate immune activation is a complicated multistep process, starting with the detection and internalization of bacteria by the macrophages. Through the invasion of *L. monocytogenes* from the phagosomes into the cytosol, the activation of nuclear factor-κB (NF-κB) is triggered, activating genes involved in innate immune response such as production of CC-chemokine ligand 2 (CCL2).[115, 117] Furthermore LLO itself stimulates the activation of different pathways such as NF-κB, mitogen-activated protein kinase (MAPK) or phosphatidylinositol pathway.[118, 126-128] Expression of CCL2 mediates the recruitment of monocytes to the site of infection, which contain the corresponding surface bound CC-chemokine receptor 2 (CCR2).[115, 129] Moreover, bacterial products such as nucleic acids, lipopolysaccharide, peptidoglycan or lipoteichoic acids, which are part of pathogen-associated molecular patterns (PAMPs) are released by the macrophage. At the cell surface of the monocytes, the PAMPs are recognized by Toll-like receptors (TLRs), which in turn bind to myeloid differentiating factor-88 (MyD88).[115, 117, 130] The signals mediated by MyD88 are vital for the activation of the recruited monocytes, which differentiate into tumour-necrosis factor (TNF) and inducible nitric-oxide synthase (iNOS)-producing dendritic cells (TipDCs).[115, 131] Finally the production of nitric oxide (NO) and TNF by TipDC results in the clearance of the pathogens.

1.3   REGULATION OF LISTERIAL VIRULENCE: PRFA

As *L. monocytogenes* survives under various environmental conditions, inside and outside a host organism, it has developed a complex regulatory mechanism to control and avoid unnecessary expression of virulence factors and pathogenesis associated enzymes.[116, 132] However, shifting from saprotrophic to parasitic life cycle does not only require the up-regulation of virulence genes but also the down-regulation of genes and bacterial systems correlated to environmental survival. For example, extracellular motility is provided by flagella-propelled motion, which is repressed intracellularly.[132]

The above-mentioned proteins, involved in invasion and intracellular replication, are tightly controlled by the transcriptional regulator PrfA in a concentration dependent manner.[116, 132] Beside these key virulence genes, several genes such as transporters,

metabolic enzymes or regulators are indirectly regulated.[132, 133] The concentration of PrfA is transcriptionally controlled by three promoters. Two are regulated by vegetative σ^A factor and/or stress σ^B factor and the third by a positive feedback of PrfA.[132, 134] One key stimulus of PrfA is the temperature as the σ^A-dependent *prfA* transcript serves as a thermoswitch. At temperatures below 30 °C the ribosomal binding site is masked by the formation of a secondary structure. Destabilization at 37 °C enables a spontaneous translation of the *prfA* mRNA upon invasion of a host.[132, 135] Yet, incubation of *L. monocytogenes* in culture broth at 37° C revealed only marginal transcription of virulence genes.[132, 136] The PrfA regulator is furthermore allosterically controlled and possesses two functional states, OFF and ON. After infection the state shifts to ON, resulting in a high input to the positive feedback autoloop.[132] Another key stimulus is the availability of different carbon sources. In contrast to intracellular available hexose phosphates, virulent gene expression is down-regulated by β-glucosides such as glucose, fructose or mannose.[122, 132, 134] PrfA and *prfA* are further influenced by environmental conditions such as osmolarity, iron concentration, pH and stress mediated by σ^B.[116, 132, 137, 138]

2   RESEARCH APPROACH AND OBJECTIVES

During infection, PrfA-dependent genes are strongly expressed compared to mere growth in culture broth. *Shetron-Rama* et al. revealed that in contrast to extracellular growth, intracellularly grown *L monocytogenes* exhibited a 50-200-fold up-regulated transcription of the virulence gene *actA*.[139] Hence, analyzing the proteome of bacteria adapted to extracellular conditions does not reveal the complete subset of pathogenesis associated enzymes.

Due to these limitations it was attempted to establish a new ABPP protocol for *in vitro* and *in situ* labeling of *Listerial* proteome during eukaryotic infection. As a proof of principle the invasive ABPP experiment should be conducted with well-known probe compounds to elucidate the gain of so far unlabeled enzyme targets. Thus the bacterial and eukaryotic proteome should be comparatively labeled to determine differences in the labeling pattern (extra-/ intracellular, healthy/infected). New targets should be identified by LC-MS/MS to assess a possible contribution in pathogenesis.

3   Results and Discussion

3.1   Establishing an Infection Protocol

For a successful establishment of an *in vitro* and *in situ* labeling protocol of intracellular bacteria, several key factors had to be optimized. These, include the initial invasion process, the amount of host cells yielding sufficient bacterial proteome, the multiplicity of infection (MOI), the duration of infection and the extraction of bacterial proteome.

For studying the invasion of *L. monocytogenes*, the murine macrophage cell line J774 was chosen as host cells. As macrophages actively internalize bacteria, the initial invasion process is accelerated. To further enhance the ingestion, bacteria were opsonized with FBS, for simplifying the recognition through the phagocytic cells.

As estimated by ABPP experiments, approximately 1×10^8 and 2×10^8 J774 infected with *L. monocytogenes* cells provide ample *Listerial* proteome for *in situ* and *in vitro* labeling, respectively. Due to this required amount of host cells, large scale cell culture techniques were applied to ensure an effective handling. Since J774 macrophages are semi-adherent cells, they are able to grow attached to cell culture flasks as well as suspended in stirrer bottles. J774 cells are hard to detach and require scraping, which causes damage and a drop of viability, however, due to crucial washing steps, the infection with *L. monocytogenes* had to be conducted with adherent cells. Thus, J774 macrophages were grown and subcultured in suspension, which provides a viability of >99%. For infection, cells were seeded out to single (175 cm^2) or triple (500 cm^2) bottomed culture flasks, 36 h before incubation with bacteria.

In addition to the number of host cells, the duration of infection and the initial quantity of bacteria affect the final amount of bacterial proteome. To promote the activation and expression of pathogenesis-associated enzymes, a moderate infection and a vivid intracellular replication of *L. monocytogenes* had to be ensured. Hence, the appropriate infection duration and the ratio of bacteria to host cells - multiplicity of infection (MOI) - were experimentally determined. Therefore, J774 macrophages were infected at MOIs of 0 (no bacteria), 10 and 100 for an overall duration of 5 h. The progress of invasion was observed under a microscope and is represented in Figure III-2 (p. 60).
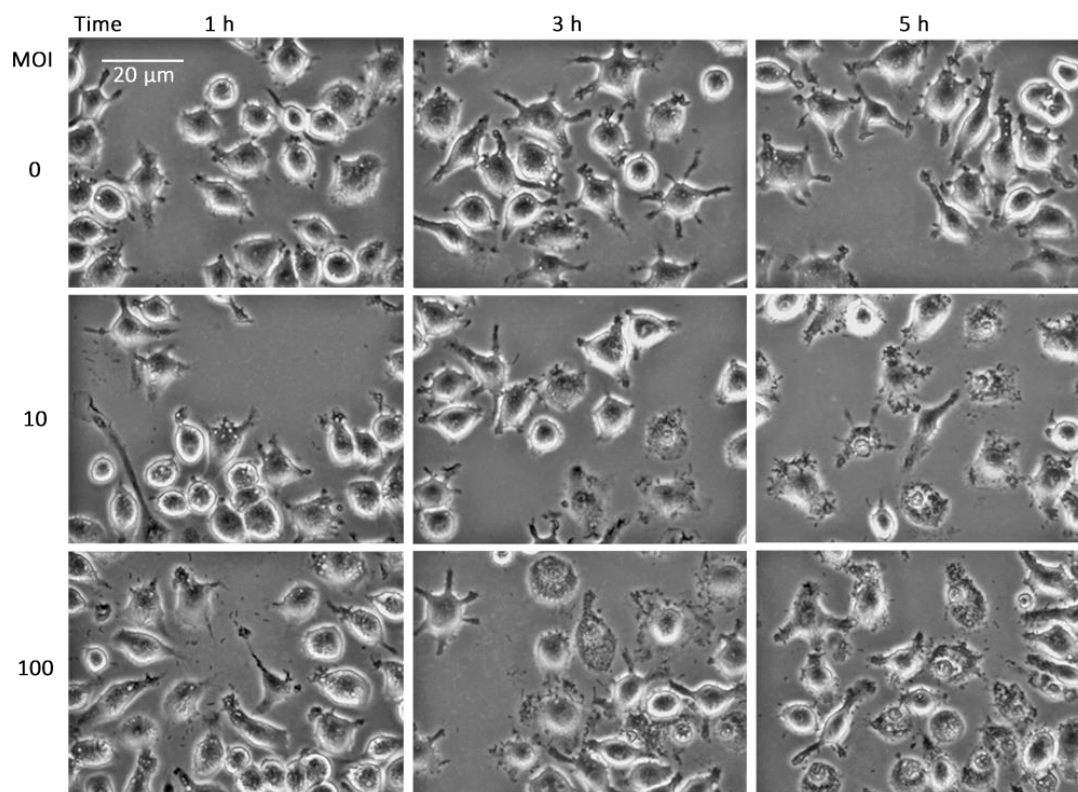
Figure III-2: Infection of J774 cells with *L. monocytogenes* at MOIs of 0 (= no bacteria), 10 and 100 for incubation times of 1 h, 3 h and 5 h.

At a MOI of 100, the host cells are already overwhelmed 3 h after initiating the infection. Incubation for another 2 h results in partial lysis of macrophages, as various extracellular bacteria can be detected. Thus, a long and vivid intracellular life cycle is not ensured at a MOI of 100. In contrast, a MOI of 10 exhibits a slowly proceeding infection, with an appropriate amount of intracellular bacteria after 5 h of infection.

To extract the *Listerial* proteome from the host cells, the macrophages were selectively lysed, with detergents such as saponins[140] and Triton X-100[141], with the latter exhibiting better results in terms of a fast lysis and a complete separation of the bacterial proteome by centrifugation.

L. monocytogenes is still able to grow at temperatures between 0.5 °C and 5.0 °C.[142] Thus, all washing and centrifugation steps after host lysis had to be conducted rapidly for preventing a return to an extracellular life cycle and the depletion of virulence-associated proteins. Subsequently, the bacterial pellet was either lysed by sonication or stored at -80 °C. The exact infection protocol is presented in Chapter V-1.2.4 (p. 82).

3.2 COMPARATIVE IN VITRO LABELING

As a first proof of principle, the *in vitro* labeling patterns of intra- versus extracellular *L. monocytogenes* and infected versus healthy J774 cells were compared. Therefore the bacteria were allowed to invade the host cells for 5 h at a MOI of 10. For comparable culture conditions, extracellular bacteria were first opsonized with FBS and subsequently incubated with eukaryotic growth medium (5 h). In addition, all washing steps and medium changes were simultaneously conducted with both infected and healthy macrophages. For isolation of the intracellular bacteria, the majority of infected host cells were lysed with Triton X-100. The remaining macrophages were detached by scraping, to obtain the infected J774 cells. After sonication, the whole cell proteomes were labeled with diverse probe compounds (Figure III-3). The structures and the labeling of β-lactone **25**, oxiran **26**, fluorophosphonate **27** and acivicin **28** are presented in Figure III-4 (p. 62).
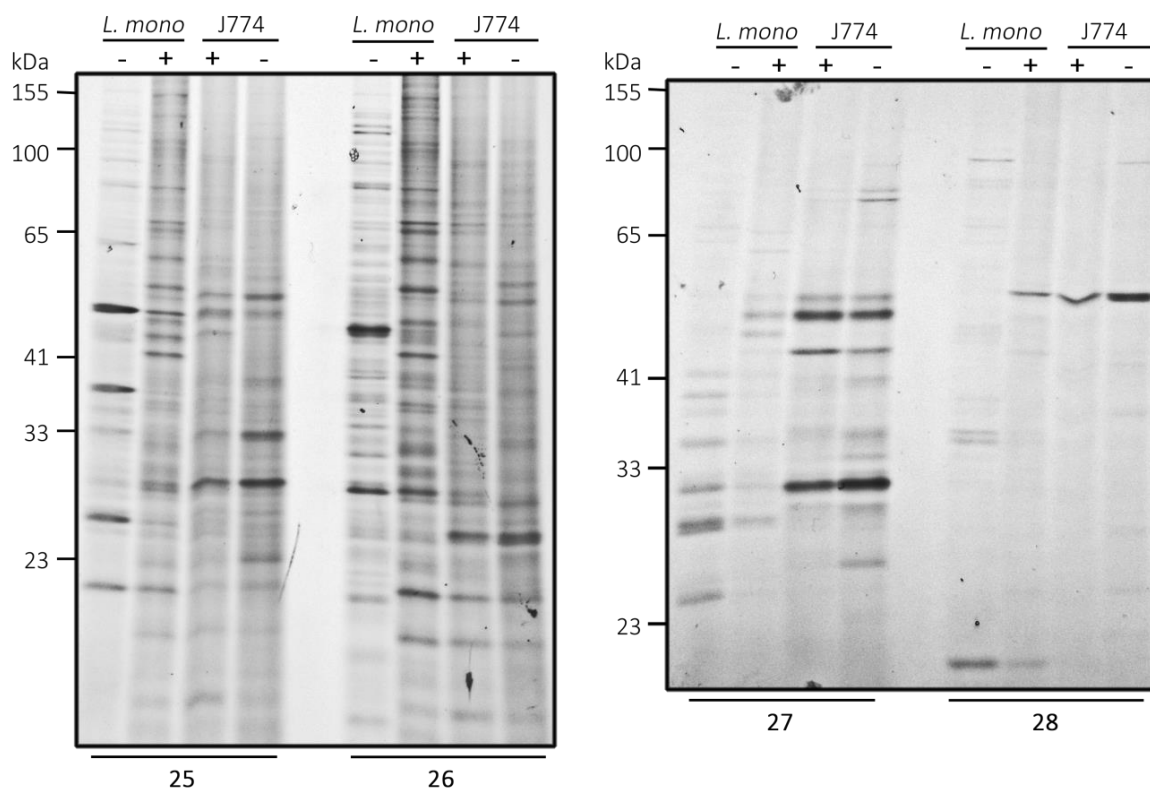
Figure III-3: Comparative *in vitro* labeling of extra- (-) versus intracellular (+) *L. monocytogenes* and infected (+) versus healthy (-) J774 macrophages with **25** (50 µM, 1 h), **26** (10 µM, 1 h), **27** (10 µM, 1 h) and **28** (50 µM, 1 h).
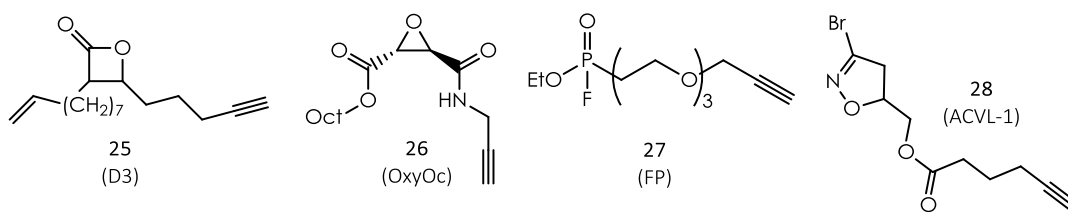
Figure III-4: Structures of β-lactone D3 (**25**), oxiran OxyOc (**26**), fluorophosphonate FP (**27**) and acivicine ACVL-1 (**28**).

Of all analyzed compounds, **25**[143-146] synthesized by Dr. Thomas Böttcher, and **26**[147] synthesized by Dr. Maximilian Pitscheider, exhibit the most promising labeling. The labeling pattern of extra- and intracellular *L. monocytogenes* are entirely different for both compounds **25** and **26**. Several so far unlabeled bands emerge in the bacterial proteome, indicating pathogenesis-associated enzymes. Smaller variations occur within the eukaryotic proteome.

3.3   COMPARATIVE IN SITU LABELING

To further evaluate the ABPP infection protocol, the feasibility of *in situ* labeling of intracellular bacteria should be determined with β-lactone **25**. After 3 h of infection, extracellular *L. monocytogenes* and infected and healthy J774 cells were incubated with 100 μM of **25** for 2 h. Thereafter the majority of infected host cells were lysed with Triton X-100 to obtain the labeled intracellular bacteria. For the detection of secreted proteins, the supernatant medium was isolated and concentrated. The comparison of *in situ* to the corresponding *in vitro* labeling with **25** is presented in .

in vitro **25** (50 µM, 1 h)   *in situ* **25** (100 µM, 2 h)
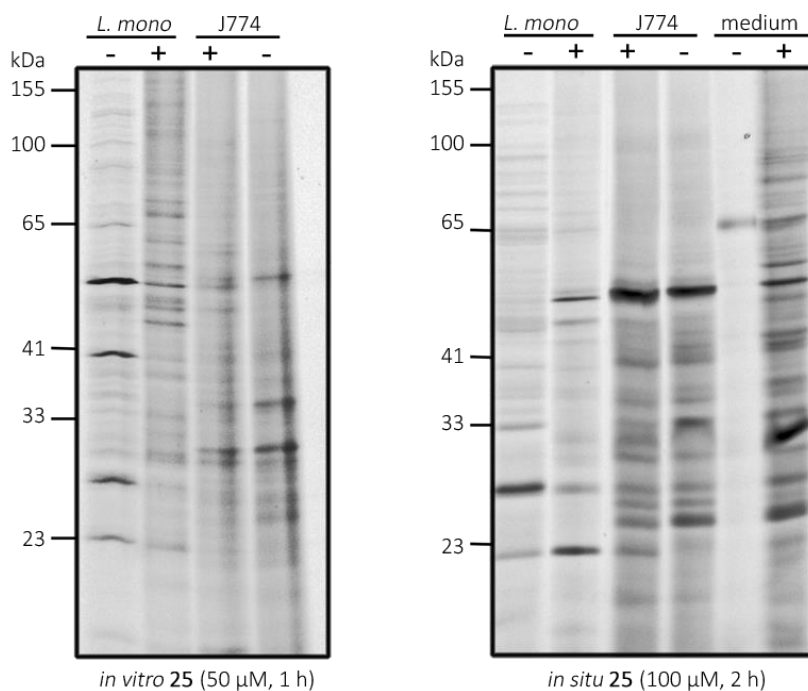
Figure III-5: Comparison of *in vitro* and *in situ* labeling with **25** of extra- (-) versus intracellular (+) *L. monocytogenes* and infected (+) versus healthy (-) J774 macrophages. In addition, *in situ* labeling of secreted proteins in the supernatant medium of infected (+) and healthy (-) macrophages.

The results demonstrate that it is possible to label bacteria intracellularly with cell permeable probes such as **25**. A direct comparison of *in vitro* and *in situ* labeling reveals differing patterns. In both cases, individual proteins are targeted with both methods. The *in situ* labeling pattern of both *L. monocytogenes* proteomes seems to differ significantly, whereas the labeling of infected and healthy J774 exhibits only small variations. Due to cell lysis, some proteins are released into the medium. Thus similar bands are obtained for the supernatant medium in addition to further probably secreted targets.

3.4   TARGET IDENTIFICATION

In a further step, the in Figure III-5 presented targets were analyzed via LC-MS/MS after biotin/avidin enrichment and trypsin digest. As a control, all labeling experiments, except the supernatant medium, were simultaneously conducted with DMSO for background determination. An overview of possible targets is given in Figure III-6 (p. 64) and the corresponding mass results are presented in Table III-1 (p. 64) for *Listerial* and in Table III-2 (p. 65) for murine protein targets.
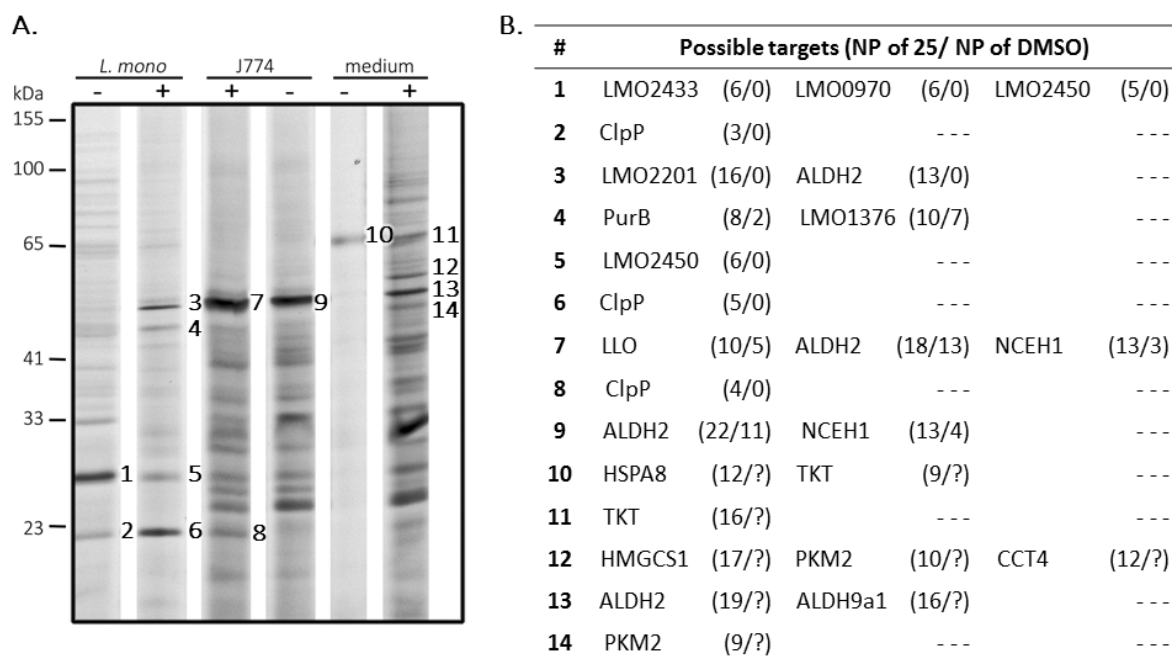
Figure III-6: **A.** Successfully analyzed bands via LC-MS/MS of *in situ* labeling with **25**. **B.** Possible targets of **25** sorted by the band number (#). The number of peptides found (NP) with probe **25** compared to the DMSO control is shown in brackets.

Table III-1: Target identification of *Listerial* proteins via LC-MS/MS. The table shows the protein accession (Acc.), molecular weight (MW), the corresponding band number (#), the protein sequence coverage (Cov.), the number of peptides (NP) and unique peptides (UNP) found and the reached peptide spectral match (PSM) and score in a single LC-MS/MS run.

Name	Acc.	MW	#	Cov.	NP	UNP	PSM	Score
LMO2433	Q8Y4K5	28.8	1	30.95	6	6	14	37.43
LMO0970, Enoyl-[acyl-carrier-protein] reductase	Q8Y8D5	28.3	1	27.10	6	6	9	22.75
LMO2450	Q8Y4I9	27.8	1	24.60	5	5	8	20.64
			5	21.77	6	6	10	24.93
ClpP, ATP-dependent Clp protease proteolytic subunit	Q9RQI6	21.6	2	18.69	3	3	7	20.48
			6	22.22	5	5	15	40.02
			8	22.22	4	4	9	24.58
LMO2201, 3-oxoacyl-[acyl-carrier-protein] synthase	Q8Y574	44.3	3	56.17	16	16	48	179.64
PurB, Adenylosuccinate lyase	Q8Y6B84	49.1	4	20.93	8	8	9	25.11

Name	Acc.	MW	#	Cov.	NP	UNP	PSM	Score
LMO1376, 6-phospho-gluconate dehydrogenase	Q8Y7B0	52.4	**4**	30.93	10	10	15	46.80
LLO, Listeriolysin O	P13128	58.7	**7**	29.49	10	10	11	33.63

Table III-2: Target identification of murine proteins via LC-MS/MS. The table shows the protein accession (Acc.), molecular weight (MW), the corresponding band number (#), the protein sequence coverage (Cov.), the number of peptides (NP) and unique peptides (UNP) found and the reached peptide spectral match (PSM) and score in a single LC-MS/MS run.

Name	Acc.	MW	#	Cov.	NP	UNP	PSM	Score
ALDH2, Aldehyde dehydrogenase, mitochondrial	P47738	56.5	**3**	29.29	13	13	26	78.17
			7	46.05	18	18	103	334.39
			9	47.40	22	21	129	401.34
			13	43.00	19	19	96	298.54
NCEH1, Neutral cholesterol ester hydrolase	Q8BLF1	45.7	**7**	35.05	13	13	42	146.25
			9	28.19	13	13	39	116.95
HSPA8, Heat shock cognate 71 kDa protein	P63017	70.8	**10**	21.83	12	12	24	77.16
TKT, Transketolase	P40142	67.6	**10**	17.98	9	9	17	43.31
			11	34.03	16	16	36	115.68
HMGCS1, Hydroxymethyl-glutaryl-CoA synthase	Q8JZK9	57.5	**12**	37.88	17	17	40	115.26
PKM2, Isoform M2 of Pyruvate kinase isozymes M1/M2	P52480-1	57.8	**12**	29.19	10	10	12	36.64
			14	23.54	9	9	14	50.08
CCT4, T-complex protein 1 subunit delta	P80315	58.0	**12**	28.01	12	12	14	40.59
ALDH9a1, Putative uncharacterized protein	Q3TG52	55.8	**13**	42.66	16	16	45	137.80

3.5 VALIDATION OF SELECTED TARGETS

3.5.1 CLPP: CASEINOLYTIC PROTEIN PROTEASE

The caseinolytic protein protease ClpP plays a major role in virulence regulation of different bacterial pathogens.[148-150] This protease is a well-known target of the β-lactone **25** in *S. aureus*, *L. monocytogenes* and other strains.[143-146] The comparative *in situ*

labeling obviously reveals an up-regulation in intracellular *L. monocytogenes*, indicated through the higher signal intensity of band #6 (Figure III-6A). In addition, preliminary experiments suggested that the detection of bacterial targets inside a host proteome, as for the emerging band #8 (Figure III-6A) which is attributed to ClpP, is restricted to high abundant proteins. Due to the small size of bacteria in relation to eukaryotic cells, their proteome is highly diluted.

3.5.2   LMO2201: SIMILAR TO 3-OXOACYL-ACP SYNTHASE

Although LMO2201 is a hypothetical protein, its gene sequence is similar to the 3-oxoacyl-[acyl-carrier-protein] synthase II alias FabF of other *Listerial* and bacterial strains. FabF is responsible for fatty acyl chain elongation and part of the type II fatty acid biosynthesis (FASII). Different antibiotic inhibitors of FabF are already known, such as cerulenin[151-153], platencin[154, 155] and platensimycin[154, 155]. For the verification of LMO2201 as target of **25**, the DNA sequence was cloned into pDEST 007 and the protein overexpressed in *E. coli* BL21. The labeling of the overexpression lysate with **25** is shown in Figure III-7.
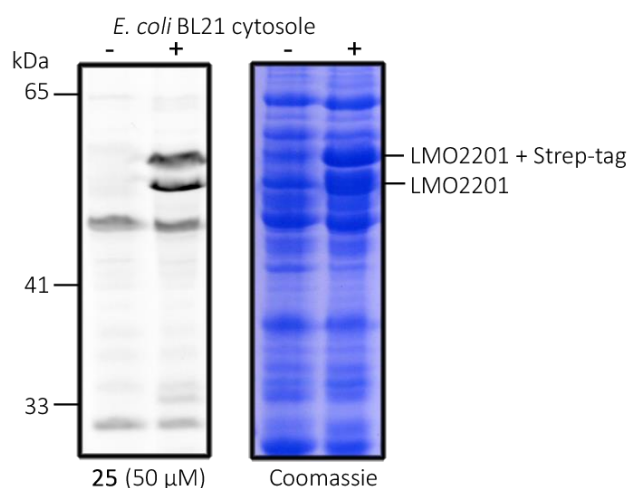
Figure III-7: Fluorescent SDS-PAGE of overexpression lysate labeled with **25** (50 µM, 1 h), compared to the corresponding coomassie staining (-= not induced, += induced). LMO2201 is expressed as a double band, with and without the Strep-tag, which are both selectively targeted.

With respect to the high amount of proteins revealed by the coomassie staining, LMO2201 is selectively targeted by **25**. Despite a molecular weight of 44.3 kDa, the

protein is running at higher weights in the SDS-PAGE, which is in line with the *in situ* labeling (band #3, Figure III-6A). LMO2201 was not detected in any analyzed probe of extracellular *L. monocytogenes*, suggesting an up-regulated expression after entering an intracellular life cycle. However, the integrative Metabolic Analysis Tool (iMAT)[156] predicts a down-regulation of the FASII biosynthesis pathway in intracellular *L. monocytogenes*, which is supported by gene expression analysis of the *fabF* gene.[157] Thus further experiments should be conducted to prove the increased expression of LMO2201. In addition the specific labeling of LMO2201 with **25** should be evaluated by binding site identification via LC-MS/MS and heat control.

3.5.3   LLO: LISTERIOLYSIN O

LLO is one of the most important virulence factors of *L. monocytogenes* and belongs to the class of cholesterol-dependent cytolysins (CDCs). These exotoxins are able to bind to the cholesterol of host membranes, which results in pore-formation via oligomerization of the CDCs.[118, 158-160] The pore-formation of LLO is pH-dependent, due to an acidic triad. At a pH of 5.5 the maximal activity is reached, which decreases drastically at higher pH-values.[118, 158-160] However, the availability of host membranes prevents LLO from inactivation at physiological temperature and pH.[160] Interestingly, peptides of LLO were solely detected in the proteome of infected macrophages (band #7, Figure III-6A) and not in intra- or extracellular *L. monocytogenes*, which is reasonable for an exotoxin required for phagosomal escape. For a further verification as target of **25**, the DNA sequence of LLO was cloned into pET 55 and the protein overexpressed in *E. coli* BL21. To prevent secretion during overexpression, the secretion signal sequence[159] was deleted by designing an appropriate forward primer for the PCR. The hemolytic activity of the overexpressed LLO was examined with several buffers on sheep blood agar plates (Heipha) after Strep-purification (Figure III-8A, p. 68).
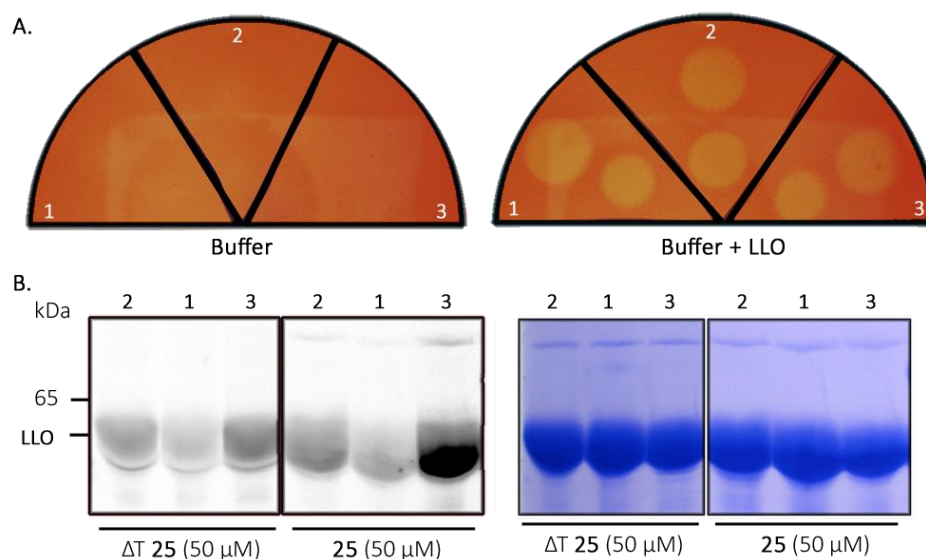
Figure III-8: A. Hemolytic activity of LLO at 37 °C in different buffers: 1= storage buffer pH 6.0, 2= PBS pH 7.4 and 3= Strep elution buffer pH 8.0. Comparable hemolysis occurs under all analyzed conditions. **B.** Labeling behavior of LLO in buffers 1-3 compared to the corresponding heat controls (ΔT) with **25** (50 µM, 1 h). Coomassie staining reveals equal amount of LLO in all lanes. The exact composition of buffers 1-3 is described in the experimental section.

The recombinantly expressed LLO exhibits a comparable hemolytic activity in all analyzed buffers. To further examine the labeling behavior of **25** under different conditions, the protein dissolved in storage buffer (pH 6.0), PBS (pH 7.4) or Strep elution buffer (pH 8.0) was first incubated for 1 h with **25** and diluted with PBS (5x) for the subsequent click reaction. The fluorescent SDS-PAGE with probe **25** (50 µM) compared to the corresponding coomassie staining is presented in Figure III-8B. The best labeling results are apparently obtained in Strep buffer 3, followed by PBS 2. The most acidic storage buffer 1 exhibits the weakest labeling. Despite heat inactivation (ΔT) LLO is still bound by **25**, however, the signal intensity decreases. This might suggest either an unspecific binding of **25**, or a high stability and/or a fast renaturation of the exotoxin. To determine the selectivity and specificity of **25** towards LLO, further experiments should be conducted such as labeling of LLO in a whole cell lysates, serial dilutions of **25** and binding site identification via LC-MS/MS. In addition, possible effects of **25** on the hemolytic activity of LLO should be analyzed by applying a hemolysis assay.

3.5.4   PKM2: Pyruvate Kinase Isozyme M2

The primary function of PKM2 is the catalysis of phosphenolypyruvate (PEP) to ADP, the last step of glycolysis.[161, 162] It also interacts with diverse biomolecules such as signaling proteins[163], transcription factors[164]and promyelocytic leukemia (PML) tumor suppressor protein[165] or pathogenesis-associated proteins such as NS5B[166] (RNA-polymerase, hepatitis C virus), PP60v-scr-tyrosine kinase[167] (oncoprotein, Rous sarcoma virus) and Opa[168] (pathogen/host cell interaction, *N. gonorrhoeae*).[162] Hence PKM2 is involved in various pathways including metabolic regulation, cellular growth, apoptosis and immunological response.[162] Interestingly PKM2 was only detected in the supernatant medium (bands #12 and #14, Figure III-6A). To verify it as target, the human recombinant analogue (ProSpec) was labeled with **25**, as presented in Figure III-9.
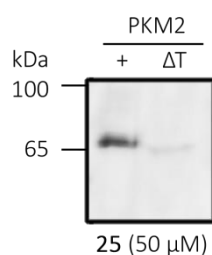
Figure III-9: Fluorescent SDS-PAGE of native (+) and heat denaturated (ΔT) recombinant PKM2 (1 µg) labeled with **25** (50 µM, 1 h).

PKM2 appears to be specifically bound by **25** as the heat control reveals a strongly decreased intensity. To determine the target selectivity, labeling of recombinant PKM2 with **25** should be conducted in whole cell lysate.

3.5.5   ALDH2: Aldehyde Dehydrogenase 2

ALDH2, the mitochondrial isoform of cytosolic ALDH1A1, exhibits a high affinity for acetaldehyde and plays a major role in the detoxification of alcohol.[79, 169-171] Other aldehydes such as 4-hydroxynonenal and acrolein are also oxidized by this enzyme.[171, 172] In addition to the dehydrogenase activity, ALDH2 functions as reductase in the biotransformation of nitroglycerin.[171, 173, 174] Peptides of ALDH2 were equally detected in all eukaryotic probes at different weights between ∼55-33 kDa, with the highest abundance in bands #7, #9 and #13 (Figure III-6A). It was also identified in the proteome

of intracellular *L. monocytogenes* (band #3, Figure III-6A), which might indicate an insufficient separation of the bacteria. To verify ALDH2 as target, the human recombinant analogue (ProSpec) was labeled with **25**, as presented in Figure III-10.
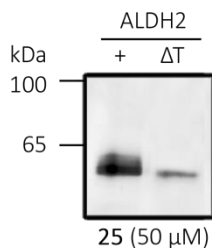
Figure III-10: Fluorescent SDS-PAGE of native (+) and heat denaturated (ΔT) recombinant ALDH2 (1 µg) labeled with **25** (50 µM, 1 h).

ALDH2 seems to be specifically bound by **25** as the heat control reveals a strongly decreased intensity. To determine the target selectivity, labeling of recombinant ALDH2 with **25** should be conducted in whole cell lysate.

3.5.6 NCEH1: NEUTRAL CHOLESTEROL ESTER HYDROLASE

The transmembrane protein NCEH1 represents a key enzyme in murine macrophages, catalyzing the hydrolysis of cholesterol ester stored in lipid droplets.[175-178] The resulting free cholesterol is effluxed by ABC transporters or other pathways. This reverse cholesterol transport is important for maintaining the intracellular cholesterol balance of mammalian cells.[178-181] Peptides of NCEH1 were detected in both the infected and healthy J774 macrophages at different weights between ∼55-33 kDa, with the highest abundance in bands #7 and #9 (Figure III-6A). To verify NCEH1 as target, the human recombinant analogue (Abnova) was labeled with **25**, as presented in Figure III-11A (p. 71).
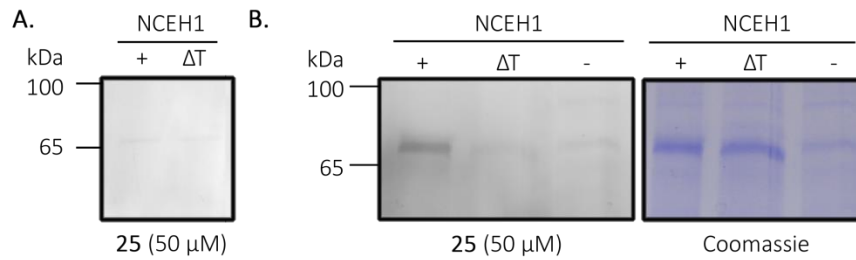
Figure III-11: Fluorescent SDS-PAGE of native (+) and heat denaturated (ΔT) recombinant NCEH1 (1 μg) labeled with **25** (50 μM, 1 h). **B.** Labeling of homologous NCEH1 overexpression lysate with **25** (50 μM, 1 h) compared to corresponding coomassie staining (+= NCEH1 vector, ΔT= heat control and -= control vector).

However, recombinant NCEH1 was not successfully labeled by **25**. As recombinant expression might lead to improper folding and thus loss of the binding site of **25**, labeling was repeated with homologous NCEH1 overexpression lysate (GenWay Biotech). The fluorescent SDS-PAGE and the corresponding coomassie staining are presented in Figure III-11B. NCEH1 exhibits solely weak labeling with **25**, which is abolished after heat denaturation. Thus it is unlikely to be a target of **25**.

4   CONCLUSION AND SUMMARY

In summary, a protocol for the proteomic labeling of intracellular *L. monocytogenes* in murine macrophages was successfully established. By the application of this new protocol it was shown that distinct proteomic changes between an extra- and intracellular life cycle of *L. monocytogenes* can be visualized *in vitro* as well as *in situ*. The *in vitro* labeling may thereby serve for the selection of suitable probe compounds for *in situ* ABPP-experiments, as presented for compounds **25**-**28**. The best *in vitro* results were obtained for β-lactone **25**, which was hence chosen for *in situ* experiments and target identification via LC-MS/MS.

Target identification yielded several interesting hits that underwent preliminary validation by labeling of the recombinantly overexpressed proteins with **25**. The *in situ* APBB experiments revealed that the virulence regulator ClpP, a known target of β-lactone **25**, is up-regulated during invasion. In addition, two so far unknown *Listerial* targets of **25**, the FabF-like LMO2201 and the virulence factor LLO, were identified in the proteome of intracellular *L. monocytogenes* and infected J774 macrophages, respectively. Thus the novel ABPP protocol contributes to the identification of pathogenesis-associated enzymes, which are not detected at an extracellular life cycle. Of the three murine hits only PKM2 and ALDH2 could be validated in contrast to NCEH1. However, PKM2 represents the most interesting eukaryotic protein, as it is already known to interact with different pathogen derived biomolecules.

5   OUTLOOK

The *in situ* labeling with **25** should be repeated to further verify the LC-MS/MS results. As the gel based separation and the following protein isolation is difficult for numerous bands, the separation should be conducted in a gel free experiment.

LLO represents the major virulence factor of *L. monocytogenes*, thus the effects of **25** on the hemolytic activity of LLO should be analyzed applying a hemolysis assay. Moreover the binding site of **25** should be identified.

As the *Listerial* FASII biosynthesis pathway is predicted to be down-regulated during infection in contrast to the experimental findings with ABPP, further experiments as stable isotope dimethyl labeling[182-184] should be conducted to prove the increased expression of LMO2201 in intracellular L. monocytogenes. Furthermore the binding site of **25** should be identified.

Finally the protocol could be extended to other pathogenic bacterial strains such as *Staphylococcus aureus* or different eukaryotic host cells.

IV Zusammenfassung

ALDEHYDDEHYDROGENASE 1 ALS NEUES TARGET DER DUOCARMYCINE

Die Duocarmycine stellen eine kleine Gruppe äußerst potenter antitumoraler Naturstoffe dar, welche ihre zytotoxische Wirkung durch sequenzspezifische Alkylierung der DNA entfalten. In Bezug auf den Mechanismus der DNA-Alkylierung können die Duocarmycine in zwei Hauptelemente unterteilt werden, die Alkylierungs- und die DNA-Bindungseinheit (Abbildung IV-1).
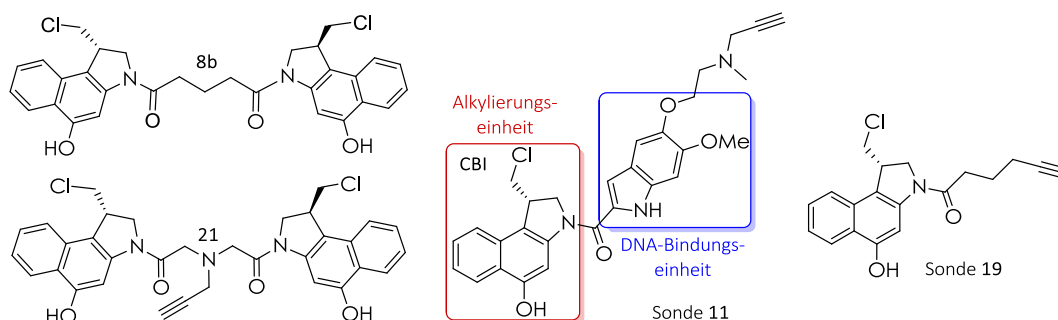
Abbildung IV-1: Aufbau der bifunctionalen Duocarmycine **8b** und **21** und der Sonden **11** und **19**.

Das in Abbildung IV-1 gezeigte bifunktionalen Duocarmycin **8b**, bestehend aus zwei CBI-Alkylierungseinheiten, die durch einen Spacer verbunden sind, stellt eines der bis dato zytotoxischsten Derivate mit einem IC$_{50}$ von 0,11 pM dar. Untersuchungen bezüglich der Alkylierungseigenschaften zeigten jedoch keine nennenswerten Interaktionen mit doppelsträngiger DNA. Daher sollten im Rahmen dieser Arbeit neue Duocarmycin-Targets mit Hilfe des aktivitätsbasierten Protein-Profilings (ABPP) identifiziert und anschließend durch diverse biochemische Methoden validiert werden.

Durch die Markierung des Proteoms von A549-Lungenkrebszellen mit **11** und die darauffolgende massenspektroskopische Analyse konnte die Aldehyddehydrogenase 1A1 (ALDH1A1) als wichtigstes Proteintarget identifizierten werden. Außerdem wurden die Cysteine 456 und 464 als Bindungsstellen der Duocarmycine mit Hilfe weiterer massenspektroskopischer Analysen identifiziert und durch Punktmutation belegt. Beide Cysteine befinden sich in der Kristallstruktur des Schafshomologs in unmittelbarer Nähe zum aktiven Zentrum, dem Cystein 303. Der Abstand beider Bindungsstellen zueinander könnte zudem eine gleichzeitige Reaktion mit beiden Alkylierungseinheiten des bifunktionalen **8b** ermöglichen. Diese Crosslinking-Hypothese konnte allerdings aufgrund geringer Diffraktion nicht durch Co-Kristallisation belegt werden. Die inhibitorischen

Eigenschaften der Verbindungen **8b** und **11** wurden zudem mit Hilfe eines zeitabhängigen ALDH1A1-Aktivitätsassays überprüft, wobei **8b** eine deutlich schnellere Inhibition bei gleichzeitig niedrigeren Konzentrationen aufwies.

Um den Anteil der ALDH1A1 an der zytotoxischen Wirkung der Duocarmycine bestimmen zu können wurden neue Derivate ohne DNA-Bindungseinheit synthetisiert, welche im Vergleich zu **11** reduzierte Zytotoxizitäten im niedrigen nanomolaren Bereich aufwiesen. ABPP-Experimente mit Verdünnungsreihen der Verbindungen **11** und **19** und A549-Zellen zeigten eine hochselektive Markierung der ALDH1A1 bei 100-fach niedrigerer Konzentration von **19** im Vergleich zu **11**. Zudem wies **19** in weiteren Aktivitätsassays eine deutlich schnellere Inhibition bei gleichzeitig niedrigeren Konzentrationen auf. *In situ*-Markierungen von A549-Zellen und anschließende Fluoreszenzmikroskopie zeigten einen drastischen Rückgang der DNA-Affinität, da das Fluoreszenzsignal von **19** und **21** nahezu ausschließlich im Zytosol der Zellen detektiert werden konnte.

Um schließlich eine direkte Verbindung zwischen der Inhibition der ALDH1A1 und der zytotoxischen Wirkung der Duocarmycine herstellen zu können, wurde ein siRNA-Knockdown der ALDH1A1 durchgeführt. Zudem wurde die Auswirkung auf das Zellwachstum mittels Proliferationsassays bestimmt. Der siRNA-Knockdown zeigte hierbei einen ähnlichen Rückgang des Zellwachstums im Vergleich zur direkten Behandlung der Zellen mit Verbindungen **19** und **21** im niedrigen nanomolaren Bereich. Somit stellt die ALDH1A1 ein wichtiges Enzym für das Zellwachstum und die Zellviabilität in A549-Zellen dar.

Bifunktionale Duocarmycin-Derivate sowie Derivate ohne DNA-Bindungseinheit entfalten somit einen Großteil ihrer Wirkung durch die Inhibition der ALDH1A1, wobei der Beitrag eventueller nicht kovalenter Targets noch nicht geklärt ist. Den Hauptgrund für die zytotoxische Wirkung von Duocarmycinen mit intakter DNA-Bindungseinheit stellt dagegen nach wie vor die sequenzspezifische DNA-Alkylierung dar.

AKTIVITÄTSBASIERTES PROTEIN-PROFILING WÄHREND DER BAKTERIELLEN INVASION

Während der Infektion einer Wirtszelle werden virulenz-assoziierte Gene pathogener

Bakterien um ein Vielfaches stärker exprimiert als im Vergleich zum extrazellulären Wachstum in Kulturmedien. Die Proteinanalyse von extrazellulär kultivierten Bakterien dürfte somit kaum die Gesamtheit aller virulenz-assoziierter Proteine erfassen können. Daher sollte im Rahmen dieser Arbeit ein ABPP-Protokoll zur *in vitro*- und *in situ*-Markierung von *listeriellem* Proteom während der Infektion eukaryotischer Wirtszellen entwickelt werden. Zudem sollten mögliche Vorteile dieser im Vergleich zur herkömmlichen Methode geprüft werden.

Das ABPP-Protokoll zur intrazellulären Markierung von *L. monocytogenes* in Mausmakrophagen wurde erfolgreich entwickelt. Darüber hinaus konnten eindeutige Unterschiede im *in vitro*-Markierungsmuster verschiedener Verbindungen im Proteom der intra- verglichen mit den extrazellulären *Listerien* beobachtet werden. Zudem zeigte das Proteom infizierter, bezogen auf das nicht infizierter Makrophagen, leichte Veränderungen in der Markierung.
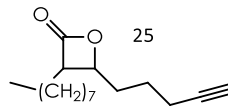
Abbildung IV-2: Structure of β-Lacton **25**.

Da sich das β-Lacton **25** (Abbildung IV-2) im *in vitro*-Experiment als vielversprechend erwies, wurde es für die *in situ*-Markierung mit anschließender massenspektroskopischer Analyse ausgewählt. Die Targetidentifizierung ergab mehrere interessante Hits, wobei 5 von 6 Targets durch Markierung der rekombinanten Enzyme prävalidiert werden konnten. Zu den bakteriellen Targets zählten, der Virulenzregulator ClpP, ein bereits bekanntes Target der β-Lactone, und zwei bis dato unbekannte Targets der β-Lactone, das FabF-ähnliche LMO2201 und der Virulenzfaktor LLO. LMO2201 wurde dabei im Proteom intrazellulär *Listerien* und LLO im Proteom infizierter Makrophagen identifiziert. Somit trägt das ABPP-Protokoll zur Identifikation neuer virulenz-assoziierter Proteine bei, welche nicht im Proteom aus herkömmlicher Kultivierung identifiziert werden konnten. Von den eukaryotischen Targets konnten nur PKM2 und ALDH2 prävalidiert werden, nicht aber NCEH1. Von diesen stellt PKM2 das interessanteste Protein dar, nachdem es für seine Interaktion mit Biomolekülen diverser Pathogene bekannt ist.

V Experimental Section

1   CELL CULTURE AND MICROBIOLOGY

1.1   MATERIAL

1.1.1   MEDIA

Media	Supplier		Composition
DMEM high glucose (4.5 g/L) without L-glutamine	PAA (USA)	+ 10% (v/v)	heat inactivated FBS
		+ 1% (v/v)	L-glutamine
DMEM low glucose (1.0 g/L) with L-glutamine	PAA (USA)	+ 10% (v/v)	heat inactivated FBS
LB	Custom made	1% (w/v)	Peptone
		0.5% (w/v)	yeast extra
		0.5 % (w/v)	NaCl
			adjusted to pH 7.5 in ddH$_2$O
BHB	Custom made	1.75% (w/v)	brain-heart-broth
		0.5% (w/v)	NaCl
		0.25% (w/v)	Na$_2$HPO$_4$
		0.2% (w/v)	D-glucose
			adjusted to pH 7.4 in ddH$_2$O
Opti-MEM I	Invitrogen (USA)		

1.1.2   AGAR PLATES

Agar Plates	Supplier
Sheep blood agar	Heipha (Germany)
Listeria selective agar (Ottaviani u. Agosti)	Heipha (Germany)

1.1.3   CELL LINES

Cell line	Species	Cell type	Medium	Supplier
A549	*Homo sapiens*	lung adenocarcinoma	DMEM high glucose	AK Tietze (Germany)
J774.1	*Mus musculus*	monocytes - macrophages	DMEM low glucose	DSMZ (Germany)

1.1.4   BACTERIAL STRAINS

Species	Strain	Medium	Supplier
Escherichia coli	BL21	LB	Novagen (Germany)
	XL1-Blue		Stratagene (Germany)
Listeria monocytogenes	EDG-e	BHB	Institute Pasteur (France)

1.1.5   BUFFER AND SOLUTIONS

Name			Composition
Trypan blue stain	0.25 g	0.5% (w/v)	Trypan blues
	0.90 g	0.9% (w/v)	NaCl
	50 mL		in ddH$_2$O, filtered
1x Trypsin/EDTA	5 mL	10% (v/v)	10x Trypsin/EDTA
	50 mL		in PBS
PBS	8.00 g	140.0 mM	NaCl
	0.20 g	2.7 mM	KCl
	1.44 g	10.0 mM	Na$_2$HPO$_4$
	0.24 g	1.8 mM	KH$_2$PO$_4$
	1000 mL		adjusted to pH 7.4 in ddH$_2$O
Washing Buffer	500 mL	10.0 mM	HEPES
	5 mL		in Hank's Balanced Salt Solution
Opsonizing Buffer	90 mL	10% (v/v)	FBS
	10 mL		in PBS
Gentamycin media	500 mL	100 µg/mL	10 mg/mL gentamycin stock
	5 mL		in DMEM low glucose
0.1% Triton-X 100	250 µL	1% (v/v)	10% Triton X-100 stock
	250 mL		in ddH$_2$O
4% Paraformaldehyde	4 g	4% (w/v)	paraformaldehyde
	100 mL		dissolved in PBS at 60 °C
0.05% Saponin	50 mg	0.05% (w/v)	saponin
	100 mL		in PBS
3% BSA, 0.1% Triton X-100	3 g	3% (w/v)	BSA
	1 mL	1% (v/v)	10% Triton X-100 stock
	99 mL		in PBS
0.5% BSA	500 mg	0.5% (w/v)	BSA
	100 mL		in PBS
DAPI stock	10 mg	1% (w/v)	DAPI
	1 mL		in ddH$_2$O

DAPI stain	1 µL	(1:20,000)	DAPI Stock
	20 mL		in ddH$_2$O
0.1% Gelatin	0.5 g	0.1% (w/v)	gelatin
	500 mL		in ddH$_2$O, autoclaved for 30 min

1.1.6   ANTIBODIES

Name	Type	Produced in	Supplier
Prestige anti-ALDH1A1	primary	rabbit	Sigma (Germany)
Atto 488 anit-rabbit lgG	secondary	goat	Sigma (Germany)

1.1.7   SIRNAS

Name	siRNA Duplex Sequenes (5' to 3')	Supplier
Silencer Select neg. control #2 = siRNA scr	-	Ambion (USA)
siRNA ALDH1A1 Moreb = siRNA #1	GGACAAUGCUGUUGAAUUUtt sense AAAUUCAACAGCAUUGUCCtt antisense	Costom made at MWG
Silencer Select s1236 = siRNA #2	CCUUCACAGGAUCAACAGAtt sense UCUGUUGAUCCUGUGAAGGct antisense	Ambion (USA)
Silencer Select s1237 = siRNA #3	GGACCAGUGCAGCAAAUCAtt sense UGAUUUGCUGCACUGGUCCaa antisense	Ambion (USA)
Silencer Select s1238 = siRNA #4	CAAUACCAAUUGAUGGAAAtt sense UUUCCAUCAAUUGGUAUUGta antisense	Ambion (USA)

1.2   METHODS

1.2.1   CRYOSTOCKS

For preparing bacterial cryostocks, a 5 mL overnight culture was pelleted at 4000 rpm for 10 min. The supernatant was discarded and the pellet was resuspended in 500 µL medium and 500 µL sterile glycerin. The cryostock was shock frozen in liquid nitrogen and stored at -80 °C.

1.2.2 CULTIVATION OF A549 CELL LINE

A549 cells were grown adherently in DMEM high glucose medium supplemented with FBS and L-glutamine at 37 °C in 5% CO_2. After reaching a confluence of 70-90% the cells were detached with 1x trypsin/EDTA and split at ratios between 1:5 and 1:10. Further experiments were conducted at confluences of 70-80%.

1.2.3 CULTIVATION OF J774 CELL LINE

After thawing, J774 cells were first grown adherently in DMEM low glucose medium supplemented with FBS and L-glutamine at 37 °C in 5% CO_2. The cells were harvested using a rubber policeman and split at 1:3 to 1:4 after reaching a confluence of $\sim$70%. At the third to fourth passage, the cell were transferred to a stirrer bottle and further cultivated in suspension at 30 rpm. To ensure a survival rate of >99%, cells were counted daily using a Neubauer improved hemozytometer and trypan blue for staining. Three times a week, the suspension culture was reduced to one fourth and the remaining cells were pelleted and resuspended in new medium. For infection experiments 7.5×10^6 or 2.1×10^7 cells were seeded out per 175 cm^2 or 500 cm^2 flask, respectively, and grown for 36 h to reach a confluence of $\sim$70%. To estimate the number of cells, one culture flask was detached and counted for every infection experiment.

1.2.4 INFECTION OF J774 CELLS WITH *L. MONOCYTOGENES*

A starter culture of *L. monocytogenes* in 5 mL BHB was inoculated by an overnight culture, freshly prepared from a cryostock, and grown for 8 h at 37 °C. Afterwards the culture was diluted in 100 mL BHB (1:100) and incubated at 37 °C overnight. The bacteria were pelleted, and resuspended in 100 mL opsonizing Buffer. After opsonization for 30 min, the bacteria were washed twice with PBS and resuspended in 100 mL DMEM low glucose without FBS. For quantifying the number of bacteria, a dilution of 1:1,000,000 (100 µL) was plated on Listeria selective agar plates and colonies were allowed to grow for 24 h at 37 °C.

J774 macrophages were initially infected with opsonized *L. monocytogenes* at a MOI of 10 for 1 h at 37 °C and 5% CO_2. The remaining bacteria-DMEM suspension (extracellular sample) was incubated at 37 °C for 6 h. In addition untreated macrophages, representing the healthy sample, were incubated with DMEM low glucose without FBS at 37 °C for 1 h at 37 °C and 5% CO_2. Afterwards infected as well as healthy cells were washed twice with washing buffer. Gentamycin medium was added for killing extracellular bacteria and the infection was allowed to prolong for 5 h. Subsequently the macrophages were washed twice with washing buffer and either lysed with cold 0.1% Triton-X 100 for 30 min on ice to gain the intracellular bacteria or detached by scraping with a rubber policeman to gain the infected or healthy J774 cells, respectively. For quantifying the number of intracellular bacteria, serial dilutions were plated on Listeria selective agar plates and colonies were allowed to grow for 24 h at 37 °C. All bacterial and eukaryotic samples were washed twice with cold PBS and stored as a pellet at -80°C.

1.2.5   IMMUNOSTAINING AND IMAGING

All solutions were filtered for immunostaining experiments. One day before experiment, coverslips were coated with 500 µL of 0.1% gelatin in 24-well plates at 37 °C and 5% CO_2 overnight. The slips were washed with PBS three times and A549 cells were seeded at a concentration of 50,000 cells per cavity 24 h prior to immunostaining. The cells were incubated with 1 µM of seco-drugs **11**, **19** or **20** for 2 h and **8b** or **21** for 4 h in DMEM high glucose at 37 °C and 5% CO_2. Lower concentrations of seco-drugs **19** and **20** with 100 nM and 10 nM were incubated for 24 h at 37 °C and 5% CO_2. The coverslips were subsequently washed three times with cold PBS, which was repeated for every further incubation step unless indicated otherwise. Afterwards the cells were fixed with 4% paraformaldehyde for 20 min at RT and permeabilized with 0.05% saponine for 20 min at RT. To evade unspecific binding of the antibodies, the samples were blocked with 3% BSA and 0.1% Triton-X 100 for 1 h at RT. Thereafter the primary anti-ALDH1A1 antibody was freshly diluted in 0.5% BSA at ratios of 1:9 – 1:19. Without further washing, the coverslips were incubated with the antibody mix at 4 °C overnight. The secondary fluorescent anti-rabbit antibody was diluted in 0.5% BSA at 1:200, applied to samples and incubated for 3 h at RT. Due to the fluorescent dye, all further incubation steps were conducted in the

dark. Afterwards the click chemistry was carried out for 1 h at RT with 1 µL rhodamine-azide (10 mM), 4 µL TCEP (52.3 mM), 12 µL TBTA (1.7 µM) in 179 µL PBS and 4 µL CuSO4 (50 mM) added last. The DNA was stained with DAPI (1:20,000) for 10 min at RT. Finally the coverslips were placed onto slide with ProLong Gold Antifade (Invitrogen) and sealed with nail polish one day later. Pictures were taken with a confocal laser scanning Fluoview FV1000 microscope (Olympus) or a fluorescent Axioplan2 microscope (Carl Zeiss). Control compounds **8b** and **20**, lacking the alkyne tag, were used to observe the background labeling caused by click chemistry. The images of seco-drugs **11**, **19** and **21** were than recorded with the same adjustments. Slides were stored at -20 °C.

1.2.6   SIRNA KNOCK DOWN OF ALDH1A1 IN A549 CELLS

For the knock down of ALDH1A1 one approved siRNA #1 (by *Moreb* et al.)[86] was synthesized by MWG and three different Silencer Select siRNAs #2-4 were purchased. A reverse transfection of A549 cells was carried out with the Lipofectamine RNAiMAX Reagent (Invitrogen) according to the manufacturer's protocol. Thus 30 pmol siRNA #1, 15 pmol siRNAs #2-4 and 15 pmol siRNA scr were separately diluted in 500 µL Opti-MEM I and gently mixed. Afterwards, 5 µL Lipofectamine was added, the samples gently mixed and incubated for 20 min at RT. The siRNA mix was transferred to a 6-well plate and 30,000 A549 cells were added in 2.5 mL DMEM high glucose. The plate was mixed by rocking and incubated for up to six days at 37 °C and 5% CO_2. After three days the medium was exchanged. To evaluate the knock down efficacy of the different siRNAs, a Western blot was carried out with actin labeling as a reference, as described in Chapter V-2.2.11.

1.2.7   PROLIFERATION ASSAY

1.2.7.1   OF SIRNAS #1 AND #3

A549 cells were reversely transfected in 6-wells with ALDH1A1 specific siRNAs #1 and #3 and the siRNA scr as described before (Chapter V-1.2.6, p. 84). The cells were cultivated for 2 days, trypsinized and seeded at a concentration of 1000 cells per cavity into two 96-well-plates. On the third and sixth day after transfection 20 µL of a filtered MTT stock

solution in PBS (5mg/mL) were added to each well and the medium thoroughly mixed by gentle pipetting. The cells were incubated for 3 h at 37 °C and 5% CO_2 to allow the MTT to be metabolized and the reaction was controlled under the microscope. Subsequently, the medium was removed and formazan resuspended in 200 µL DMSO by placing the well-plates on a shaking table for 2 min and 700 rpm. The optical density was readout at $\lambda = 570$ nm and $\lambda = 630$ nm with an Infinite 200 PRO NanoQuant microplate reader (Tecan). To determine the number of replication after 3 days of growth, the measured densities of the sixth day after transfection was divided by the densities of the third day after transfection. The numbers of replication of siRNA #1 and #3 were then calculated in relation to siRNA scr, which was set to 100%. Three independent replicates were conducted, each containing 6x wells of a 96-wells plate for one siRNA and one time point. The knock down efficiency of siRNA #1 and #3 was controlled via Western blot (Chapter V-2.2.11, p. 94) whilst the proliferation assay.

1.2.7.2 OF SECO-DRUGS 19 AND 21

To determine the effect of seco-drugs **19** and **21** on the proliferation of A549 cells, the proliferation assay in Chapter V-1.2.7.1 (p. 84) was slightly modified. Therefore, A549 cells were reversely transfected in 6-wells with siRNA scr and grown for 2 days. The cells were trypsinized and seeded at a concentration of 1000 cells per cavity into two 96-well-plates. On the third day after transfection different concentrations of seco-drugs **19** and **21** were added in DMEM high glucose to one 96-well-plate and the cells were grown for 3 days. The optical density and the number of replication were determined as described before (Chapter V-1.2.7.1, p. 84). Three independent replicates were conducted each containing 6x wells of a 96-wells plate for one time point and one concentration. The results were compared to the siRNA induced reduction of proliferation.

2 PROTEOMICS

2.1 MATERIAL

2.1.1 BUFFERS AND STAINS

Name			Composition
2xSDS-Loading buffer	496.00 mg	63 mM	Tris HCl
	5.00 mL	10% (v/v)	glycerine
	1.25 mg	0.0025% (w/v)	Bromphenol Blue
	1.00 g	2% (w/v)	sodium dodecyl sulfate
	2.50 mL	5% (v/v)	β-mercaptoethanol
	42.50 mL		in ddH$_2$O
Coomassie stain	2.5 g	0.25 % (w/v)	Coomassie Brilliant Blue
	100 mL	10 % (v/v)	glacial acetic acid
	500 mL	50 % (v/v)	ethanol absolute
	400 mL		in ddH$_2$O
Coomassie destainer	100 mL	10 % (v/v)	glacial acetic acid
	200 mL	20 % (v/v)	ethanol absolute
	700 mL		in ddH$_2$O
Storage buffer	409.0 mg	140.0 mM	NaCl
	14.9 mg	4.0 mM	KCl
	71.0 mg	10.0 mM	Na$_2$HPO$_4$
	3.9 mg	0.5 mM	DTT
	50 mL		adjusted to pH 6.0 in ddH$_2$O

2.1.2 REPORTER TAGS[185]

Rhodamin azide   Trifunctional Linker
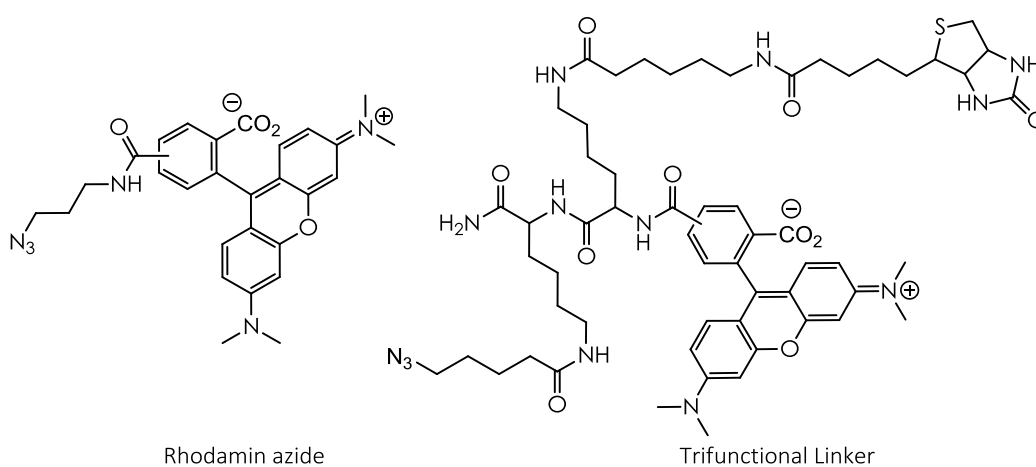
2.1.3 ANTIBODIES

Name	Type	Produced in	Supplier
Polyclonal anti-ALDH1A1	primary	rabbit	Abcam (UK)
Alexa Fluor 488 anti-rabbit IgG	secondary	donkey	Invitrogen (USA)
Anti-rabbit IgG HRP conjugate	secondary	donkey	Pierce (USA)
Polyclonal anti-Actin	primary	goat	Santa Cruz (USA)
Alexa Fluor 488 anti-goat IgG	secondary	donkey	Invitrogen (USA)
Anti-goat IgG HRP conjugate	secondary	donkey	Pierce (USA)

2.1.4 PROTEINS

Name	Supplier
ALDH1A1	ProSpec (Israel)
	Abcam (UK)
ALDH2	ProSpec (Israel)
PKM2	ProSpec (Israel)
NCEH1	Abnova (Taiwan)
	GenWay (USA)
TEV	custom made

2.1.5 CRYSTALLIZATION SCREENING SUITES

Name	Screen Size	Crystals	Supplier
PEG Suite	96	+	Qiagen (Germany)
PEG II Suite	96	+	Qiagen (Germany)
PACT Suit	96	+	Qiagen (Germany)
Wizard I and II Suite	96	+	Emerald BioSystems (USA)
pHClear Suite	96	-	Qiagen (Germany)
Protein Complex Suite	96	-	Qiagen (Germany)
AmSO$_4$ Suite	96	-	Qiagen (Germany)
JCSG Suite	96	-	Qiagen (Germany)
Classic II Suite	96	-	Qiagen (Germany)
Cryo Suite	96	-	Qiagen (Germany)
Kinase Suite	96	-	Jena Bioscience (Germany)

2.1.6   STOCK SOLUTIONS FOR CRYSTALLIZATION

Name			Composition
PEG 1000	100g	50% (w/v)	PEG 1000
	200 mL		in in ddH$_2$O
PEG 1500	100g	50% (w/v)	PEG 1500
	200 mL		in in ddH$_2$O
PEG 3350	125 g	50% (w/v)	PEG 3350
	250 mL		in in ddH$_2$O
PEG 8000	75 g	50% (w/v)	PEG 8000
	150 mL		in in ddH$_2$O
Bis Tris propane pH 8.5	25.00 g	1.0 M	Bis Tris propane
	88.5		adjusted to pH 8.5 in ddH$_2$O
HEPES pH 8.0	47.66 g	1.0 M	HEPES
	200 mL		adjusted to pH 8.0 in ddH$_2$O
HEPES pH 7.5	47.66 g	1.0 M	HEPES
	200 mL		adjusted to pH 7.5 in ddH$_2$O
CHES pH 9.5	41.46 g	1.0 M	CHES
	200 mL		adjusted to pH 9.5 in ddH$_2$O
MES pH 6.5	29.24 g	1.0 M	HEPES
	150 mL		adjusted to pH 6.5 in ddH$_2$O
PCB pH 7.0	3.84 g	0.4 M	sodium propionate
	4.28 g	0.2 M	sodium cacodylate trihydrate
	11.29 g	0.4 M	Bis Tris propane
	100 mL		adjusted to pH 7.0 in ddH$_2$O
Sodium formate	42.50 g	2.5 M	sodium formate
	250 mL		in ddH$_2$O
NaCl	29.22 g	2.5 M	NaCl
	200 mL		in ddH$_2$O
CaCl$_2$	73.51 g	2.5 M	CaCl$_2$
	200 mL		in ddH$_2$O

2.2   PROTEIN PROFILING PROTEOMICS

2.2.1   *IN VITRO* LABELING

2.2.1.1   SECO-DRUGS

For analytical *in vitro* studies A549 cells were grown to 70-90% confluence in 25 cm^2 culture flasks. The cells were detached with 1x trypsin/EDTA, washed with PBS and lysed by sonication in PBS with a Bandelin Sonopuls with 1 x 20 sec pulsed at 80% max. power

under ice cooling. Afterwards lysates were labeled with seco-drugs with varying concentrations for 4 h at RT. The samples were subjected to click chemistry as described in Chapter V-2.2.6 (p. 91).

2.2.1.2   INFECTION

For analytical *in vitro* studies J774 cells were grown to ∼70% confluence in 4x 500 cm^2 culture flasks for intracellular *L. monocytogenes* and in 2x 175 cm^2 culture flasks each for infected and healthy macrophages. The infection was conducted as described in Chapter V-1.2.4 (p. 82) and the resulting pellets, including the extracellular bacteria, were sonicated in PBS with a Bandelin Sonopuls with 7 x 20 sec pulsed at 100% max. power under ice cooling. Afterwards lysates were labeled with probes **25**-**28** for 1 h at RT. The samples were subjected to click chemistry as described in Chapter V-2.2.6 (p. 91).

2.2.2   *IN SITU* LABELING

2.2.2.1   SECO-DRUGS

For analytical or preparative *in situ* studies A549 cells were grown to 70-90% confluence in 6-Well-plates or 25 cm^2 culture flasks, respectively. The seco-drugs were used as freshly prepared dilutions in DMSO of a 100 mM stock, stored at -80 °C. After removal of the growth medium, the seco-drugs were added with varying concentrations in 2 mL DMEM high glucose at a final DMSO concentration of 0.1%. In addition a control was prepared with DMSO for background determination. The cells were than incubated for 4 h at 37 °C and 5% CO$_2$, subsequently washed with 1 mL PBS and detached with 1x trypsin/EDTA. Afterwards they were resuspended in medium, washed with PBS and lysed by sonication in PBS with a Bandelin Sonopuls with 1 x 20 sec pulsed at 80% max. power under ice cooling. The analytical and preparative samples were subjected to click chemistry as described in Chapter V-2.2.6 and V-2.2.7 (p. 92), respectively.

2.2.2.2   INFECTION

For analytical and preparative *in situ* studies J774 cells were grown to ～70% confluence in 10x 175 cm^2 culture flasks for the intracellular *L. monocytogenes* and in 3x 175 cm^2 culture flasks each for infected and healthy macrophages. The infection, described in Chapter V-1.2.4 (p. 82), was slightly modified. Thus 4 h after the initial infection 2/3 of the flasks were incubated with 100 µM β-lactone **25** for 2 h at 37 °C and 5% CO$_2$, whereas 1/3 was incubated with DMSO for background determination. In addition 25 mL of the extracellular *L. monocytogenes* were labeled with **25** or DMSO for 2 h at 37 °C, respectively. Subsequently the macrophages were washed twice with washing buffer and the supernatant medium was concentrated by centrifugation, applying an Amicon filter unit (MWCO 10 kDa, Milipore). The samples for intracellular bacteria were lysed with cold 0.1% Triton-X 100 for 30 min on ice and the samples for infected or healthy macrophages were detached by scraping with a rubber policeman. All bacterial and eukaryotic probes were washed twice with cold PBS and the pellets were lysed by sonication in PBS with a Bandelin Sonopuls with 7 x 20 sec pulsed at 100% max. power under ice cooling. The analytical and preparative samples were subjected to click chemistry as described in Chapter V-2.2.6 and V-2.2.7 (p. 91), respectively.

2.2.3   COMPETITIVE LABELING

The competitive labeling was conducted with 0.5 µg of purchased recombinant ALDH1A1 and a 10- to 40-fold excess of the competitor **8b** to probe **11**. ALDH1A1 was first incubated with either **8b** or DMSO as a control for 12 h at RT. Subsequently, the samples were labeled with 5 µM **11** for 6 h at RT and subjected to click chemistry as described in Chapter V-2.2.6 (p. 91).

2.2.4   HEAT CONTROL

For heat denaturation 2% SDS (w/v) were added to the proteome, which was subsequently heated for 15 min at 96 °C. Thereafter the proteome was allowed to cool to RT and it was further treated as the corresponding positive controls.

2.2.5 PROTEOME CONCENTRATION

2.2.5.1 BRADFORD ASSAY

The Bradford Assay represents a quick and semiquantitative method to determine the concentration of proteins in solution. In contrast to the BCA Protein Assay (Chapter V-2.2.5.2), it is compatible with reducing agents. The Bradford reagent, Roti-Quant (Roth) was freshly diluted with ddH$_2$O (1:4) and the solution was filtered. To set up a standard curve, serial dilutions in ddH$_2$O of 0, 0.25, 0.5, 0.75, 1.0 and 1.5 mg/mL BSA were prepared, to yield a total volume of 40 µL. Afterwards, the serial dilutions and the proteome samples were incubated with 2 mL Roti-Quant solution for 1 min, which induces a complex formation between Brilliant Blue G and the proteins. The OD$_{595}$ of the formed complex was finally measured with a BioPhotometer (Eppendorf).

2.2.5.2 BCA PROTEIN ASSAY

The BCA Protein Assay represents a more sensitive and less variable method in comparison to the Bradford Assay (Chapter V-2.2.5.1). In addition it is compatible with detergents. The Roti-Quant universal (Roth) reagents 1 and 2 were freshly mixed at a ratio of 15:1. To set up a standard curve, serial dilution in ddH$_2$O of 0, 25, 50, 100, 200 and 400 µg/mL BSA were prepared, to yield a total volume of 50 µL. Afterwards, the serial dilutions and the proteome samples were incubated with 100 µL Roti-Quant universal mix for 15 min at 60 °C, which induces the formation of a Cu^{2+}-protein complex. The following reduction of Cu^{2+} to Cu^{1+} results in a Cu^{1+}-BCA complex. The absorption of the Cu^{1+}-BCA complex was finally measured at $\lambda = 503$ nm in 96-well-plates with an Infinite 200 PRO NanoQuant microplate reader (Tecan). All measurements were carried out as triplicates.

2.2.6 ANALYTICAL STUDIES

For analytical studies rhodamine azide was appended to the labeled proteins via click chemistry. Therefore 0.5 µL rhodamine-azide (10 mM), 1 µL TCEP (52.3 mM) and 3 µL TBTA (1.7 µM) were added to 47 µL proteome (1-2 mg/mL) at once. Subsequently the cycloaddition was initiated by the addition of 1 µL CuSO$_4$ (50 mM). The reaction mix was

gently vortexed and incubated for 1 h at RT. Afterwards the click chemistry was quenched by the addition of 50 µL 2xSDS-loading buffer and 50 µL of the resulting proteome mixture were applied on a 10% polyacrylamide gel. After SDS-PAGE, fluorescence was recorded in a Fujifilm Las-4000 Luminescent Image Analyzer with a Fujinon VRF43LMD3 Lens and a 575DF20 filter. Subsequently to the fluorescent readout, the gel was stained with coomassie overnight at RT. Afterwards it was incubated with comassie destainer for several hours and finally with H_2O.

2.2.7 PREPARATIVE ENRICHMENT

For preparative enrichment a trifunctional linker containing rhodamine, biotine and an azide was appended to the labeled proteins. Therefore 1 µL trifunctional linker (10 mM), 10 µL TCEP (52.3 mM) and 30 µL TBTA (1.7 µM) were added to 500 µL proteome (2 mg/mL) at once. Subsequently the cycloaddition was initiated by the addition of 10 µL $CuSO_4$ (50 mM). The reaction mix was gently vortexed and incubated for 1 h at RT. To control for unspecific protein binding on avidin-agarose beads, the enrichment was carried out with labeled samples and their corresponding DMSO control. After click chemistry, proteins were precipitated using an equal volume of cold acetone at -21 °C overnight. The samples were centrifuged at 13,000 rpm for 10 min and the supernatant was discarded. The resulting pellet was washed twice with 200 µL cold methanol and resuspended by sonication. Subsequently, the pellet was dissolved in 1 mL 0.4% SDS in PBS by sonication and incubated under gentle mixing with 50 µL of avidin-agarose beads (Sigma-Aldrich) for 1-3 h at RT. The beads were washed three times with 1 mL of 0.2% SDS in PBS, twice with 1 mL of 6 M urea and three times with 1 mL 0.2% SDS in PBS. The proteins were dissociated from the beads by the addition of 50 µL of 2xSDS-loading buffer and heating for 6 min at 96 °C. The complete samples were applied on a 10% SDS-PAGE and the fluorescence was recorded in a Fujifilm Las-4000 Luminescent Image Analyzer with a Fujinon VRF43LMD3 Lens and a 575DF20 filter. The enriched gel bands as well as the corresponding DMSO controls were isolated, washed and digested via trypsin or chymotrypsin as described previously.[186] The MS-analysis is described in Chapter V-2.2.9 (p. 93).

2.2.8 BINDING SITE IDENTIFICATION

To discover the binding site of the duocarmycin derivative in ALDH1A1, the recombinant enzyme was labeled with **8b** and **11.** Therefore 1 µL of **8b** (2.5 µM) and **11** (10 µM) was incubated with 11 µg and 50 µg ALDH1A1, respectively, in 100 µL Tris-HCl for 4-12 h at RT. Afterwards, the buffer was exchanged to NH_4HCO_3 (25 mM), using a centrifugal filter device (MWCO 30 kDa, Milipore). Finally 1 µL chymotrypsin (0.01 nmol) and 1 µL $CaCl_2$ (100 mM) were added and the digestion mix was incubated for 16 h at RT. After chymotryptic digest, the peptides were desalted with ZipTips (Milipore), separated by LC and analyzed by high resolution mass spectra, as described in Chapter V-2.2.9 (p. 93).

2.2.9 MASS SPECTROMETRY AND BIOINFORMATICS

The digested peptides were loaded onto a Dionex C18 Nano Trap Column (100 µm) and subsequently eluted and separated by a Dionex C18 PepMap 100 (3 µm) column. The separation was followed by tandem and high resolution MS using a coupled Dionex Ultimate 3000 LC-Thermo Finnegan LTQ-FT MS system. For analyzing the mass spectrometry data, the software "BioWorks" and "Proteome Discoverer 1.3" (Thermo Sientific) were applied in case of seco-drug **11** and β-lactone **25**, respectively, using the SEQUEST algorithm to search against the corresponding databases. The search was limited to peptide fragments of the respective digestion method (trypsin / chymotrypsin), two missed cleavage sites, monoisotopic precursor ions and a peptide tolerance of <10 ppm. Filters were set to further refine the search results. The X_{corr} vs. charge state filter was set to X_{corr} values of 1.5, 2.0 and 2.5 for charge states +1, +2 and +3, respectively. The number of different peptides has to be ≥ 2 and the peptide probability filter was set to < 0.001. These filter values are similar to others previously reported for SEQUEST analysis.[187]

2.2.10 PROTEIN CONCENTRATION

The concentration of purified recombinant proteins was determined using the Infinite 200 PRO NanoQuant microplate reader (Tecan). 1.5 µL protein solution was applied to the NanoQuant Plate and measured at λ = 280 nm and 310 nm for correction, which

resulted in OD_{280c}. In addition 1.5 µL protein buffer was measured for background determination (OD_{280c_BG}). In combination with the slice thickness d and the protein specific extinction coefficient ε the protein concentration c was calculated according to the following equation.

$$c = \frac{OD_{280c} - OD_{280c\_BG}}{d \times \varepsilon}$$

Extinction coefficients were obtained by the ExPASy Protparam tool (Swiss Institute of Bioinformatics).

2.2.11 WESTERN BLOT (IMMUNOBLOTTING)

To determine the total amount of protein of all cell lysates a BCA assay was performed using Roti-Quant Universal Reagenz 1 and 2 (Roth) according to manufacturer's protocol. The absorption was then measured in triplicates at $\lambda = 503$ nm with an Infinite 200 PRO NanoQuant microplate reader (Tecan) and the amount of protein adjusted to 2 mg/mL. If the cells were pretreated with seco-drug **19**, rhodamine was attached by click chemistry as described before. After separation by 12% SDS-Page the proteins were transferred to a nitrocellulose membrane (Whatman) at 100 V for 90 min using a Mini Trans-Blot Cell (Biorad). The membrane was then blocked with 5% milk for 1 h and incubated with primary antibody overnight at 4 °C and subsequently with secondary antibody for 2 h at RT. Fluorescence of secondary antibodies and rhodamine was recorded in a Chemidoc MP System (Biorad) and the data was analyzed by the Image Labe image acquisition and analysis software (Biorad). Primary antibodies used for immunoblotting were rabbit anti-ALDH1A1 (Abcam) and goat anti-actin (Santa Cruz). Secondary antibodies used Figure II-26B (p. 40) were Alexa Fluor 488 donkey anti-rabbit (Invitrogen) and Alexa Fluor 488 donkey anti-goat (Invitrogen). Secondary antibodies used in Supplementary Figure II-33 (p. 46) and Figure II-34C (p. 47) were Pierce donkey anti-rabbit HRP and Pierce donkey anti-goat HRP.

2.3 FUNCTIONAL PROTEOMICS

2.3.1 TIME-DEPENDENT ALDH1A1 *IN VITRO* ACTIVITY ASSAY

2.3.1.1 PURCHASED ALDH1A1

The ALDH1A1 activity assay was slightly modified from existing protocols.[188] To ensure the formation of the corresponding drug, seco-drugs **8b** and **11** were pre-incubated in Tris-HCl (50 mM; pH 8.5) for 2 h at 25 °C at different concentrations. Subsequently, 1 µg ALDH1A1 was added to give an enzyme concentration of 360 nM in a total volume of 50 µL. The incubation proceeded for 1 h, 2 h, 4 h, 8 h and 24 h at 25 °C. Afterwards, 50 µL substrate mixture containing 50 mM Tris-HCl, 100 mM KCl, 5 mM β-mercaptoethanol, 1 mM β-NAD$^+$ and 100 µM retinal were added to initiate the enzymatic reaction. The product formation of NADH was monitored by measuring the absorption increase at $\lambda = 340$ nm at 37 °C in 96-well-plates with an Infinite 200 PRO NanoQuant microplate reader (Tecan). Heat denatured and not inhibited ALDH1A1 served as negative and positive controls, respectively. All measurements were carried out as triplicates.

2.3.1.2 A549 LYSATES

To ensure the formation of the corresponding drug, seco-drug **8b** and **11** were pre-incubated in Tris-HCl (50 mM; pH 8.5) for 2 h at 25 °C at different concentrations. Subsequently, 2 µL A549 lysate was added to give a total volume of 50 µL and incubated for different periods of time at 25 °C. Afterwards, 50 µL substrate mixture containing 50 mM Tris-HCl, 100 mM KCl, 5 mM β-mercaptoethanol, 1 mM β-NAD$^+$ and 10 mM propanal were added to initiate the enzymatic reaction. The product formation of NADH was monitored by measuring the absorption increase at $\lambda = 340$ nm at 37 °C in 96-well-plates with an Infinite 200 PRO NanoQuant microplate reader (Tecan). Lysates treated with 1% DMSO and heat denatured lysates served as positive and negative controls, respectively. All measurements were carried out as triplicates and repeated with substrate mixture lacking propanal to determine the rate of NAD$^+$ reduction by other enzymes. Reduction by other enzymes was not observed.

2.3.1.3 RECOMBINANT AND PURIFIED ALDH1A1

To ensure the formation of the corresponding drug, seco-drug **11**, **19** and **21** were pre-incubated in PBS for 1 h at 30 °C at different concentrations. 1 µL purified wild type ALDH1A1 (4 µM; Chapter V-3.2.4.3, p. 109) was added to give an enzyme concentration of 80 nM in a total volume of 50 µL. The incubation proceeded for 3 h, 8 h and 24 h at 30 °C. Afterwards, 50 µL substrate mixture containing 50 mM Tris-HCl, 100 mM KCl, 5 mM β-mercaptoethanol, 1 mM β-NAD$^+$ and 10 mM propanal were added to initiate the enzymatic reaction. The product formation of NADH was monitored by measuring the absorption increase at λ = 340 nm at 37 °C in 96-well-plates with an Infinite 200 PRO NanoQuant microplate reader (Tecan). All measurements were carried out as triplicates.

2.3.2 ESTIMATION OF THE CONCENTRATION OF ALDH1A1 IN A549 LYSATE

To estimate the concentration of ALDH1A1 in A549 lysates, a serial dilution of recombinant ALDH1A1 and different volumes of A549 cell lysate were labeled with **11**. Afterwards, the fluorescent scans were analyzed by Multi Gauge (Fujifilm) to determine the absorption of the single bands within the tagged areas (Figure V-1A/B).
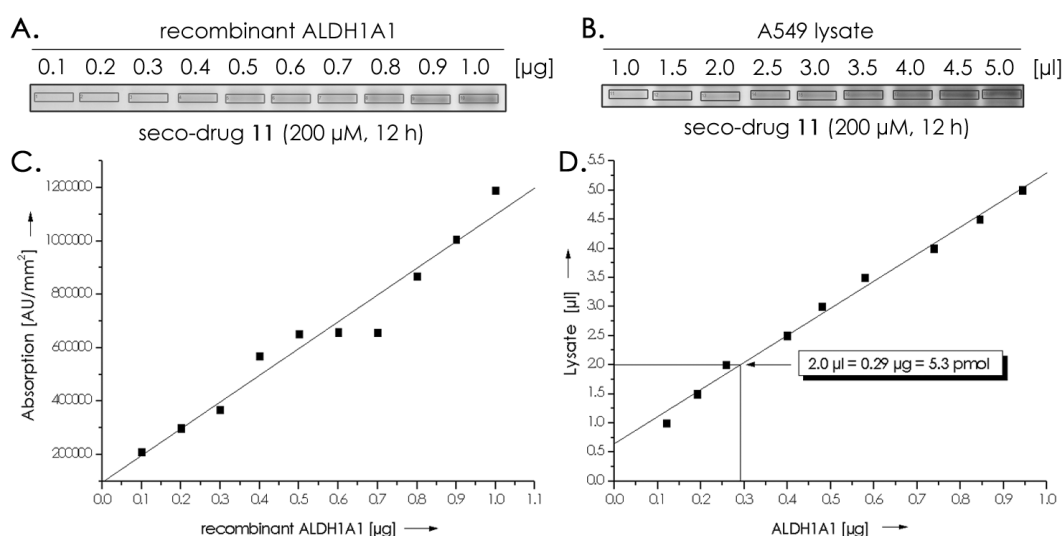
Figure V-1 (previous page): Estimation of the concentration of ALDH1A1 in A549 lysate. **A.** Fluorescent SDS analysis of recombinant ALDH1A1 labeled with seco-drug **11** (200 µM, 12 h). **B.** Fluorescent SDS analysis of A549 lysate labeled with seco-drug **11** (200 µM, 12 h). **C.** Absorption curve of recombinant ALDH1A1. **D.** Linear fit of different A549 lysate volumes against the extrapolated amount of ALDH1A1.[73]

A standard curve of absorption against the amount of recombinant ALDH1A1 was applied to determine a relation between absorption and the deployed amount of ALDH1A1 (Figure V-1C). The amount of ALDH1A1 contained in A549 lysate was then extrapolated from the measured absorption values and plotted against the volume of A549 lysate (Figure V-1D). The linear fit reveals an approximate amount of 0.29 µg ALDH1A1 contained in 2.0 µL of A549 lysate, the volume applied in the activity assay, which corresponds to 5.3 pmol or 106 nM (50 µL).

2.3.3 HEMOLYTIC ACTIVITY

To control for the hemolytic activity, 5 µg/µL purified LLO (Chapter V-3.2.4.5, p. 110) was dissolved in three different buffers: Strep elution buffer (pH 8.0), storage buffer (pH 6.0) and PBS (pH 7.4). 5 µL and 10 µL of each buffer mix were added to a 5% sheep blood agar plate and incubated at 37 °C overnight. In addition, the experiment was simultaneously conducted with pure buffer solutions. Hemolysis of the erythrocytes resulted in a color change to yellow, which indicated LLO activity.

2.4 STRUCTURAL PROTEOMICS

2.4.1 CRYSTALLIZATION OF RECOMBINANT ALDH1A1-STREP

For the initial screening of ALDH1A1-Strep, high throughput screens were conducted with a Phoenix robot (Art Robbins Instruments) in a 96-well format at 20 °C and 70% humidity. At first ALDH1A1 was freshly isolated, purified (Chapter V-3.2.4.1, p. 108) and concentrate to 10 mg/mL in Tris-HCl (100 mM, pH 8.5). Subsequently, the protein was screened against various crystallization screening suits (Chapter V-2.1.5, p. 87) in a 200 nL scale. Therefore the different defined solutions were transferred into Intelli-Plates 96-3 (Art Robbins Instruments). Afterwards ALDH1A1 was added to droplets of the varying reservoir solution in ratios of 1:1, 1:2 and 1:3 (protein:reservoir) and the plates

were hermetically sealed with a transparent plastic foil by the Quick Combi Sealer Plus (HJ-Bioanalytik). Crystals were allowed to grow at 4 °C and 20 °C for two weeks by the sitting drop vapor diffusion method. Crystals were obtained at 4 °C within the PACT suit at the following composition:

Crystallization suite	Temperature	Composition	
PACT suite	4 °C	100 mM	Bis Tris propane (pH 8.5)
		200 mM	sodium formate
		20% (w/v)	PEG 3350

The initial hit conditions were manually optimized in SuperClear Pregreased 24-well plates (Crystalgen) in a 3-4 µL scale, applying the hanging drop vapor diffusion method. The composition of each reservoir was slightly modified and calculated with MakeTray (Hampton Research) for the stock solutions in Chapter V-2.1.6 (p. 88) and a total reservoir volume of 1 mL. 1-2 µL of ALDH1A1 (5 mg/mL or 10 mg/mL) were added to 2 µL reservoir solution on plastic cover slips in ratios of 1:1 and 1:2 and gently mixed by pipetting. After two weeks at 4 °C, crystals were obtained under following conditions:

Concentration	Temperature	Ratio	Composition	
5 mg/mL	4 °C	1:1	100 mM	Bis Tris propane (pH 8.5)
			150-200 mM	sodium formate
			19-20% (w/v)	PEG 3350
10 mg/mL	4 °C	2:1	100 mM	Bis Tris propane (pH 8.5)
			10-40 mM	sodium formate
			11-12% (w/v)	PEG 3350

The resulting crystals were either initially analyzed at the X8 PROTEUM in-house generator or shock frozen in cryo buffer and stored in liquid nitrogen.

2.4.2 CRYSTALLIZATION OF RECOMBINANT WILD TYPE ALDH1A1

ALDH1A1 was freshly isolated, digested, purified (Chapter V-3.2.4.3, p. 109) and concentrate to 6 mg/mL, 12 mg/mL and 20 mg/mL in Tris-HCl (100 mM, pH 8.5).

Subsequently, the protein was screened against various crystallization screening suits (Chapter V-2.1.5, p. 87) in a 200 nL scale with a Phoenix robot (Art Robbins Instruments). Three different concentrations of ALDH1A1 were added to droplets of the varying reservoir solution in a ratio of 1:1 and the plates were hermetically sealed. Crystals were allowed to grow at 4 °C and 20 °C for 1-2 weeks. Crystal were obtained at 4 °C within the Wizard suit and at 20 °C within the PEG and the PEG II suite at the following compositions:

Crystallization suite	Temperature	Composition	
Wizard I and II suite	4 °C	100 mM	CHES (pH 9.5)
		200 mM	NaCl
		10% (w/v)	PEG 8000
PEG suite	20 °C	100 mM	MES (pH 6.5)
		25% (w/v)	PEG 1000
PEG II suite	20 °C	100 mM	HEPES (pH 7.5)
		20% (w/v)	PEG 1500
PEG II suite	20 °C	100 mM	HEPES (pH 7.5)
		25% (w/v)	PEG 1000

The initial hit conditions were manually optimized in a 4 µL scale. 2 µL of ALDH1A1 (4-38.0 mg/mL) were added to 2 µL reservoir solution on glass cover slips in a ratio of 1:1 and gently mixed by pipetting. The plates were incubated at 4 °C or 20 °C for 1-2 weeks. Crystals were obtained at 4°C under following conditions:

Concentration	Temperature	Ratio	Composition	
28 mg/mL	4 °C	1:1	100 mM	CHES (pH 9.5)
			300 mM	NaCl
			16% (w/v)	PEG 8000
38 mg/mL	4 °C	1:1	100 mM	CHES (pH 9.5)
			150 mM	NaCl
			4% (w/v)	PEG 8000
4 mg/mL	4 °C	1:1	100 mM	Bis Tris propane (pH 8.5)
			250 mM	sodium formate
			21% (w/v)	PEG 3350

The resulting crystals were either initially analyzed at the X8 PROTEUM in-house generator or shock frozen in cryo buffer and stored in liquid nitrogen.

2.4.3   ADDITIVES

ALDH1A1 was freshly isolated, digested, purified (Chapter V-3.2.4.3, p. 109) and concentrate to 5 mg/mL, 10 mg/mL and 20 mg/mL in a solution of 50 mM Tris-HCl (pH 8.5), 100 mM KCl, 5 mM β-mercaptoethanol and 1 mM β-NAD$^+$. Subsequently, the protein was screened against various crystallization screening suits (Chapter V-2.1.5, p. 87) in a 200 nL scale with a Phoenix robot (Art Robbins Instruments). Three different concentrations of ALDH1A1 were added to droplets of the varying reservoir solution in a ratio of 1:1 and the plates were hermetically sealed. Crystals were allowed to grow at 4 °C and 20 °C for several weeks. After ～5 days crystal were obtained at 4 °C within the PACT suit at the following composition:

Crystallization suite	Temperature	Composition	
PACT	4 °C	100 mM	PCB (pH 7.0)
		25% (w/v)	PEG 1500

The initial hit conditions were manually optimized in a 3 µL scale. 1 µL of ALDH1A1 (5 mg/mL and 10 mg/mL) were added to 2 µL reservoir solution on glass cover slips in a ratio of 1:2 and gently mixed by pipetting. The plates were incubated at 4 °C for two weeks. After one day crystals were observed at 4°C under following conditions:

Concentration	Temperature	Ratio	Composition	
10 mg/mL	4 °C	1:2	100 mM	PCB (pH 7.0)
			29% (w/v)	PEG 1500

However, the crystals could not be reproduced.

2.4.4 CRYSTAL DEHYDRATION

Easy crystal dehydration can be achieved by incubating the crystal with saturated salt solutions in a closed environment. Due to the salts specific relative humidity, the solvent content can be decreased by vapor diffusion in a reproducible and gradual dehydration. Depending on the salt, relative humidities of 11% (LiCl) to 97% (K_2SO_4) can be achieved at RT according to *Rockland* et al.[99] However, the range between 68-93% represents the most relevant relative humidities for protein crystallography.

Salt		Solubility g/mL	Relative humidity
Potassium sulfate	K_2SO_4	0.12	97%
Potassium nitrate	KNO_3	0.38	93%
Potassium chloride	KCl	0.40	86%
Sodium chloride	NaCl	0.37	75%

For dehydration 20 µL of the above described salt solutions (freshly prepared) were injected into MicroRT capillaries (MiTeGen) with gel-loading pipette tips. Crystals obtained in Chapter V-2.4.1 (p. 97) were harvested and the capillaries were drawn over the mounting loops and fixed at the goniometer bases to create a sealed environment. Afterwards, crystals and salt solutions were allowed to equilibrate for 0.5 h to 2 h at RT. Thereafter they were either initially analyzed at the X8 PROTEUM in-house generator or shock frozen and stored in liquid nitrogen.

2.4.5 DATA COLLECTION

Initial X-ray diffraction analysis was conducted at the X8 PROTEUM in-house generator, featuring a MICROSTAR microfocus CuKα rotating anode X-ray source, a PLATINUM[135] CCD detector and a 4-cirlce KAPPA goniometer. In addition, one dataset was collected at the PXI beamline of Swiss Light Source (SLS), Villigen, Switzerland, consisting of 180 frames with 1 ° oscillation and 30% beam transmission. Data processing was performed by using the program package XDS (Kabsch[189]). The crystal structure of human ALDH1A1 was solved by molecular replacement, using the coordinates of sheep ALDH1A1 (PDB code 1BXS) with the program PHASER (McCoy[190]) The model analysis was performed with COOT (Emsley, Cowtan[92, 191]).

3 GENOMICS

3.1 MATERIAL

3.1.1 BUFFERS

Name			Composition
50x TAE buffer stock	242 g	2.0 M	Trisma base
	57 mL	1.0 M	glacial acetic acid
	29 g	0.1 M	EDTA
	1000 mL		adjusted to pH 7.0 in ddH$_2$O
1x TAE buffer	20 mL	2% (v/v)	50x TAE buffer stock
	980 mL		in ddH$_2$O
TE buffer	12.1 mg	10 mM	Trisma Base
	2.9 mg	1 mM	EDTA
	10 mL		adjusted to pH 8.0 in ddH$_2$O
6x DNA loading buffer	250 mg	0.25% (w/v)	Bromephenol blue
	250 mg	0.25% (w/v)	xylen cyanol
	33 mL	33% (v/v)	Tris-HCl (150 mM)
	60 mL	60% (v/v)	glycerin
	7 mL		in ddH$_2$O
10000x ATET stock	20 mg	2 g/L	anhydrotetracyclin
	10 mL		in DMF
1000x IPTG stock	2.38 g	1 M	IPTG
	10 mL		in ddH$_2$O
Strep binding buffer	15.8 g	100.0 mM	Tris-HCl
	8.8 g	150.0 mM	NaCl
	0.3 g	1.0 mM	EDTA
	1000 mL		adjusted to pH 8.0 in ddH$_2$O
Strep elution buffer	27 mg	2.5 mM	desthiobiotin
	50 mL		in strep binding buffer
TEV cleavage buffer	394.0 mg	50 mM	Tris-HCl
	7.3 mg	0.5 mM	EDTA
	7.7 mg	1 mM	DTT
	50 mL		adjusted to pH 8.0 in ddH$_2$O
Gefi buffer	3.16 g	20 mM	Tris-HCl
	5.87 g	100 mM	NaCl
	1000 mL		adjusted to pH 7.0 in ddH$_2$O

3.1.2 ENZYMES

Name	Supplier
Phusion High Fidelity DNA Polymerase	NEB (Germany)
BP Clonase II enzyme mix	Invitrogen (USA)
LR Clonase II enzyme mix	Invitrogen (USA)
DpnI	Promega (USA)

3.1.3 PLASMIDS

Name	Tags	Promotor	Res	Supplier
pDONR 201	-	-	Kan	Invitrogen (USA)
pDEST 007	N-Strep	tet	Amp	Custom made
pET 55	N-Strep, C-His	T7	Amp	Novagen (Germany)
ALDH1A1- Gateway® PLUS Shuttle Clone	-	-	Kan	Gene Copeia (USA)
TEV-ALDH1A1-ovis-pMK-RQ	-	-	Kan	GeneArt (Germany)

3.1.4 PRIMERS

Name		Primer Sequence (5' to 3')
ALDH1A1	forw	GGAACAGTGTGGGTGAATGCCTATGGCGTGGTAAGTGC
C456A	rev	GCACTTACCACGCCATAGGCATTCACCCACACTGTTCC
ALDH1A1	forw	CGTGGTAAGTGCCCAGGCCCCCTTTGGTGGATTC
C464A	rev	GAATCCACCAAAGGGGGCCTGGGCACTTACCACG
ALDH-TEV	for	GGGGACAAGTTTGTACAAAAAAGCAGGCTTTGAGAATCTTTATTTTCAGTCATCCTCAGGCACGCCAG
	rev	GGGGACCACTTTGTACAAGAAAGCTGGGTGTTATGAGTTCTTCTGAGAGATTTTCACTG
LLO	for	GGGGACAAGTTTGTACAAAAAAGCAGGCTTTGATGCATCTGCATTCAATAA
	rev	GGGGACCACTTTGTACAAGAAAGCTGGGTGTTATTCGATTGGATTATCTACT
LMO2201	for	GGGGACAAGTTTGTACAAAAAAGCAGGCTTTATGGATAAGAGAAGAGTAGT
	rev	GGGGACCACTTTGTACAAGAAAGCTGGGTGTTAGTCTTCTATTCTTTTAAATAC

3.2   METHODS

3.2.1   PCR FOR GATEWAY

The Gateway Technology (Invitrogen) requires *att*B recombination sites for cloning PCR products into DONR-vectors. Primers were thus designed to contain the corresponding *att*B sites in addition to the partial DNA-sequence of the desired protein:

forward primer: *att*B1 = GGGGACAAGTTTGTACAAAAAAGCAGGCTTT

reverse primer: *att*B2 = GGGGACCACTTTGTACAAGAAAGCTGGGTG

The PCR reactions were performed with a CFX96 System (BioRad) applying the following temperature program:

Initial denaturation	98 °C	3:00 min
35-50 cycles	98 °C	0:10 min
	45-72 °C	0:30 min
	72 °C	0:30 min/kb
Final extension	72 °C	5:00 min
	4 °C	hold

3.2.1.1   SITE-DIRECTED MUTAGENESIS OF *ALDH1A1*

To exchange the cysteines 456 and 464 for alanine, the point mutations were introduced by mismatch PCR. Thus two mismatching primers for each cysteine were designed with the QuickChange Primer Design Program (Agilent Technologies) and synthesized at MWG as presented in Chapter V-3.1.4 (p. 103). The mismatch, an exchange of two DNA-bases, was created in the middle of each primer. However, to successfully create a double mutant, the primer sequences of the different cysteines were not allowed to overlap. Both strands of a double-stranded template DNA plasmid were replicated in a mutagenic primer-directed PCR, applying Phusion High Fidelity DNA polymerase. An ALDH1A1 ORFEXPRESS Gateway PLUS Shuttle Clone served as DNA template of wild type cDNA.

At first the single point mutations were introduced. Therefore 50 μL PCR reaction mixture were prepared containing 36.1 μL ddH$_2$O, 10 μL 5x GC or 5x HF buffer (NEB), 0.8 μL

forward and reverse primer of either Cys456 or Cys464 (10 nM), 1 µL dNTPs (10 mM) and 0.8 µL plasmid DNA (125 ng/µL). To prevent primer degradation caused by the exonuclease activity of Phusion, 0.2 µL of the DNA polymerase were added and the PCR reaction was subsequently performed. After 35 cycles a good amplification was detected at annealing temperatures between 56-59 °C for the HF buffer mix. The resulting PCR products were purified by an agarose gel and the isolated bands were extracted with an E.Z.N.A. MicroElutet Gel Extraction kit (OMEGA bio-tek). The DNA concentration was measured using an Infinite 200 PRO NanoQuant microplate reader (Tecan). To remove the unmutated parental DNA, the PCR products were digested with the endonuclease DpnI, specific for methylated and hemimethylated DNA. Therefore 1 µL of DpnI was added to 15 µL purified PCR product and 1.7 µL RE 10x Buffer B (Promega). The digestion mixture was incubated for 2 h at 37 °C. As the template DNA is implemented in a Gateway pDONR vector, the PCR products can directly be subjected to the LR cloning reaction. However, due to low concentrations, the plasmids were first amplified into super competent *E. coli* XL1-Blue cells.

To create the double mutant, the wild type DNA template was exchanged for the amplified and purified plasmid of either single mutant. Afterwards the PCR was performed as described before applying the opposing mutant primers. The resulting PCR products were purified, isolated and the parental DNA was digested with DpnI.

3.2.1.2   CONSTRUCTION OF *ALDH1A1-TEV*

To obtain the pure ALDH1A1 by TEV-digest after Strep purification, a TEV restriction site was introduced. Therefore the forward primer in Chapter V-3.1.4 (p. 103) was designed to implement the TEV specific sequence between the *att*L1 site and the ORF of the ORFEXPRESS Gateway PLUS Shuttle Clone to gain: *att*L1-TEV-ALDH1A1. According to Phusion manufacturer's protocol 20 µL PCR reaction mixture were prepared containing 11.8 µL ddH$_2$O, 4 µL 5x GC or 5x HF buffer (NEB), 1 µL forward and reverse primer (10 nM), 0.4 µL dNTPs (10 mM), 0.6 µL DMSO and 1 µL plasmid DNA (5 ng/µL). Finally 0.5 µL of the Phusion DNA polymerase were added and the PCR reaction was subsequently performed. After 35 cycles a comparable amplification was detected over a broad range of annealing temperatures with 48-72 °C. The resulting PCR products were

purified by an agarose gel and the isolated bands were extracted with an E.Z.N.A. MicroElutet Gel Extraction kit (OMEGA bio-tek). The DNA concentration was measured using an Infinite 200 PRO NanoQuant microplate reader (Tecan).

3.2.1.3   COLONY PCR OF *HLY* (LLO)

To prevent secretion of LLO whilst overexpression the secretional sequence of the *hly* gene, the first 75 DNA bases, was deleted by designing an appropriate forward primer (Chapter V-3.1.4, 103). Furthermore the PCR reaction was conducted with 1 µL of an *L. monocytogenes* overnight culture instead of the genomic DNA. Thus the initial denaturation of the PCR program was extended to 10 min to disrupt the bacterial. 20 µL PCR reaction mixture were prepared containing 11.8 µL ddH$_2$O, 4 µL 5x GC or 5x HF buffer (NEB), 1 µL forward and reverse primer (10 nM), 0.4 µL dNTPs (10 mM) and 0.6 µL DMSO. Finally 0.2 µL of the Phusion DNA polymerase were added and the PCR reaction was subsequently performed. After 40 cycles a comparable amplification was detected over a range of 49-63 °C annealing temperatures with a maximum at 52 °C for the GC buffer mix. The resulting PCR products were purified and isolated as described before.

3.2.1.4   COLONY PCR OF *LMO2201*

The forward primer of *LMO2201* (Chapter V-3.1.4, p. 103) still contains the start codon. Hence two gene products can be observed after overexpression as another start codon is present upstream of the Strep-tag, the original protein and a homologue including a Strep-tag. The PCR reaction was conducted with 1 µL of an *L. monocytogenes* overnight culture instead of the genomic DNA and the initial denaturation was extended to 10 min. 20 µL PCR reaction mixture were prepared containing 11.8 µL ddH$_2$O, 4 µL 5x GC or 5x HF buffer (NEB), 1 µL forward and reverse primer (10 nM), 0.4 µL dNTPs (10 mM) and 0.6 µL DMSO. Finally 0.2 µL of the Phusion DNA polymerase were added and the PCR reaction was subsequently performed. After 50 cycles amplification was only detected at annealing temperatures of around 50 °C in GC buffer mix. The resulting PCR products were purified and isolated as described before.

3.2.2 CONSTRUCTION OF SHEEP *ALDH1A1-TEV*

For crystallization of sheep ALDH1A1, a Gateway entry clone with an *att*L1-TEV-ALDH1A1-*att*L2 insert was designed. The codons were optimized by GeneOptimizer (GeneArt) for expression in *E. coli*. Afterward the optimized gene was synthesized by GeneArt and cloned into pKM-RQ containing a kanamycin resistance. The purified plasmid was subjected to LR Cloning Reaction to finally yield expression ready BL21 clones (pDEST 007).

3.2.3 GATEWAY TECHNOLOGY

3.2.3.1 BP CLONING REACTION

The BP cloning reaction enables the transfer of *att*B-PCR products into vector systems containing *att*P recombination sites, such as pDONR 201. The recombination of *att*B and *att*P results in the exchange of the vector insert, an *att*P flanked *ccdB* gene, for the PCR product and in the creation of *att*L sites. The BP cloning mix was prepared as follows:

- 150 ng *att*B-PCR product
- 150 ng pDONR 201
- ad 8 µL TE buffer
- 2 µL BP Clonase II enzyme mix, added last

The BP cloning mix was incubated overnight at RT. The resulting *att*L-entry clone was added to 50 µL of super competent *E. coli* XL1-Blue cells and incubated for 30 min on ice. The transformation was initiated via heat shock at 42 °C for 40 sec. The cells were grown for 2 h in 200 µL kanamycin LB (25 µL/mL) at 37 °C and plated on kanamycin LB agar plates for clone selection. After 12-24 h at 37 °C single clones were picked and grown in 10 mL kanamycin LB overnight at 37 °C. A cryostock was made as described in Chapter V-1.2.1 (p. 81) and the plasmid was isolated by E.Z.N.A. Plasmid Mini kit (OMEGA bio-tek) according to the manufacturer's protocol. The DNA concentration was measured using an Infinite 200 PRO NanoQuant microplate reader (Tecan) and the validity of the expression vector was proved by DNA sequencing.

3.2.3.2 LR CLONING REACTION

The LR cloning reaction enables the transfer of *att*L-flanked inserts into expression vector systems containing *att*R recombination sites, such as pDEST 007 and pET 55. The recombination of *att*L and *att*R results in the exchange of the *att*R flanked *ccdB* gene for the *att*L-entry clone insert and in the creation of *att*B sites. The LR cloning mix was prepared as follows:

- 150 ng *att*L-entry clone
- 150 ng pDEST 007 / pET 55
- ad 8 µL TE buffer
- 2 µL BP Clonase II enzyme mix, added last

The LR cloning mix was incubated overnight at RT. The resulting *att*B-expression clone was transformed into super competent *E. coli* XL1-Blue cells as described before and selected on ampicillin LB agar plates (100 µg/mL). The plasmid was isolated by E.Z.N.A. Plasmid Mini kit (OMEGA bio-tek) according to the manufacturer's protocol. For overexpression the plasmid was retransformed into competent *E. coli* BL21 cells. The DNA concentration was measured using an Infinite 200 PRO NanoQuant microplate reader (Tecan) and the validity of the expression vector was proved by DNA sequencing.

3.2.4 OVEREXPRESSION OF RECOMBINANT PROTEINS

3.2.4.1 ALDH1A1-STREP

The recombinant BL21 clone of wild type ALDH1A1 (Chapter V-3.2.1.1, p. 104) was grown in ampicillin LB medium (100 µg/mL) at 37 °C until an OD_{600} of 600 was reached. Afterwards expression was induced with IPTG (1:1000) and the culture was further incubated at 37 °C for 5 h. The cells were washed twice with PBS, resuspended in strep binding buffer and lysed by sonication for 20 min at 80% max. power under ice cooling with a Bandelin Sonopuls instrument. The soluble fraction was separated via centrifugation for 45 min at 18,000 rpm and further purified by an ÄKTA system (GE Healthcare) and applied on a StrepTrap HP 5 mL column (GE Healthcare). After washing with binding buffer, the ALDH1A1 was eluted with elution buffer and the suitable fractions were concentrated with an Amicon filter unit (MWCO 10 kDa, Milipore). Finally

the enzyme was purified via size exclusion with an ÄKTA system over a HiLoad 16/60 Superdex 200 prep grade column (GE Healthcare) and stored at -80 °C in 50 mM Tris-HCl pH 7.5 containing 10% glycerin. However, for crystallographic experiments, ALDH1A1 was freshly overexpressed and purified.

3.2.4.2 MUTANTS OF ALDH1A1-STREP

The recombinant BL21 clones of ALDH1A1 wildtype, 456, 464 and the double mutant (Chapter V-3.2.1.1, p. 104) were grown in ampicillin LB medium (100 µg/mL) at 37 °C until an OD_{600} of 800 was reached. Afterwards expression was induced with ATET (1:10,000) and the culture was further incubated at 37 °C for 5 h. The cells were washed twice with PBS and lysed by sonication in PBS with a Bandelin Sonopuls with 3 x 20 sec pulsed at 80% max. power under ice cooling. The cytosolic fraction was separated via centrifugation for 15 min at 10,000 rpm. The lysates were stored at -80 °C.

3.2.4.3 WILD TYPE ALDH1A1

The recombinant BL21 clones of ALDH1A1-TEV (Chapter V-3.2.1.2, p. 105) were grown in ampicillin LB medium (100 µg/mL) at 37 °C until an OD_{600} of 600 was reached. Afterwards expression was induced with ATET (1:10,000) and the culture was further incubated at 18 °C overnight. The cells were washed twice with PBS, resuspended in strep binding buffer and lysed by sonication for 20 min at 80% max. power under ice cooling with a Bandelin Sonopuls instrument. The soluble fraction was separated via centrifugation for 45 min at 18,000 rpm and further purified by an ÄKTA system (GE Healthcare) and applied on a StrepTrap HP 5 mL column (GE Healthcare). After washing with binding buffer, the ALDH1A1 was eluted with elution buffer and the suitable fractions were concentrated with an Amicon filter unit (MWCO 10 kDa, Milipore). Thereafter a TEV digest was performed overnight at 4 °C in TEV cleavage buffer with a ration of ALDH1A1 to TEV protease of 100:1. Finally the enzyme was purified by gel filtration with an ÄKTA system over a HiLoad 16/60 Superdex 200 prep grade column (GE Healthcare) and stored at -80 °C in 50 mM Tris-HCl pH 7.5 containing 10% glycerin. However, for crystallographic experiments, ALDH1A1 was freshly overexpressed and purified.

3.2.4.4   LMO2201-STREP

The recombinant BL21 clones of LMO2201 (Chapter V-3.2.1.4, p. 106) were grown in ampicillin LB medium (100 µg/mL) at 37 °C until an OD_{600} of 600 was reached. Afterwards expression was induced with IPTG (1:1000) and the culture was further incubated at 22 °C overnight. The cells were washed twice with PBS and lysed by sonication in PBS with a Bandelin Sonopuls with 7 x 20 sec pulsed at 100% max. power under ice cooling. The cytosolic fraction was separated via centrifugation for 15 min at 10,000 rpm. The lysates were stored at -80 °C.

3.2.4.5   LLO-STREP

The recombinant BL21 clones of LLO (Chapter V-3.2.1.3, p. 106) were grown in ampicillin LB medium (100 µg/mL) at 30 °C until an OD_{600} of 400 was reached. Afterwards expression was induced with IPTG (1:1000) and the culture was further incubated at 22 °C overnight. The cells were washed twice with PBS, resuspended in strep binding buffer and lysed by sonication for 20 min at 80% max. power under ice cooling with a Bandelin Sonopuls instrument. The soluble fraction was separated via centrifugation for 45 min at 18000 rpm and further purified by an ÄKTA system (GE Healthcare) and applied on a StrepTrap HP 5 mL column (GE Healthcare). After washing with binding buffer, the ALDH1A1 was eluted with elution buffer and the suitable fractions were concentrated with an Amicon filter unit (MWCO 10 kDa, Milipore). To control for hemolytic activity, the elution buffer was exchanged for PBS and storage buffer. The samples were stored at 4 °C for two weeks.

VI Bibliography

1. G. A. Holt, A. Chandra, "Herbs in the modern healthcare environment - an overview of uses, legalities, and the role of the healthcare professional" *Clin. Res. Regul. Aff.* **2002**, *19*, 83-107.

2. E. Ravina, *The evolution of drug discovery - From traditional medicines to modern drugs*. Wiley-VCH, Weinheim, **2011**.

3. G. Ebbell, *The papyrus Ebers: the greatest Egyptian medical document*. Levin & Munksgaard, Copenhagen, **1937**.

4. F. W. Sertürner, "Über das Morphium, eine neue salzfähige Grundlage, und die Mekonsäure, als Hauptbestandteile des Opiums" *Ann. Phys.* **1817**, *25*, 56-89.

5. J. Drews, "Drug discovery: a historical perspective" *Science* **2000**, *287*, 1960-1964.

6. P. Ehrlich, *Gesammelte Arbeiten*. F. Himmelweit, Ed., Springer-Verlag, Berlin, **1957**.

7. A. Fleming, "On the antibacterial action of cultures of a penicillium, with special reference to their use in the isolation of B. influenza" *Br. J. Exp. Pathol.* **1929**, *10*, 226-236.

8. G. Domagk, "Chemotherapie der bakteriellen Infektionen" *Angew. Chem.* **1935**, *48*, 657-676.

9. R. J. Sommer, A. Streit, "Comparative genetics and genomics of nematodes: genome structure, development, and lifestyle" *Annu. Rev. Genet.* **2011**, *45*, 1-20.

10. M. Clamp, B. Fry, M. Kamal, X. Xie, J. Cuff, M. F. Lin, M. Kellis, K. Lindblad-Toh, E. S. Lander, "Distinguishing protein-coding and noncoding genes in the human genome" *Proc. Natl. Acad. Sci. U.S.A.* **2007**, *104*, 19428-19433.

11. R. M. Twyman, *Principles of proteomics*. BIOS Scientific Publishers, Abingdon, Oxfordshire, **2004**.

12. O. N. Jensen, "Modification-specific proteomics: characterization of post-translational modifications by mass spectrometry" *Curr. Opin. Chem. Biol.* **2004**, *8*, 33-41.

13. R. A. Copeland, M. R. Harpel, P. J. Tummino, "Targeting enzyme inhibitors in drug discovery" *Expert Opin. Ther. Targets* **2007**, *11*, 967-978.

14. R. A. Copeland, *Evaluation of enzyme inhibitors in drug discovery*. Wiley, New Jersey, **2005**.

15. P. Imming, C. Sinning, A. Meyer, "Drugs, their targets and the nature and number of drug targets" *Nat. Rev. Drug Discov.* **2006**, *5*, 821-834.

16. D. C. Swinney, J. Anthony, "How were new medicines discovered?" *Nat. Rev. Drug Discov.* **2011**, *10*, 507-519.

17. F. Zhu, Z. Shi, C. Qin, L. Tao, X. Liu, F. Xu, L. Zhang, Y. Song, J. Zhang, B. Han, P. Zhang, Y. Chen, "Therapeutic target database update 2012: a resource for facilitating target-oriented drug discovery" *Nucleic Acids Res.* **2012**, *40*, D1128-1136.

18. T. Ito, K. Ota, H. Kubota, Y. Yamaguchi, T. Chiba, K. Sakuraba, M. Yoshida, "Roles for the two-hybrid system in exploration of the yeast protein interactome" *Mol. Cell. Proteomics* **2002**, *1*, 561-566.

19. H. Zhu, M. Bilgin, M. Snyder, "Proteomics" *Annu. Rev. Biochem.* **2003**, *72*, 783-812.

20. G. MacBeath, "Protein microarrays and proteomics" *Nat. Genet.* **2002**, *32 Suppl*, 526-532.

21. M. B. Nodwell, S. A. Sieber, "ABPP methodology: introduction and overview" *Top. Curr. Chem.* **2012**, *324*, 1-41.

22. T. Böttcher, M. Pitscheider, S. A. Sieber, "Natural products and their biological targets: proteomic and metabolomic labeling strategies" *Angew. Chem. Int. Ed. Engl.* **2010**, *49*, 2680-2698.

23. M. J. Evans, B. F. Cravatt, "Mechanism-based profiling of enzyme families" *Chem. Rev.* **2006**, *106*, 3279-3301.

24. B. F. Cravatt, A. T. Wright, J. W. Kozarich, "Activity-based protein profiling: from enzyme chemistry to proteomic chemistry" *Annu. Rev. Biochem.* **2008**, *77*, 383-414.

25. M. Fonovic, M. Bogyo, "Activity based probes for proteases: applications to biomarker discovery, molecular imaging and drug screening" *Curr. Pharm. Des.* **2007**, *13*, 253-261.

26. M. Fonovic, M. Bogyo, "Activity-based probes as a tool for functional proteomic analysis of proteases" *Expert Rev. Proteomics.* **2008**, *5*, 721-730.

27. B. M. Cullen, I. M. Halliday, G. Kay, J. Nelson, B. Walker, "The application of a novel biotinylated affinity label for the detection of a cathepsin B-like precursor produced by breast-tumour cells in culture" *Biochem. J.* **1992**, *283 (Pt 2)*, 461-465.

28. C. M. Kam, A. S. Abuelyaman, Z. Li, D. Hudig, J. C. Powers, "Biotinylated isocoumarins, new inhibitors and reagents for detection, localization, and isolation of serine proteases" *Bioconjugate Chem.* **1993**, *4*, 560-567.

29. A. S. Abuelyaman, D. Hudig, S. L. Woodard, J. C. Powers, "Fluorescent derivatives of diphenyl [1-(N-peptidylamino)alkyl]phosphonate esters: synthesis and use in the inhibition and cellular localization of serine proteases" *Bioconjugate Chem.* **1994**, *5*, 400-405.

30. R. R. Rando, "Mechanism-based irreversible enzyme inhibitors" *Methods Enzymol.* **1977**, *46*, 28-41.

31. C. Drahl, B. F. Cravatt, E. J. Sorensen, "Protein-reactive natural products" *Angew. Chem. Int. Ed. Engl.* **2005**, *44*, 5788-5809.

32. E. Weerapana, G. M. Simon, B. F. Cravatt, "Disparate proteome reactivity profiles of carbon electrophiles" *Nat. Chem. Biol.* **2008**, *4*, 405-407.

33. R. Huisgen, *1,3 Dipolar Cycloaddition chemistry*. Wiley, New York, **1984**.

34. V. V. Rostovtsev, L. G. Green, V. V. Fokin, K. B. Sharpless, "A stepwise huisgen cycloaddition process: copper(I)-catalyzed regioselective "ligation" of azides and terminal alkynes" *Angew. Chem. Int. Ed. Engl.* **2002**, *41*, 2596-2599.

35. C. W. Tornoe, C. Christensen, M. Meldal, "Peptidotriazoles on solid phase: [1,2,3]-triazoles by regiospecific copper(i)-catalyzed 1,3-dipolar cycloadditions of terminal alkynes to azides" *J. Org. Chem.* **2002**, *67*, 3057-3064.

36. L. J. Hanka, A. Dietz, S. A. Gerpheide, S. L. Kuentzel, D. G. Martin, "CC-1065 (NSC-298223), a new antitumor antibiotic. Production, in vitro biological activity, microbiological assays and taxonomy of the producing microorganism" *J. Antibiot. (Tokyo)* **1978**, *31*, 1211-1217.

37. D. G. Martin, C. G. Chidester, D. J. Duchamp, S. A. Mizsak, "Structure of CC-1065 (NSC-298223), a new antitumor antibiotic" *J. Antibiot. (Tokyo)* **1980**, *33*, 902-903.

38. D. A. Boger, S. A. Munk, "DNA alkylation properties of enhanced functional analogs of CC-1065 incorporating the 1,2,9,9a-tetrahydrocyclopropa[1,2-c]benz[1,2-e]indol-4-one (CBI) alkylation subunit" *J. Am. Chem. Soc.* **1992**, *114*, 5488-5496.

39. B. K. Bhuyan, K. A. Newell, S. L. Crampton, D. D. Von Hoff, "CC-1065 (NSC 298223), a most potent antitumor agent: kinetics of inhibition of growth, DNA synthesis, and cell survival" *Cancer Res.* **1982**, *42*, 3532-3537.

40. M. Ichimura, T. Ogawa, K. Takahashi, E. Kobayashi, I. Kawamoto, T. Yasuzawa, I. Takahashi, H. Nakano, "Duocarmycin SA, a new antitumor antibiotic from Streptomyces sp" *J. Antibiot. (Tokyo)* **1990**, *43*, 1037-1038.

41. T. Yasuzawa, Y. Saitoh, M. Ichimura, I. Takahashi, H. Sano, "Structure of duocarmycin SA, a potent antitumor antibiotic" *J. Antibiot. (Tokyo)* **1991**, *44*, 445-447.

42. T. Ogawa, M. Ichimura, S. Katsumata, M. Morimoto, K. Takahashi, "New antitumor antibiotics, duocarmycins B1 and B2" *J. Antibiot. (Tokyo)* **1989**, *42*, 1299-1301.

43. E. Kobayashi, A. Okamoto, M. Asada, M. Okabe, S. Nagamura, A. Asai, H. Saito, K. Gomi, T. Hirata, "Characteristics of antitumor activity of KW-2189, a novel water-soluble derivative of duocarmycin, against murine and human tumors" *Cancer Res.* **1994**, *54*, 2404-2410.

44. S. R. Alberts, V. J. Suman, H. C. Pitot, J. K. Camoriano, J. Rubin, "Use of KW-2189, a DNA minor groove-binding agent, in patients with hepatocellular carcinoma: a north central cancer treatment group (NCCTG) phase II clinical trial" *J. Gastrointest. Cancer.* **2007**, *38*, 10-14.

45. C. G. Chidester, Krueger, W.C., Mizsak, S.A., Duchamp. D.J., Martin, D.G., "The structure of CC-1065, a potent antitumor agent, and its binding to DNA" *J. Am. Chem. Soc.* **1981**, *103*, 7629-7635.

46. L. H. Hurley, V. L. Reynolds, D. H. Swenson, G. L. Petzold, T. A. Scahill, "Reaction of the antitumor antibiotic CC-1065 with DNA: structure of a DNA adduct with DNA sequence specificity" *Science* **1984**, *226*, 843-844.

47. D. L. Boger, D. S. Johnson, "CC-1065 and the duocarmycins: unraveling the keys to a new class of naturally derived DNA alkylating agents" *Proc. Natl. Acad. Sci. U.S.A.* **1995**, *92*, 3642-3649.

48. D. A. Boger, B. Bollinger, D. L. Hertzog, D. S. Johnson, H. Cai, P. Mésini, R. M. Garbaccio, Q. Jin, P. A. Kitos, "Reversed and sandwiched analogs of duocarmycin SA: Establishment of the origin of the sequence-selective alkylation of DNA and new insights into the source of catalysis" *J. Am. Chem. Soc.* **1997**, *119*, 4987-4998.

49. D. L. Boger, T. Ishizaki, R. J. Wysocki, S. A. Munk, P. A. Kitos, O. Suntornwat, "Total Synthesis and Evaluation of (+/-)-N-(Tert-Butyloxycarbonyl)-Cbi, (+/-)-Cbi-Cdpi1, and (+/-)-Cbi-Cdpi2 - Cc-1065 Functional Agents Incorporating the Equivalent 1,2,9,9a-Tetrahydrocycloprop[1,2-C]Benz[1,2-E]Indol-4-One (Cbi) Left-Hand Subunit" *J. Am. Chem. Soc.* **1989**, *111*, 6461-6463.

50. D. L. Boger, B. J. Invergo, R. S. Coleman, H. Zarrinmayeh, P. A. Kitos, S. C. Thompson, T. Leong, L. W. McLaughlin, "A demonstration of the intrinsic importance of stabilizing hydrophobic binding and non-covalent van der Waals contacts dominant in the non-covalent CC-1065/B-DNA binding" *Chem. Biol. Interact.* **1990**, *73*, 29-52.

51. K. S. MacMillan, D. L. Boger, "Fundamental relationships between structure, reactivity, and biological activity for the duocarmycins and CC-1065" *J. Med. Chem.* **2009**, *52*, 5771-5780.

52. F. Behrendt, Thesis, Georg-August-Universität Göttingen **2011**.

53. D. A. Boger, W. Yun, "Role of the CC-1065 and duocarmycin N2 substituent: Validation of a direct relationship between solvolysis chemical stability and in vitro biological potency" *J. Am. Chem. Soc.* **1994**, *116*, 5523-5524.

54. D. L. Boger, R. J. Wysocki, "Total Synthesis of (+/-)-N-(Phenylsulfonyl)-Ci and (+/-)-N-(Tert-Butyloxycarbonyl)-Ci, (+/-)-Ci-Cdpi1, and (+/-)-Ci-Cdpi2 - Cc-1065 Functional Analogs Incorporating the Parent 1,2,7,7a-Tetrahydrocycloprop[1,2-C]Indol-4-One (Ci) Left-Hand Subunit" *J. Org. Chem.* **1989**, *54*, 1238-1240.

55. D. A. Boger, T. Ishizaki, "Synthesis of N-(tert-butyloxycarbony1)-CBI,CBI, CBI-CDPI1 and CBI-CDPI2: Enhanced functional analogues of CC-1065incorporating the 1,2,9,9a-tetrahydrocyclopropa[c]benz[e]indol-4-one (CBI) left-hand subunit" *J. Org. Chem.* **1990**, *55*, 5823-5832.

56. D. L. Boger, T. Ishizaki, H. Zarrinmayeh, P. A. Kitos, O. Suntornwat, "A potent, simple derivative of an analog of the CC-1065 alkylation subunit" *Bioorg. Med. Chem. Lett.* **1991**, *1*, 55-58.

57. D. A. Boger, K. Machiya, D. L. Hertzog, P. A. Kitos, D. Holmes, "Total synthesis and preliminary evaluation of (+)- and ent-(-)-duocarmycin SA" *J. Am. Chem. Soc.* **1993**, *115*, 9025-9036.

58. L. F. Tietze, B. Krewe, H. Frauendorf, "Probing the mechanism of action of potential anticancer agents at a molecular level using electrospray ionisation Fourier transform ion cyclotron resonance mass spectrometry" *Eur. J. Mass. Spectrom.* **2009**, *15*, 661-672.

59. L. F. Tietze, B. Krewer, "Antibody-directed enzyme prodrug therapy: a promising approach for a selective treatment of cancer based on prodrugs and monoclonal antibodies" *Chem. Biol. Drug. Des.* **2009**, *74*, 205-211.

60. K. D. Bagshawe, "Antibody directed enzymes revive anti-cancer prodrugs concept" *Br. J. Cancer* **1987**, *56*, 531-532.

61. K. D. Bagshawe, "Antibody-directed enzyme prodrug therapy (ADEPT) for cancer" *Expert Rev. Anticancer. Ther.* **2006**, *6*, 1421-1431.

62. K. D. Bagshawe, "Targeting: the ADEPT story so far" *Curr. Drug Targets* **2009**, *10*, 152-157.

63. G. Xu, H. L. McLeod, "Strategies for enzyme/prodrug cancer therapy" *Clin. Cancer Res.* **2001**, *7*, 3314-3324.

64. W. A. Denny, "Tumor-activated prodrugs--a new approach to cancer therapy" *Cancer Invest.* **2004**, *22*, 604-619.

65. L. F. Tietze, F. Major, I. Schuberth, D. A. Spiegl, B. Krewer, K. Maksimenka, G. Bringmann, J. Magull, "Selective treatment of cancer: synthesis, biological evaluation and structural elucidation of novel analogues of the antibiotic CC-1065 and the duocarmycins" *Chemistry* **2007**, *13*, 4396-4409.

66. L. F. Tietze, K. Schmuck, H. J. Schuster, M. Muller, I. Schuberth, "Synthesis and biological evaluation of prodrugs based on the natural antibiotic duocarmycin for use in ADEPT and PMT" *Chemistry* **2011**, *17*, 1922-1929.

67. L. F. Tietze, F. Major, I. Schuberth, "Antitumor agents: development of highly potent glycosidic duocarmycin analogues for selective cancer therapy" *Angew. Chem. Int. Ed. Engl.* **2006**, *45*, 6574-6577.

68. R. Braid, S. Winstein, "Neighboring carbon and hydrogen. Li. dienones from Ar1[UNK]-3 participation. Isolation and behavior of spiro(2,5)octa-1,4-diene-3-one" *J. Am. Chem. Soc.* **1963**, *85*, 567-578.

69. W. S. Murphy, S. Wattanasin, "Anionic cyclization of phenols" *Chem. Soc. Rev.* **1983**, *12*, 213-250.

70. R. C. Kelly, I. Gebhard, N. Wicnienski, P. A. Aristoff, P. D. Johnson, D. G. Martin, "Coupling of cyclopropapyrroloindole (CPI) derivatives. The preparation of CC-1065, ent-CC-1065, and analogues" *J. Am. Chem. Soc.* **1987**, *109*, 6837-6838.

71. L. F. Tietze, J. M. von Hof, M. Muller, B. Krewer, I. Schuberth, "Glycosidic prodrugs of highly potent bifunctional duocarmycin derivatives for selective treatment of cancer" *Angew. Chem. Int. Ed. Engl.* **2010**, *49*, 7336-7339.

72. J. P. Parrish, D. B. Kastrinsky, F. Stauffer, M. P. Hedrick, I. Hwang, D. L. Boger, "Establishment of substituent effects in the DNA binding subunit of CBI analogues of the duocarmycins and CC-1065" *Bioorg. Med. Chem.* **2003**, *11*, 3815-3838.

73. T. Wirth, K. Schmuck, L. F. Tietze, S. A. Sieber, "Duocarmycin analogues target aldehyde dehydrogenase 1 in lung cancer cells" *Angew. Chem. Int. Ed. Engl.* **2012**, *51*, 2874-2877.

74. L. F. Tietze, J. M. von Hof, B. Krewer, M. Muller, F. Major, H. J. Schuster, I. Schuberth, F. Alves, "Asymmetric synthesis and biological evaluation of glycosidic prodrugs for a selective cancer therapy" *ChemMedChem* **2008**, *3*, 1946-1955.

75. L. F. Tietze, H. J. Schuster, S. M. Hampel, S. Ruhl, R. Pfoh, "Enantio- and diastereoselective synthesis of duocarmycine-based prodrugs for a selective treatment of cancer by epoxide opening" *Chemistry* **2008**, *14*, 895-901.

76. L. F. Tietze, F. Major, "Synthesis of new water-soluble DNA-binding subunits for analogues of the cytotoxic antibiotic CC-1065 and their prodrugs" *Eur. J. Org. Chem.* **2006**, 2314-2321.

77. K. Schmuck, Thesis, Georg-August-Universität Göttingen **2011**.

78. L. Gonzalez-Segura, H. Riveros-Rosas, A. G. Diaz-Sanchez, A. Julian-Sanchez, R. A. Munoz-Clares, "Potential monovalent cation-binding sites in aldehyde dehydrogenases" *Chem. Biol. Interact.* **2013**.

79. A. Yoshida, A. Rzhetsky, L. C. Hsu, C. Chang, "Human aldehyde dehydrogenase gene family" *Eur. J. Biochem.* **1998**, *251*, 549-557.

80. C. Kahlert, F. Bergmann, J. Beck, T. Welsch, C. Mogler, E. Herpel, S. Dutta, T. Niemietz, M. Koch, J. Weitz, "Low expression of aldehyde dehydrogenase 1A1 (ALDH1A1) is a prognostic marker for poor survival in pancreatic cancer" *BMC Cancer* **2011**, *11*, 275.

81. K. Morimoto, S. J. Kim, T. Tanei, K. Shimazu, Y. Tanji, T. Taguchi, Y. Tamaki, N. Terada, S. Noguchi, "Stem cell marker aldehyde dehydrogenase 1-positive breast cancers are characterized by negative estrogen receptor, positive human epidermal growth factor receptor type 2, and high Ki67 expression" *Cancer Sci.* **2009**, *100*, 1062-1068.

82. F. Jiang, Q. Qiu, A. Khanna, N. W. Todd, J. Deepak, L. Xing, H. Wang, Z. Liu, Y. Su, S. A. Stass, R. L. Katz, "Aldehyde dehydrogenase 1 is a tumor stem cell-associated marker in lung cancer" *Mol. Cancer Res.* **2009**, *7*, 330-338.

83. M. Patel, L. Lu, D. S. Zander, L. Sreerama, D. Coco, J. S. Moreb, "ALDH1A1 and ALDH3A1 expression in lung cancers: correlation with histologic type and potential precursors" *Lung Cancer* **2008**, *59*, 340-349.

84. K. D. Bunting, A. J. Townsend, "De novo expression of transfected human class 1 aldehyde dehydrogenase (ALDH) causes resistance to oxazaphosphorine anti-cancer alkylating agents in hamster V79 cell lines. Elevated class 1 ALDH activity is closely correlated with reduction in DNA interstrand cross-linking and lethality" *J. Biol. Chem.* **1996**, *271*, 11884-11890.

85. J. S. Moreb, A. Gabr, G. R. Vartikar, S. Gowda, J. R. Zucali, D. Mohuczy, "Retinoic acid down-regulates aldehyde dehydrogenase and increases cytotoxicity of 4-hydroperoxycyclophosphamide and acetaldehyde" *J. Pharmacol. Exp. Ther.* **2005**, *312*, 339-345.

86. J. S. Moreb, D. Mohuczy, B. Ostmark, J. R. Zucali, "RNAi-mediated knockdown of aldehyde dehydrogenase class-1A1 and class-3A1 is specific and reveals that each contributes equally to the resistance against 4-hydroperoxycyclophosphamide" *Cancer Chemother. Pharmacol.* **2007**, *59*, 127-136.

87. C. N. Landen, Jr., B. Goodman, A. A. Katre, A. D. Steg, A. M. Nick, R. L. Stone, L. D. Miller, P. V. Mejia, N. B. Jennings, D. M. Gershenson, R. C. Bast, Jr., R. L. Coleman, G. Lopez-Berestein, A. K. Sood, "Targeting aldehyde dehydrogenase cancer stem cells in ovarian cancer" *Mol. Cancer Ther.* **2010**, *9*, 3186-3199.

88. J. S. Moreb, H. V. Baker, L. J. Chang, M. Amaya, M. C. Lopez, B. Ostmark, W. Chou, "ALDH isozymes downregulation affects cell growth, cell motility and gene expression in lung cancer cells" *Mol. Cancer* **2008**, *7*, 87.

89. S. A. Moore, H. M. Baker, T. J. Blythe, K. E. Kitson, T. M. Kitson, E. N. Baker, "A structural explanation for the retinal specificity of class 1 ALDH enzymes" *Adv. Exp. Med. Biol.* **1999**, *463*, 27-38.

90. S. A. Moore, H. M. Baker, T. J. Blythe, K. E. Kitson, T. M. Kitson, E. N. Baker, "Sheep liver cytosolic aldehyde dehydrogenase: the structure reveals the basis for the retinal specificity of class 1 aldehyde dehydrogenases" *Structure* **1998**, *6*, 1541-1551.

91. L. Ni, J. Zhou, T. D. Hurley, H. Weiner, "Human liver mitochondrial aldehyde dehydrogenase: three-dimensional structure and the restoration of solubility and activity of chimeric forms" *Protein Sci.* **1999**, *8*, 2784-2790.

92. P. Emsley, B. Lohkamp, W. G. Scott, K. Cowtan, "Features and development of Coot" *Acta Crystallogr., Sect.: D Biol.* **2010**, *66*, 486-501.

93. The PyMOL Molecular Graphics System, v1.3, Schrödinger.

94. D. Blow, *Outline of crystallography for biologists*. Oxford University Press, New York, **2002**.

95. M. A. Larkin, G. Blackshields, N. P. Brown, R. Chenna, P. A. McGettigan, H. McWilliam, F. Valentin, I. M. Wallace, A. Wilm, R. Lopez, J. D. Thompson, T. J. Gibson, D. G. Higgins, "Clustal W and Clustal X version 2.0" *Bioinformatics* **2007**, *23*, 2947-2948.

96. M. Goujon, H. McWilliam, W. Li, F. Valentin, S. Squizzato, J. Paern, R. Lopez, "A new bioinformatics analysis tools framework at EMBL-EBI" *Nucleic Acids Res.* **2010**, *38*, W695-699.

97. F. C. Bernstein, T. F. Koetzle, G. J. Williams, E. F. Meyer, Jr., M. D. Brice, J. R. Rodgers, O. Kennard, T. Shimanouchi, M. Tasumi, "The Protein Data Bank: a computer-based archival file for macromolecular structures" *J. Mol. Biol.* **1977**, *112*, 535-542.

98. H. E. Huxley, J. C. Kendrew, "Discontinuous lattice changes in haemoglobin crystals" *Acta Crystallogr., Sect.: D Biol.* **1953**, *6*, 76-80.

99. L. B. Rockland, "Saturated salt solutions for static control of relative humidity between 5° and 40° C" *Anal. Chem.* **1960**, *32*, 1375-1376.

100. I. Dobrianov, S. Kriminski, C. L. Caylor, S. G. Lemay, C. Kimmer, A. Kisselev, K. D. Finkelstein, R. E. Thorne, "Dynamic response of tetragonal lysozyme crystals to changes in relative humidity: implications for post-growth crystal treatments" *Acta Crystallogr., Sect.: D Biol.* **2001**, *57*, 61-68.

101. B. Heras, J. L. Martin, "Post-crystallization treatments for improving diffraction quality of protein crystals" *Acta Crystallogr., Sect.: D Biol.* **2005**, *61*, 1173-1180.

102. J. P. Lam, D. C. Mays, J. J. Lipsky, "Inhibition of recombinant human mitochondrial and cytosolic aldehyde dehydrogenases by two candidates for the active metabolites of disulfiram" *Biochemistry* **1997**, *36*, 13748-13754.

103. B. S. Mayhew, D. R. Jones, S. D. Hall, "An in vitro model for predicting in vivo inhibition of cytochrome P450 3A4 by metabolic intermediate complex formation" *Drug. Metab. Dispos.* **2000**, *28*, 1031-1037.

104. B. F. Krippendorff, R. Neuhaus, P. Lienau, A. Reichel, W. Huisinga, "Mechanism-based inhibition: deriving K(I) and k(inact) directly from time-dependent IC(50) values" *J. Biomol. Screen.* **2009**, *14*, 913-923.

105. R. Kitz, I. B. Wilson, "Esters of methanesulfonic acid as irreversible inhibitors of acetylcholinesterase" *J. Biol. Chem.* **1962**, *237*, 3245-3249.

106. F. Ghanbari, K. Rowland-Yeo, J. C. Bloomer, S. E. Clarke, M. S. Lennard, G. T. Tucker, A. Rostami-Hodjegan, "A critical evaluation of the experimental design of studies of mechanism based enzyme inhibition, with implications for in vitro-in vivo extrapolation" *Curr. Drug Metab.* **2006**, *7*, 315-334.

107. T. S. Maurer, H. Fung, "Comparison of methods for analyzing kinetic data from mechanism-based enzyme inactivation: application to nitric oxide synthase" *AAPS PharmSci.* **2000**, *2*, 1-10.

108. J. S. Moreb, D. Ucar, S. Han, J. K. Amory, A. S. Goldstein, B. Ostmark, L. J. Chang, "The enzymatic activity of human aldehyde dehydrogenases 1A2 and 2 (ALDH1A2 and ALDH2) is detected by Aldefluor, inhibited by diethylaminobenzaldehyde and has significant effects on cell proliferation and drug resistance" *Chem. Biol. Interact.* **2012**, *195*, 52-60.

109. M. Tercel, S. P. McManaway, E. Leung, H. D. Liyanage, G. L. Lu, F. B. Pruijn, "The Cytotoxicity of Duocarmycin Analogues is Mediated through Alkylation of DNA, not Aldehyde Dehydrogenase 1: A Comment" *Angew. Chem. Int. Ed. Engl.* **2013**.

110. D. L. Boger, H. W. Schmitt, B. E. Fink, M. P. Hedrick, "Parallel synthesis and evaluation of 132 (+)-1,2,9,9a-tetrahydrocyclopropa[c]benz[e]indol-4-one (CBI) analogues of CC-1065 and the duocarmycins defining the contribution of the DNA-binding domain" *J. Org. Chem.* **2001**, *66*, 6654-6661.

111. D. A. Boger, N. Han, C. M. Tarby, C. W. Boyce, H. Cai, Q. Jin, P. A. Kitos, "Synthesis, chemical properties, and preliminary evaluation of substituted CBI Analogs of CC-1065 and the duocarmycins incorporating the 7-Cyano-1,2,9,9a-tetrahydrocyclopropa[c]benz[e]indol-4-one alkylation subunit: Hammett quantitation of the magnitude of electronic effects on functional reactivity" *J. Org. Chem.* **1996**, *61*, 4894-4912.

112. D. A. Boger, R. S. Coleman, B. J. Invergo, S. M. Sakya, T. Ishizaki, S. A. Munk, H. Zarrinmayeh, P. A. Kitos, S. C. Thompson, "Synthesis and Evaluation of Aborted and Extended CC- 1065 Functional Analogues: (+)- and (-)-CPI-PDE-I$_1$, (+)- and (-)-CPI-CDPI$_1$, and (+/-)-, (+)-, and (-)-CPI-CDPI$_3$. Preparation of Key Partial Structures and Definition of

an Additional Functional Role of the CC-1065 Central and Right-Hand Subunits" *J. Am. Chem. Soc.* **1990**, *112*, 4623-4632.

113. T. Wirth, G. F. Pestel, V. Ganal, T. Kirmeier, I. Schuberth, T. Rein, L. F. Tietze, S. A. Sieber, "The two faces of potent antitumor duocarmycin based drugs: A structural dissection reveals disparate motifs for DNA versus ALDH1A1 affinity" *Angew. Chem. Int. Ed. Engl.* **2013**, *in press*.

114. P. Cossart, P. J. Sansonetti, "Bacterial invasion: the paradigms of enteroinvasive pathogens" *Science* **2004**, *304*, 242-248.

115. E. G. Pamer, "Immune responses to Listeria monocytogenes" *Nat. Rev. Immunol.* **2004**, *4*, 812-823.

116. M. Hamon, H. Bierne, P. Cossart, "Listeria monocytogenes: a multifaceted model" *Nat. Rev. Microbiol.* **2006**, *4*, 423-434.

117. M. Schuppler, M. J. Loessner, "The Opportunistic Pathogen Listeria monocytogenes: Pathogenicity and Interaction with the Mucosal Immune System" *Int. J. Inflam.* **2010**, *2010*, 704321.

118. M. A. Hamon, D. Ribet, F. Stavru, P. Cossart, "Listeriolysin O: the Swiss army knife of Listeria" *Trends Microbiol.* **2012**, *20*, 360-368.

119. J. L. Gaillard, P. Berche, C. Frehel, E. Gouin, P. Cossart, "Entry of L. monocytogenes into cells is mediated by internalin, a repeat protein reminiscent of surface antigens from gram-positive cocci" *Cell* **1991**, *65*, 1127-1141.

120. Y. Shen, M. Naujokas, M. Park, K. Ireton, "InlB-dependent internalization of Listeria is mediated by the Met receptor tyrosine kinase" *Cell* **2000**, *103*, 501-510.

121. Z. Wei, L. A. Zenewicz, H. Goldfine, "Listeria monocytogenes phosphatidylinositol-specific phospholipase C has evolved for virulence by greatly reduced activity on GPI anchors" *Proc. Natl. Acad. Sci. U.S.A.* **2005**, *102*, 12927-12931.

122. I. Chico-Calero, M. Suarez, B. Gonzalez-Zorn, M. Scortti, J. Slaghuis, W. Goebel, J. A. Vazquez-Boland, "Hpt, a bacterial homolog of the microsomal glucose- 6-phosphate translocase, mediates rapid intracellular proliferation in Listeria" *Proc. Natl. Acad. Sci. U.S.A.* **2002**, *99*, 431-436.

123. M. O'Riordan, M. A. Moors, D. A. Portnoy, "Listeria intracellular growth and virulence require host-derived lipoic acid" *Science* **2003**, *302*, 462-464.

124. C. Kocks, E. Gouin, M. Tabouret, P. Berche, H. Ohayon, P. Cossart, "L. monocytogenes-induced actin assembly requires the actA gene product, a surface protein" *Cell* **1992**, *68*, 521-531.

125. E. R. Unanue, "Studies in listeriosis show the strong symbiosis between the innate cellular system and the T-cell response" *Immunol. Rev.* **1997**, *158*, 11-25.

126. S. Kayal, A. Lilienbaum, C. Poyart, S. Memet, A. Israel, P. Berche, "Listeriolysin O-dependent activation of endothelial cells during infection with Listeria monocytogenes: activation of NF-kappa B and upregulation of adhesion molecules and chemokines" *Mol. Microbiol.* **1999**, *31*, 1709-1722.

127. P. Tang, I. Rosenshine, P. Cossart, B. B. Finlay, "Listeriolysin O activates mitogen-activated protein kinase in eucaryotic cells" *Infect. Immun.* **1996**, *64*, 2359-2361.

128. U. Sibelius, T. Chakraborty, B. Krogel, J. Wolf, F. Rose, R. Schmidt, J. Wehland, W. Seeger, F. Grimminger, "The listerial exotoxins listeriolysin and phosphatidylinositol-specific phospholipase C synergize to elicit endothelial cell phosphoinositide metabolism" *J. Immunol.* **1996**, *157*, 4055-4060.

129. N. V. Serbina, W. Kuziel, R. Flavell, S. Akira, B. Rollins, E. G. Pamer, "Sequential MyD88-independent and -dependent activation of innate immune responses to intracellular bacterial infection" *Immunity* **2003**, *19*, 891-901.

130. E. Seki, H. Tsutsui, N. M. Tsuji, N. Hayashi, K. Adachi, H. Nakano, S. Futatsugi-Yumikura, O. Takeuchi, K. Hoshino, S. Akira, J. Fujimoto, K. Nakanishi, "Critical roles of myeloid

differentiation factor 88-dependent proinflammatory cytokine release in early phase clearance of Listeria monocytogenes in mice" *J. Immunol.* **2002**, *169*, 3863-3868.

131. N. V. Serbina, T. P. Salazar-Mather, C. A. Biron, W. A. Kuziel, E. G. Pamer, "TNF/iNOS-producing dendritic cells mediate innate immune defense against bacterial infection" *Immunity* **2003**, *19*, 59-70.

132. A. de las Heras, R. J. Cain, M. K. Bielecka, J. A. Vazquez-Boland, "Regulation of Listeria virulence: PrfA master and commander" *Curr. Opin. Microbiol.* **2011**, *14*, 118-127.

133. E. Milohanic, P. Glaser, J. Y. Coppee, L. Frangeul, Y. Vega, J. A. Vazquez-Boland, F. Kunst, P. Cossart, C. Buchrieser, "Transcriptome analysis of Listeria monocytogenes identifies three groups of genes differently regulated by PrfA" *Mol. Microbiol.* **2003**, *47*, 1613-1625.

134. M. Scortti, H. J. Monzo, L. Lacharme-Lora, D. A. Lewis, J. A. Vazquez-Boland, "The PrfA virulence regulon" *Microbes Infect.* **2007**, *9*, 1196-1207.

135. J. Johansson, P. Mandin, A. Renzoni, C. Chiaruttini, M. Springer, P. Cossart, "An RNA thermosensor controls expression of virulence genes in Listeria monocytogenes" *Cell* **2002**, *110*, 551-561.

136. M. T. Ripio, G. Dominguez-Bernal, M. Suarez, K. Brehm, P. Berche, J. A. Vazquez-Boland, "Transcriptional activation of virulence genes in wild-type strains of Listeria monocytogenes in response to a change in the extracellular medium composition" *Res. Microbiol.* **1996**, *147*, 371-384.

137. J. Kreft, J. A. Vazquez-Boland, "Regulation of virulence genes in Listeria" *Int. J. Med. Microbiol.* **2001**, *291*, 145-157.

138. U. Schwab, B. Bowen, C. Nadon, M. Wiedmann, K. J. Boor, "The Listeria monocytogenes prfAP2 promoter is regulated by sigma B in a growth phase dependent manner" *FEMS Microbiol. Lett.* **2005**, *245*, 329-336.

139. L. M. Shetron-Rama, H. Marquis, H. G. Bouwer, N. E. Freitag, "Intracellular induction of Listeria monocytogenes actA expression" *Infect. Immun.* **2002**, *70*, 1087-1096.

140. J. M. Augustin, V. Kuzina, S. B. Andersen, S. Bak, "Molecular activities, biosynthesis and evolution of triterpenoid saponins" *Phytochemistry* **2011**, *72*, 435-457.

141. D. Koley, A. J. Bard, "Triton X-100 concentration effects on membrane permeability of a single HeLa cell by scanning electrochemical microscopy (SECM)" *Proc. Natl. Acad. Sci. U.S.A.* **2010**, *107*, 16783-16787.

142. S. Tienungoon, D. A. Ratkowsky, T. A. McMeekin, T. Ross, "Growth limits of Listeria monocytogenes as a function of temperature, pH, NaCl, and lactic acid" *Appl. Environ. Microbiol.* **2000**, *66*, 4979-4987.

143. T. Böttcher, S. A. Sieber, "Beta-lactones as specific inhibitors of ClpP attenuate the production of extracellular virulence factors of Staphylococcus aureus" *J. Am. Chem. Soc.* **2008**, *130*, 14400-14401.

144. T. Böttcher, S. A. Sieber, "Beta-lactones as privileged structures for the active-site labeling of versatile bacterial enzyme classes" *Angew. Chem. Int. Ed. Engl.* **2008**, *47*, 4600-4603.

145. T. Böttcher, S. A. Sieber, "Beta-lactones decrease the intracellular virulence of Listeria monocytogenes in macrophages" *ChemMedChem* **2009**, *4*, 1260-1263.

146. T. Böttcher, S. A. Sieber, "Structurally refined beta-lactones as potent inhibitors of devastating bacterial virulence factors" *ChemBioChem* **2009**, *10*, 663-666.

147. M. Pitscheider, N. Mäusbacher, S. A. Sieber, "Antibiotic activity and target discovery of three-membered natural product-derived heterocycles in pathogenic bacteria" *Chem. Sci.* **2012**, *3*, 2035-2041.

148. O. Gaillot, E. Pellegrini, S. Bregenholt, S. Nair, P. Berche, "The ClpP serine protease is essential for the intracellular parasitism and virulence of Listeria monocytogenes" *Mol. Microbiol.* **2000**, *35*, 1286-1294.

149. A. Michel, F. Agerer, C. R. Hauck, M. Herrmann, J. Ullrich, J. Hacker, K. Ohlsen, "Global regulatory impact of ClpP protease of Staphylococcus aureus on regulons involved in

virulence, oxidative stress response, autolysis, and DNA repair" *J. Bacteriol.* **2006**, *188*, 5783-5796.

150. Y. M. Ibrahim, A. R. Kerr, N. A. Silva, T. J. Mitchell, "Contribution of the ATP-dependent protease ClpCP to the autolysis and virulence of Streptococcus pneumoniae" *Infect. Immun.* **2005**, *73*, 730-740.

151. M. Moche, G. Schneider, P. Edwards, K. Dehesh, Y. Lindqvist, "Structure of the complex between the antibiotic cerulenin and its target, beta-ketoacyl-acyl carrier protein synthase" *J. Biol. Chem.* **1999**, *274*, 6031-6034.

152. K. Zhu, X. Ding, M. Julotok, B. J. Wilkinson, "Exogenous isoleucine and fatty acid shortening ensure the high content of anteiso-C15:0 fatty acid required for low-temperature growth of Listeria monocytogenes" *Appl. Environ. Microbiol.* **2005**, *71*, 8002-8007.

153. K. Young, H. Jayasuriya, J. G. Ondeyka, K. Herath, C. Zhang, S. Kodali, A. Galgoci, R. Painter, V. Brown-Driver, R. Yamamoto, L. L. Silver, Y. Zheng, J. I. Ventura, J. Sigmund, S. Ha, A. Basilio, F. Vicente, J. R. Tormo, F. Pelaez, P. Youngman, D. Cully, J. F. Barrett, D. Schmatz, S. B. Singh, J. Wang, "Discovery of FabH/FabF inhibitors from natural products" *Antimicrob. Agents. Chemother.* **2006**, *50*, 519-526.

154. J. Wang, S. Kodali, S. H. Lee, A. Galgoci, R. Painter, K. Dorso, F. Racine, M. Motyl, L. Hernandez, E. Tinney, S. L. Colletti, K. Herath, R. Cummings, O. Salazar, I. Gonzalez, A. Basilio, F. Vicente, O. Genilloud, F. Pelaez, H. Jayasuriya, K. Young, D. F. Cully, S. B. Singh, "Discovery of platencin, a dual FabF and FabH inhibitor with in vivo antibiotic properties" *Proc. Natl. Acad. Sci. U.S.A.* **2007**, *104*, 7612-7616.

155. E. Martens, A. L. Demain, "Platensimycin and platencin: promising antibiotics for future application in human medicine" *J. Antibiot. (Tokyo)* **2011**, *64*, 705-710.

156. H. Zur, E. Ruppin, T. Shlomi, "iMAT: an integrative metabolic analysis tool" *Bioinformatics* **2010**, *26*, 3140-3142.

157. L. Lobel, N. Sigal, I. Borovok, E. Ruppin, A. A. Herskovits, "Integrative genomic analysis identifies isoleucine and CodY as regulators of Listeria monocytogenes virulence" *PLoS Genet.* **2012**, *8*, e1002887.

158. I. J. Glomski, M. M. Gedde, A. W. Tsang, J. A. Swanson, D. A. Portnoy, "The Listeria monocytogenes hemolysin has an acidic pH optimum to compartmentalize activity and prevent damage to infected host cells" *J. Cell. Biol.* **2002**, *156*, 1029-1038.

159. C. Giammarini, F. Andreoni, G. Amagliani, A. Casiere, S. Barocci, M. Magnani, "High-level expression of the Listeria monocytogenes listeriolysin O in Escherichia coli and preliminary characterization of the purified protein" *Protein Expr. Purif.* **2003**, *28*, 78-85.

160. S. Vadia, E. Arnett, A. C. Haghighat, E. M. Wilson-Kubalek, R. K. Tweten, S. Seveau, "The pore-forming toxin listeriolysin O mediates a novel entry pathway of L. monocytogenes into human hepatocytes" *PLoS Pathog.* **2011**, *7*, e1002356.

161. F. J. Kayne, N. C. Price, "Amino acid effector binding to rabbit muscle pyruvate kinase" *Arch. Biochem. Biophys.* **1973**, *159*, 292-296.

162. V. Gupta, R. N. Bamezai, "Human pyruvate kinase M2: a multifunctional protein" *Protein Sci.* **2010**, *19*, 2031-2044.

163. S. Mazurek, H. C. Drexler, J. Troppmair, E. Eigenbrodt, U. R. Rapp, "Regulation of pyruvate kinase type M2 by A-Raf: a possible glycolytic stop or go mechanism" *Anticancer Res.* **2007**, *27*, 3963-3971.

164. J. Lee, H. K. Kim, Y. M. Han, J. Kim, "Pyruvate kinase isozyme type M2 (PKM2) interacts and cooperates with Oct-4 in regulating transcription" *Int. J. Biochem. Cell. Biol.* **2008**, *40*, 1043-1054.

165. N. Shimada, T. Shinagawa, S. Ishii, "Modulation of M2-type pyruvate kinase activity by the cytoplasmic PML tumor suppressor protein" *Genes Cells* **2008**, *13*, 245-254.

166. X. Wu, Y. Zhou, K. Zhang, Q. Liu, D. Guo, "Isoform-specific interaction of pyruvate kinase with hepatitis C virus NS5B" *FEBS Lett.* **2008**, *582*, 2155-2160.

167. P. Presek, H. Glossmann, E. Eigenbrodt, W. Schoner, H. Rubsamen, R. R. Friis, H. Bauer, "Similarities between a phosphoprotein (pp60src)-associated protein kinase of Rous sarcoma virus and a cyclic adenosine 3':5'-monophosphate-independent protein kinase that phosphorylates pyruvate kinase type M2" *Cancer Res.* **1980**, *40*, 1733-1741.

168. J. M. Williams, G. C. Chen, L. Zhu, R. F. Rest, "Using the yeast two-hybrid system to identify human epithelial cell proteins that bind gonococcal Opa proteins: intracellular gonococci bind pyruvate kinase via their Opa proteins and require host pyruvate for growth" *Mol. Microbiol.* **1998**, *27*, 171-186.

169. J. Hempel, R. Kaiser, H. Jornvall, "Mitochondrial aldehyde dehydrogenase from human liver. Primary structure, differences in relation to the cytosolic enzyme, and functional correlations" *Eur. J. Biochem.* **1985**, *153*, 13-28.

170. A. A. Klyosov, L. G. Rashkovetsky, M. K. Tahir, W. M. Keung, "Possible role of liver cytosolic and mitochondrial aldehyde dehydrogenases in acetaldehyde metabolism" *Biochemistry* **1996**, *35*, 4445-4456.

171. C. H. Chen, L. Sun, D. Mochly-Rosen, "Mitochondrial aldehyde dehydrogenase and cardiac diseases" *Cardiovasc. Res.* **2010**, *88*, 51-57.

172. D. R. Petersen, J. A. Doorn, "Reactions of 4-hydroxynonenal with proteins and cellular targets" *Free Radic. Biol. Med.* **2004**, *37*, 937-945.

173. Z. Chen, M. W. Foster, J. Zhang, L. Mao, H. A. Rockman, T. Kawamoto, K. Kitagawa, K. I. Nakayama, D. T. Hess, J. S. Stamler, "An essential role for mitochondrial aldehyde dehydrogenase in nitroglycerin bioactivation" *Proc. Natl. Acad. Sci. U.S.A.* **2005**, *102*, 12159-12164.

174. Z. Chen, J. S. Stamler, "Bioactivation of nitroglycerin by the mitochondrial aldehyde dehydrogenase" *Trends Cardiovasc. Med.* **2006**, *16*, 259-265.

175. H. Okazaki, M. Igarashi, M. Nishi, M. Sekiya, M. Tajima, S. Takase, M. Takanashi, K. Ohta, Y. Tamura, S. Okazaki, N. Yahagi, K. Ohashi, M. Amemiya-Kudo, Y. Nakagawa, R. Nagai, T. Kadowaki, J. Osuga, S. Ishibashi, "Identification of neutral cholesterol ester hydrolase, a key enzyme removing cholesterol from macrophages" *J. Biol. Chem.* **2008**, *283*, 33357-33364.

176. M. Igarashi, J. Osuga, M. Isshiki, M. Sekiya, H. Okazaki, S. Takase, M. Takanashi, K. Ohta, M. Kumagai, M. Nishi, T. Fujita, R. Nagai, T. Kadowaki, S. Ishibashi, "Targeting of neutral cholesterol ester hydrolase to the endoplasmic reticulum via its N-terminal sequence" *J. Lipid. Res.* **2010**, *51*, 274-285.

177. M. Igarashi, J. Osuga, H. Uozaki, M. Sekiya, S. Nagashima, M. Takahashi, S. Takase, M. Takanashi, Y. Li, K. Ohta, M. Kumagai, M. Nishi, M. Hosokawa, C. Fledelius, P. Jacobsen, H. Yagyu, M. Fukayama, R. Nagai, T. Kadowaki, K. Ohashi, S. Ishibashi, "The critical role of neutral cholesterol ester hydrolase 1 in cholesterol removal from human macrophages" *Circ. Res.* **2010**, *107*, 1387-1395.

178. M. Sekiya, J. Osuga, M. Igarashi, H. Okazaki, S. Ishibashi, "The role of neutral cholesterol ester hydrolysis in macrophage foam cells" *J. Atheroscler. Thromb.* **2011**, *18*, 359-364.

179. M. S. Brown, J. L. Goldstein, M. Krieger, Y. K. Ho, R. G. Anderson, "Reversible accumulation of cholesteryl esters in macrophages incubated with acetylated lipoproteins" *J. Cell. Biol.* **1979**, *82*, 597-613.

180. C. Cavelier, I. Lorenzi, L. Rohrer, A. von Eckardstein, "Lipid efflux by the ATP-binding cassette transporters ABCA1 and ABCG1" *Biochim. Biophys. Acta* **2006**, *1761*, 655-666.

181. X. Wang, H. L. Collins, M. Ranalletta, I. V. Fuki, J. T. Billheimer, G. H. Rothblat, A. R. Tall, D. J. Rader, "Macrophage ABCA1 and ABCG1, but not SR-BI, promote macrophage reverse cholesterol transport in vivo" *J. Clin. Invest.* **2007**, *117*, 2216-2224.

182. J. L. Hsu, S. Y. Huang, N. H. Chow, S. H. Chen, "Stable-isotope dimethyl labeling for quantitative proteomics" *Anal. Chem.* **2003**, *75*, 6843-6852.

183. P. J. Boersema, R. Raijmakers, S. Lemeer, S. Mohammed, A. J. Heck, "Multiplex peptide stable isotope dimethyl labeling for quantitative proteomics" *Nat. Protoc.* **2009**, *4*, 484-494.

184. D. Kovanich, S. Cappadona, R. Raijmakers, S. Mohammed, A. Scholten, A. J. Heck, "Applications of stable isotope dimethyl labeling in quantitative proteomics" *Anal. Bioanal. Chem.* **2012**, *404*, 991-1009.

185. J. Eirich, J. L. Burkhart, A. Ullrich, G. C. Rudolf, A. Vollmar, S. Zahler, U. Kazmaier, S. A. Sieber, "Pretubulysin derived probes as novel tools for monitoring the microtubule network via activity-based protein profiling and fluorescence microscopy" *Mol. Biosyst.* **2012**, *8*, 2067-2075.

186. S. A. Sieber, S. Niessen, H. S. Hoover, B. F. Cravatt, "Proteomic profiling of metalloprotease activities with cocktails of active-site probes" *Nat. Chem. Biol.* **2006**, *2*, 274-281.

187. S. P. Mirza, B. D. Halligan, A. S. Greene, M. Olivier, "Improved method for the analysis of membrane proteins by mass spectrometry" *Physiol. Genomics* **2007**, *30*, 89-94.

188. J. S. Moreb, C. Maccow, M. Schweder, J. Hecomovich, "Expression of antisense RNA to aldehyde dehydrogenase class-1 sensitizes tumor cells to 4-hydroperoxycyclophosphamide in vitro" *J. Pharmacol. Exp. Ther.* **2000**, *293*, 390-396.

189. W. Kabsch, "Automatic processing of rotation diffraction data from crystals of initially unknown symmetry and cell constants" *J. Appl. Crystallogr.* **1993**, *26*, 795-800.

190. A. J. McCoy, R. W. Grosse-Kunstleve, P. D. Adams, M. D. Winn, L. C. Storoni, R. J. Read, "Phaser crystallographic software" *J. Appl. Crystallogr.* **2007**, *40*, 658-674.

191. P. Emsley, K. Cowtan, "Coot: model-building tools for molecular graphics" *Acta Crystallogr., Sect.: D Biol.* **2004**, *60*, 2126-2132.

1. T. Wirth, K. Schmuck, L. F. Tietze, S. A. Sieber, "Duocarmycin analogues target aldehyde dehydrogenase 1 in lung cancer cells" *Angew. Chem. Int. Ed. Engl.* **2012**, *51*, 2874-2877.

2. T. Wirth, G. F. Pestel, V. Ganal, T. Kirmeier, I. Schuberth, T. Rein, L. F. Tietze, S. A. Sieber, "The two faces of potent antitumor duocarmycin based drugs: A structural dissection reveals disparate motifs for DNA versus ALDH1A1 affinity" *Angew. Chem. Int. Ed. Engl.* **2013**, *in press*.

Tanja Wirth

geb. 09. September 1984 in Füssen

Akademische Ausbildung

02/2010 – 06/2013	**Technische Universität München**
	Promotion Am Lehrstuhl für Organische Chemie II
	Thema der Dissertation: *„Aldehyde Dehydrogenase 1 – A Novel Target of Duocarmycins "* and *„Activity Based Protein Profiling during Bacterial Invasion"*
	Unter Anleitung von Prof. Dr. Stephan A. Sieber

12/2007 – 11/2009	**Ludwig-Maximilians Universität München**
	Studium der Chemie
	Abschluss Master of Science
	Thema der Masterarbeit: *„Bakterielle Invasion in eukaryo-tische Zellen – Chemische Methoden zur Identifizierung pathogenese-assoziierter Enzyme"*
	Unter Anleitung von Prof. Dr. Stephan A. Sieber

10/2004 – 12/2007	**Ludwig-Maximilians Universität München**
	Studium der Chemie und Biochemie
	Abschluss Bachelor of Science
	Thema der Bachelorarbeit: *„Synthese und Kristallstruktur des ersten Erdalkalioxonitridosilikats mit Schichtstruktur"*
	Unter Anleitung von Prof. Dr. Wolfgang Schnick

Schulische Ausbildung

09/1995 – 07/2004	Gymnasium Füssen
09/1991 – 07/1995	Grundschule Füssen